Noninvasive Imaging of Three-dimensional Ventricular Electrical Activity

A DISSERTATION
SUBMITTED TO THE FACULTY OF THE GRADUATE SCHOOL
OF THE UNIVERSITY OF MINNESOTA
BY

Chengzong Han

IN PARTIAL FULFILLMENT OF THE REQUIREMENTS
FOR THE DEGREE OF
DOCTOR OF PHILOSOPHY

Prof. Bin He, Advisor

August, 2012

Acknowledgements

I would like to express my most sincerely appreciation to my advisor, Prof. Bin He, for his guidance and assistance over the past six years. His insightful advice and consistent support help me to make steady progress in my dissertation research. I also greatly thank the members of my dissertation committee, Dr. Jianping Wang, Dr. Alena Talkachova and Dr. Shai Ashkenazi, for their time, support and valuable comments.

I would like to thank Dr. Steven M. Pogwid, Professor at the University of Alabama at Birmingham, for his collaboration, useful discussion, and access to resources in his animal lab. I also would like to acknowledge many collaborators in Dr. Pogwizd's lab, especially Dr. Cheryl R. Killingsworth, Ms. Sharon Melnick, and Mr. Dennis Rollins for collaborating in the animal surgery, data acquisition, and providing expertise in cardiac electrophysiology experiments.

I am also indebted to many lab colleagues who have worked in the Biomedical Functional Imaging and Neuroengineering Laboratory at the University of Minnesota, who have contributed a lot to the research contained in this dissertation. Special thanks to Dr. Chenguang Liu and Dr. Zhongming Liu, for their great help in cardiac electrical imaging and animal experiment especially at the initial stage of my research, for their very helpful discussion on data analysis and interpretation, and for being brothers in taking care of me both in life and research in the past six years. I also graciously thank Dr. Dakun Lai, for his great assistance and useful discussion in animal experiment in the

past years. I also would like to thank Ms. Zhaoye Zhou and Mr. Long Yu for their great help and useful discussion in animal experiment and data analysis, and for being wonderful team members.

Finally, I am grateful to all other lab members whom I have worked with: Dr. Xin Zhang, Dr. Lei Ding, Dr. Yingchun Zhang, Dr. Xiaoxiao Bai, Dr. Xu Li, Dr. Christopher Wilke, Dr. Rongmin Xia, Dr. Qingyu Ma, Dr. Nuo Gao, Dr. Xiaotong Zhang, Dr. Gang Wang, Dr. Gang Hu, Dr. Yakang Dai, Dr. Han Yuan, Dr. Audrey Royer, Dr. Lin Yang, Mr. Leo Mariappan, Mr. Yunfeng Lu, Mr. Keith Jamison, Ms. Huishi Zhang, Mr. Jiaen Liu, Ms. Nessa Johnson, Mr. Alexander Doud, Ms. Kaitlin Cassady, Mr. Abhrajeet Roy, Mr. Bryan Baxter, and Mr. Haijun Shan. Thanks to them for their help in my study and life, and for being friends.

Dedication

This dissertation is dedicated to my parents, Yongqing Han and Guoding Feng, for their unwavering love and support throughout my life, and for encouraging me to do everything to the best of my life. I also would like to dedicate this dissertation to my dear wife, Hanhuai Shan, for her tremendous love, encouragement, patience, and support during all these years.

Abstract

Noninvasive imaging of cardiac electrical activity is of great importance and can facilitate basic cardiovascular research and clinical diagnosis and management of various malignant cardiac arrhythmias. This dissertation research is aimed to investigate a novel physical-model-based 3-dimensional cardiac electrical imaging (3DCEI) approach. The 3DCEI approach is developed by mathematically combining high-density body surface electrocardiograms (ECGs) with the anatomical information. Computer simulation study and animal experiments were conducted to rigorously evaluate the performance of 3DCEI. The simulation results demonstrate that 3DCEI can localize the origin of activation and image the activation sequence throughout the three-dimensional ventricular myocardium. The performance of 3DCEI was also experimentally and rigorously evaluated through well-controlled animal validation studies in both the small animal model (rabbit) and large animal model (canine), with the aid of simultaneous intramural recordings from intra-cardiac mapping using plunge-needle electrodes inserted in the ventricular myocardium. The clinical relevance of 3DCEI was further demonstrated by investigating 3DCEI in cardiac arrhythmias from animal models with experimentally-induced cardiovascular diseases. The consistent agreement between the non-invasively imaged activation sequences and its directly measured counterparts in both the rabbit heart and canine heart implies that 3DCEI is feasible in reconstructing the spatial patterns of ventricular activation sequences, localizing the arrhythmogenic foci, and imaging dynamically changing arrhythmia on a beat-to-beat basis. The promising results presented in this dissertation study suggest that this cardiac electrical imaging

approach may provide an important alternative for non-invasively imaging cardiac electrical activity throughout ventricular myocardium and may potentially become an important tool to facilitate clinical diagnosis and treatments of malignant ventricular arrhythmias.

Table of Contents

LIST OF TABLES IX

LIST OF FIGURES X

INTRODUCTION 1

1.1. Overview 1

1.2. Motivations and Significance 3

1.3. Scope of the Dissertation 5

BACKGROUND 7

2.1. Cardiac Electrical Activity 7

2.2. Cardiac Arrhythmias and Electrophysiological Mapping 8

2.3. Electrocardiography and Body Surface Potential Mapping 10

2.2. Cardiac Electrical Imaging 11

2.2.1. ECG Forward Problem 11

2.2.2. ECG Inverse Problem 14

2.3. Intracavitary Potential-based Inverse Solution 17

THREE-DIMENSIONAL CARDIAC ELECTRICAL IMAGING 18

2.1. Biophysical Principles and Equivalent Source Model 18

3.2. Imaging Principles 21

3.2.1. Forward Problem 21

3.2.2. Inverse Problem 22

3.2. Computer Simulation Study 23

3.2.1. Preliminary Results 26

3.2.2. Discussion 28

EXPERIMENTAL INVESTIGATION IN NORMAL RABBIT HEART 34
4.1. Introduction 34
4.2. Study Design 35
4.2.1. Simultaneous Body Surface Potential Mapping and 3D Intra-cardiac Mapping 35
4.2.2. Ultra Fast Computed Tomography 38
4.2.3. 3D Intra-cardiac Mapping 39
4.2.4. Data Analysis and Statistical Analysis 40
4.3. Results 42
4.3.1. Validation during Pacing 42
4.3.2. Norepinephrine-induced Ventricular Arrhythmias 48
4.4. Discussion 51
EXPERIMENTAL INVESTIGATION IN NORMAL CANINE HEART 56
5.1. Introduction 56
5.2. Study Design 57
5.2.1. Canine Model and Experimental Procedures 57
5.2.2. Data Analysis 59
5.3. Results 62
5.3.1. Experimentation and Modeling 62
5.3.2. Pacing in the Canine Heart 62
5.3.3. Ventricular Arrhythmias in the Canine Heart 65
5.4. Discussion 68
EXPERIMENTAL INVESTIGATION OF VENTRICULAR ARRHYTHMIA MECHANISMS . 75
6.1. Ventricular Arrhythmias during Drug-induced QT Prolongation in the Rabbit Heart 75
6.1.1. Introduction 75

6.1.2. Study Design 76
6.1.3. Results 80
6.1.4. Discussion 86
6.2. Ventricular Arrhythmias in a Canine Model of Nonischemic Heart Failure 88
6.2.1. Introduction 88
6.2.2. Study Design 89
6.2.3. Results 91
6.2.4. Discussion 94
CONCLUSIONS AND FUTURE WORK 96
7.1. Conclusions 96
7.2. Future Work 98
LITERATURE CITED 101
APPENDIX A - COPYRIGHT PERMISSIONS 115
APPENDIX B – VITA 118

List of Tables

Table 1. Simulation results of imaging the 3D ventricular activation sequence induced by single-site pacing……...……..P30

Table 2. Simulation results of imaging the 3D ventricular activation sequence induced by dual-site pacing……P31

Table 3. Quantitative comparison between measured and imaged activation sequences in single-site LV pacing in the rabbit heart……..P44

Table 4. Quantitative comparison between measured and imaged activation sequences in single-site RV and septal pacing in the rabbit heart..……..P45

Table 5. Quantitative comparison between measured and imaged activation sequences in simultaneous dual-site pacing in the rabbit heart..……..P47

Table 6. Quantitative comparison between measured and imaged activation sequences in norepinephrine induced VT in rabbit heart…….....P48

Table 7. Quantitative comparison between measured activation sequence and imaged activation sequence during single-site LV pacing in the canine heart…….P63

Table 8. Quantitative comparison between measured activation sequence and imaged activation sequence during single-site RV pacing in the canine heart……P64

Table 9. Quantitative comparison between measured activation sequence and imaged activation sequence in norepinephrine induced VT in the canine heart……..P69

Table 10. Summary of ventricular arrhythmias induced during the infusion of clofilium and phenylephrine in the rabbit heart……..P80

List of Figures

Fig.1. ECG forward problem and inverse problem in cardiac electrical imaging.……..P12

Fig.2. The relation between transmembrane potential, equivalent current density and activation time ……P20

Fig.3. Comparison between the forward activation sequence and imaged activation sequence during the single-site pacing in computer simulation.…….P24

Fig.4. Comparison between the forward activation sequence and imaged activation sequence during the dual-site pacing in computer simulation.……P26

Fig.5. Relative error under single-site pacing with varying electrode numbers and noise levels in computer simulation study……P28

Fig.6. Localization error under single-site pacing with varying electrode numbers and noise levels in computer simulation study…….....P29

Fig.7. Schematic diagram of the experimental protocol for validating the 3DCEI technique in rabbit.……..P36

Fig.8. Comparison between activation sequence measured via 3D intra-cardiac mapping and activation sequence imaged by 3DCEI during pacing in rabbit ……..P43

Fig.9. Comparison between the measured activation sequence and the imaged activation sequence during septum pacing in rabbit…….P46

Fig.10. Comparison between the measured activation sequence and the imaged activation sequence during norepinephrine induced VT in rabbit ……...P50

Fig.11. Schematic diagram of the experimental protocol for validating the 3DCEI technique in canine.…….P58

Fig.12. Comparison between the measured activation sequence and the imaged activation sequence during pacing in canine.……...P61

Fig.13. Comparison between the measured activation sequence and the imaged activation sequence for monomorphic VTs in canine.…….P66

Fig.14. Comparison between the measured activation sequence and the imaged activation sequence for polymorphic VT in canine……..P68

Fig.15. The drug infusion protocol for inducing torsades de pointes in rabbit..…….P78

Fig.16. Comparison between the measured activation sequence and the imaged activation sequence for PVC induced by phenylephrine and clofilium in rabbit.....P81

Fig.17. Comparison between the measured activation sequence and the imaged activation sequence for couplet induced by phenylephrine and clofilium in rabbit.....P82

Fig.18. Comparison between the measured activation sequence and the imaged activation sequence for torsades de pointes in rabbit.....P84

Fig.19. Comparison between the measured activation sequence and the imaged activation sequence for VT induced by phenylephrine and clofilium in rabbit.....P85

Fig.20. Comparison between the measured activation sequence and the imaged activation sequence for spontaneous VT in heart failure canine……..P91

Fig.21. Comparison between the measured activation sequence and the imaged activation sequence for norepinephrine induced VT in heart failure canine……P93

Chapter 1

Introduction

1.1. Overview

A group of conditions in which the electrical activity of the heart is irregular or is faster or slower than normal, called cardiac arrhythmias, constitutes a major cause of death and disability among the world's population. Particularly, in the United States alone, ventricular arrhythmias are the major causes of nearly 400,000 deaths per year (Myerburg et al., 1993). Ventricular arrhythmias could occur in patients with either structurally normal (e.g., idiopathic arrhythmia) or abnormal (e.g., congestive heart failure) hearts, and may degenerate into ventricular fibrillation (VF), an irregular fast heart rhythm that could even lead to sudden cardiac death. Both pharmacological treatments (Kuck et al., 2000) and electrical stimulation treatments (pacemaker (Hayes et al., 2000) and defibrillator (Kerber, 2000; DiMarco, 2003)) are developed and used for the intervention of these malignant arrhythmias. In addition, substrate modification is also achieved through radio-frequency ablation (Stevenson & Delacretaz, 2000) to eliminate critical sites in the heart that initiate the arrhythmias.

Understanding the electrical activity of the heart and its underlying mechanisms is of the great importance for both basic science research and clinical medicine. Cardiac electrophysiological mapping emerges as an important tool to aid in both the basic research of the arrhythmia mechanisms (Pogwizd et al., 1998) and the clinical treatments

(e.g., guiding catheter ablation (Zeppenfeld et al., 2007) or optimizing cardiac resynchronization therapy (Spragg et al., 2010)) of malignant arrhythmias. Importantly, advancements have been made to map and localize cardiac electrical activity from the endocardium using catheter technology, which results in two mapping systems that are currently used in the clinical setting (Taccardi et al., 1987; Gepstein et al., 1997; Schalij et al., 1998). Though successful, these catheter-based mapping techniques require invasive procedure to place the mapping catheter and also require fluoroscopic and/or magnetic guidance to accurately steer the mapping catheter in the heart. It is a complex procedure which takes considerable time and needs to keep patients in lengthened periods of cardiac arrhythmias. In some cases, because of the hemodynamic instability of the patient's arrhythmias, such catheter-based mapping procedure may be difficult to perform.

Therefore, noninvasive diagnosis and imaging of cardiac electrical activity of arrhythmia would be of enormous value for numerous patients by allowing cardiologists to focus the intervention at the source of the arrhythmia without the need for lengthy invasive cardiac mapping. Current routine noninvasive detection and interpretation of the cardiac electrical activity is widely performed using 12-lead electrocardiogram (ECG), which records the time-varying electrical potentials on the body surface generated by the cardiac electrical sources. However, from a fundamental point of view, it is highly desirable to non-invasively image and localize the cardiac electrical activity directly in the heart from the body surface ECGs. Many investigations have been made to develop such noninvasive cardiac electrical imaging techniques to image the epicardial potentials

(Barr et al., 1977; Franzone et al., 1978; Yamashita & Takahashi, 1984; Throne & Olson, 1994; Shahidi et al., 1994; Oster et al., 1997; Greensite & Huiskamp, 1998; MacLeod & Brooks, 1998), activation sequence on the heart surface (Cuppen & van Oosterom, 1984; Huiskamp & Greensite, 1997; Pullan et al., 2001; Tilg et al., 2002; Greensite, 2004), and the cardiac electrical activity throughout three-dimentional (3D) myocardium (He & Wu, 2001; Li & He, 2001; He et al., 2002, 2003; Ohyu et al., 2002; Skipa et al., 2002; Zhang et al., 2005; Liu et al., 2006a; Liu et al., 2006b; Nielsen et al., 2007; Liu et al., 2008; Han et al., 2008; Wang et al., 2011a; Han et al., 2011, 2012). By providing detailed and regional information of the electrical activity of the heart, such techniques are of great clinical value in diagnosis and intervention of those malignant arrhythmias.

1.2. Motivations and Significance

The present dissertation study aims to rigorously evaluate and validate a novel physical-model-based three-dimensional (3D) cardiac electrical imaging (3DCEI) technique. By combining the functional information obtained from multiple-channel body surface ECGs with the subject-specific anatomical information, the 3DCEI technique could provide detailed and localized information of the cardiac electrical activity for each individual. This 3DCEI technique has a unique feature of imaging and localizing the cardiac electrical activity throughout the 3D myocardium, which represents an important alternative to other heart surface-based imaging techniques. Furthermore, rigorously validation of 3DCEI through both well designed computational study and experimental

investigations during different electrophysiological conditions could quantify the performance of 3DCEI and thus represents an important step towards further translating this technique into clinical use.

Due to the fact that arrhythmias typically originate from the subendocardium (and, at times, from epicardium or even intramural sites (Pogwizd et al., 1998)), it is of enormous value for the physician to image cardiac electrical activity and precisely localize the origin of arrhythmias throughout the 3D myocardium. The 3DCEI is a novel approach that can image the cardiac activation sequence and localize the site of origin of activation throughout 3D myocardium. It could overcome the limitation of the invasive catheter-based mapping techniques that are currently used in the clinics and advance the current noninvasive cardiac electrical imaging techniques that are bounded to heart surface. Furthermore, a rigorous validation study during both normal and abnormal electrophysiological conditions could demonstrate the potential of 3DCEI for accurately localizing arrhythmia areas and characterizing the arrhythmia mechanisms inside the heart, thus providing the cardiologists a short cut. The rigorous validation of this noninvasive imaging approach may also provide an alternative for noninvasive imaging of cardiac activation, thus facilitating the clinical diagnosis of arrhythmias and the presurgical planning by substantially reducing risks and expenses associated with the invasive procedures that are currently employed in clinical settings.

1.3. Scope of the Dissertation

In chapter 2, a brief literature review is given on the electrical activity of the human heart, the ECG, and the background knowledge of noninvasive cardiac electrical imaging techniques. Important previous investigations pertinent to the present study are also described.

In chapter 3, the physical-model-based 3DCEI approach is described. Rigorous computer simulations are conducted to evaluate the performance of the 3DCEI approach for localization of origin of cardiac activation and estimation of cardiac activation sequence. Single-site pacing and dual-site pacing protocols in realistic geometry model are used in the computer simulation study.

In chapter 4, experimental investigation in the rabbit heart is conducted to validate the performance of the physical-model-based 3DCEI approach. The estimated initiation of cardiac activation and the cardiac activation sequence are compared with simultaneous measurements from invasive 3D intra-cardiac mapping through plunge-needle electrodes in rabbits in a closed-chest condition. Validation study is performed under different electrophysiological conditions including pacing and norepinephrine-induced ventricular arrhythmias, and reasonable and consistent results are obtained.

In chapter 5, we extend the experimental investigation of the 3DCEI approach in the canine heart, which provides closer approximation to the human heart in terms of cardiac size and electrophysiological characters. The noninvasive imaging results are again compared with the simultaneous measurements from 3D intra-cardiac mapping. The reasonable results demonstrate the feasibility of this novel 3DCEI approach in such large

animal model.

In chapter 6, we perform the experimental investigation of arrhythmia mechanisms by applying the 3DCEI approach. This experimental investigation can be categorized into 2 groups: investigating arrhythmia mechanisms during drug-induce QT prolongation in rabbit heart, and investigating arrhythmia mechanisms associated with nonischemic heart failure in a canine model. These studies further demonstrate clinical relevance of 3DCEI and define the potential clinical role of 3DCEI.

In chapter 7, the major contributions of the present dissertation research are summarized. Recommendations for future works are also discussed.

The cited literatures, copyright transfer approval and the vita of the author are listed at the end of this dissertation.

Chapter 2

Background

2.1. Cardiac Electrical Activity

The electrical activity of the heart provides the fundamental of the heart functions as a pump distributing blood to the lungs and peripheral organs (Widmaier et al., 2005). Within a single cardiac cycle, the normal intrinsic electrical conduction of the heart allows electrical impulse propagation to be transmitted from the sinoatrial (SA) node through both atria and then forward to the atrioventricular (AV) node. Normal physiology allows further propagation from the AV node to purkinje fibers, their respective bundle branches, and the ventricles. This time ordered electrical conduction system initiates a depolarization wavefront that spread throughout the myocardium tissue and thus causes efficient and coordinated contraction of the cardiac muscle tissue to provide selective blood perfusion through both the lungs and systemic circulation.

In general, the cardiac electrical activity of myocardium tissue is the result of electrochemical reactions of these excitable cells (Malmivuo & Plonsey, 1995). The depolarization occurs due to an inflow of sodium ions across the cell membranes. A repolarization phrase subsequently follows as a result of potassium ion outflow. The transient shift from a resting state to an excited state of cardiac cell defines the action potential, a time dependent voltage function, travels from excited, or depolarized, cells to neighboring resting cells via low resistance intercellular connectors.

2.2. Cardiac Arrhythmias and Electrophysiological Mapping

A group of conditions in which the electrical activity of the heart is irregular or is faster or slower than normal, called cardiac arrhythmias, constitutes a major cause of death and disability among the world's population. Among these ventricular arrhythmias, ventricular tachycardia (VT) is a kind of regular and repetitive fast heart rhythm which originates in the ventricles of the heart. VT can occur in patients with either structurally normal (e.g., idiopathic VT) or abnormal (e.g., congestive heart failure) hearts, and may degenerate into ventricular fibrillation (VF), an irregular fast heart rhythm that could even lead to sudden cardiac death, and thus is considered as a life-threatening arrhythmia. In the past decades, pharmacological treatment of these arrhythmias has been developed and used; however it has been shown that pharmacological treatment is difficult considering the significant proarrhythmic effects of many antiarrhythmic agents (DiMarco, 2003). Recently, electrical stimulation technologies, including implantable and wearable defibrillators (Kerber, 2000; DiMarco, 2003), cardiac pacemakers (Hayes et al., 2000), and cardiac resynchronization therapy (Abraham et al., 2002) have been developed for the treatment of these maglignant arrhythmias and their arrhythmogenic substrates. In addition, substrate modification has been achieved with radio-frequency ablation delivered at the tip of a steerable catheter inserted into the heart through a blood vessel (Wood & Morady, 1999; Stevenson & Delacretaz, 2000). In order to eliminate critical sites in the heart that initiate the arrhythmias, such cardiac ablation techniques

require precise localization of the arrhythmia substrates arrhythmias.

Cardiac electrophysiological mapping emerges as an important tool to aid in diagnosis (e.g., characterizing the electrophysiological substrates and mechanisms of VT (Pogwizd et al., 1998)) and clinical treatments (e.g., guiding catheter ablation (Zeppenfeld et al., 2007) or implantation of cardiac resynchronization therapy (Spragg et al., 2010)) of ventricular arrhythmias. In the past decade, important advancements have been made to map and localize cardiac electrical activity from the endocardium using catheter technology. There are two mapping systems that are currently used in the clinical setting. One is the CARTO electroanatomical mapping system. This is a non-fluorescent electroanatomic catheter mapping technique developed using electromagnetic guidance of the catheter positioning (Gepstein et al., 1997; Schalij et al., 1998). Based on this technique, the investigators are able to record endocardial monophasic action potentials (Li et al., 2003), to describe the endocardial electrophysiological substrate for VT (Hsia et al., 2003), and to characterize endocardial ventricular activation as a guide for catheter ablation in patients with arrythmogenic right ventricular dysplasia (Reithmann et al., 2003). Another one is the Ensite system, which uses a cavitary noncontact multielectrode catheter-probe (that can record beat-to-beat electrical potentials in the blood-filled cavity (Taccardi et al., 1987)) to explore the inverse reconstruction of endocardial potentials from the potential measurements made on the catheter probe (Khoury et al., 1998; Liu et al., 1998; Gornick et al., 1999; Kadish et al., 1999; Jia et al., 2000). Though successful, these catheter-based mapping techniques require invasive procedure to place the mapping catheter and also require fluoroscopic and/or magnetic guidance to accurately steer the

mapping catheter in the heart. It is a complex procedure which takes considerable time and needs to keep patients in lengthened periods of cardiac arrhythmias. In some cases, because of the hemodynamic instability of the patient's arrhythmias, such catheter-based mapping procedure is difficult to perform.

2.3. Electrocardiography and Body Surface Potential Mapping

The thoracic detection of the electrical activity of the heart over a period of time, as recorded by electrodes attached to the outer surface of the skin is the electrocardiogram (ECG). Current clinically routine noninvasive detection of the cardiac electrical activity is widely performed using 12-lead ECG system. The 12-lead ECG system includes three bipolar limb leads (lead I to lead III) (Einthoven, 1906), six unipolar precordial leads (lead V1 to V6) (Wilson et al., 1934) with reference to the Wilson's Central Terminal (WCT) (Wilson et al., 1944), and three segmented unipolar leads (aVR, aVL, and aVF) (Goldberger, 1942). Important diagnosis information could be obtained from the interpretation of the waveform of ECG signals.

Investigations have also been made in developing body surface potential maps (BSPMs) techniques, which record a number of ECGs from the multiple sites of the torso to depict the instant spatial distribution of these ECG signals over the surface of the torso (Taccardi, 1963). In the past 40 years, BSPMs and its variant have been shown by many experimental and clinical studies to have higher diagnostic power and be more informative than did the 12-lead ECG (Abildskov et al., 1976; Mehra et al., 1983; Mirvis, 1988; He & Cohen, 1992; Flowers & Horan, 1995; Akahoshi et al., 1997). However,

BSPMs have disadvantages in that they cannot provide a detailed electrical source distribution within the heart, considering the "smearing" effects of heart-torso volume conductor model, which attenuate, distort, and smooth the electrical signals over the body surface (Mirvis et al., 1977; Okamoto et al., 1983; Gulrajani et al., 1984). As a consequence, many important electrophysiological events do not produce distinguishable effects on the body surface, although they can be observed on the cardiac surface or within myocardium.

2.2. Cardiac Electrical Imaging

2.2.1. ECG Forward Problem

Noninvasive cardiac electrical imaging overcomes the limitation of 12-lead ECG and BSPM by imaging and localizing the electrical activity directly in the heart. The cardiac electrical imaging techniques include ECG forward problem and ECG inverse problem (See Fig.1). The ECG forward problem provides the precondition for such noninvasive cardiac electrical imaging techniques through mathematically modeling the electrical field between heart and torso. The ECG forward problem entails the calculation of densely sampled body surface potentials, starting from the assumed equivalent cardiac sources models (e.g., equivalent current density, transmembrane potential, or epicardial/pericardial potentials) to represent the cardiac electrical activity. Usually, the sources are immersed in a heart-torso volume conductor whose electrical properties and geometry are known.

In general, the electrical field of the heart-torso volume conductor (Malmivuo & Plonsey, 1995) can be governed by the partial differential equations (Poisson's equation or Laplace's equation depending on the assumption of the equivalent source models). In forward problem, such partial differential equations could be discretized into a set of linear equations. Several very important assumptions are hidden behind the forward problem (Nash & Pullan, 2005). First, the quasistatic approximation is applied in the field, which means at each time instant the body surface potential distribution is solely determined by the simultaneous electrical status of the heart sources. Therefore the forward problem can be thought of as a series of timely independent problems. Second, in

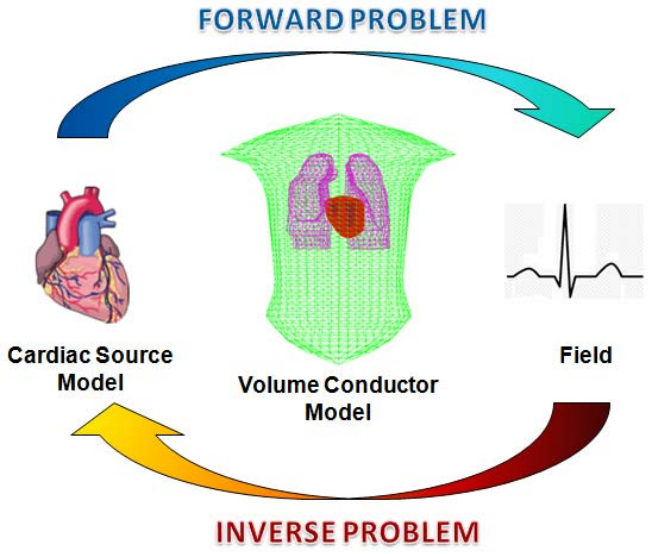

Fig. 1, ECG forward problem and ECG inverse problem in cardiac electrical imaging.

most cases, the transfer matrix is assumed to be constant over the time interval during the calculation, ignoring the cardiac motion. Conventional imaging modalities like computed

tomography (CT) or magnetic resonance imaging (MRI) are usually used to obtain the heart torso geometry. The forward problem has a unique solution; it is always possible to calculate the electrical field with certain accuracy, given the details of the source and volume conductor (Malmivuo & Plonsey, 1995).

The computational approaches to the forward problem have been detailed in the review papers by Gulrajani (Gulrajani, 1998a, 1998b, 2004). In general, they can be mainly categorized into 2 groups: the surface method and the volume method. The surface method is also termed the boundary element methods (BEM) (Gelernter & Swihart, 1964; Barr et al., 1966; Barr et al., 1977), in which only the interfaces between different torso regions/organs are taken into consideration and are digitized and represented in the numerical torso model. The different regions/organs are assumed to have isotropic conductivity, and the conductivities may vary between different regions. In the volume method, the entire three-dimentional (3D) space is represented numerically be a combination of tetrahedral and hexahedral (Gulrajani, 2005), and it is the only way to incorporate the varying conductivity of individual regions. Usually the volume methods include finite element method (Yamashita & Takahashi, 1984; Franzone et al., 1985; Pilkington et al., 1985), finite difference method (Walker & Kilpatrick, 1987), and the finite volume method (Abboud et al., 1994, Rosenfeld et al., 1996). Compared with BEM, the volume methods usually are computationally more demanding. Therefore, there are a few studies in combining both the surface method and the volume method, to take the advantage of any computational savings afforded by the surface method, while at the same time also allow the handling of anisotropies (Pullan, 1996; Fischer et al., 2000).

2.2.2. ECG Inverse Problem

The ECG inverse problem is to reconstruct the source distribution over specified volume conductor from body surface potentials through certain mathematical manipulation (He & Liu, 2010). Obviously, it is the ECG inverse problem that has clinical importance in medical application of bioelectric phenomena (Malmivuo & Plonsey, 1995). However, the ECG inverse problem does not possess a mathematically unique solution, and there are infinite equivalent cardiac sources which may contribute to the same body surface potential distribution.

In the past decades, many investigations have been made to overcome the difficulty of non-uniqueness of ECG inverse problem by using different formulations of equivalent cardiac electrical generators. In one of these formulations, cardiac electrical activity has been modeled using a few moving current dipoles (Mirvis et al., 1977; Gulrajani et al., 1984; Armoundas et al., 2003; Lai et al., 2010). Due to the distributed nature of cardiac electrical activity, considerable experimental evidence indicates that distributed source models are more needed in order to model the distributed cardiac electrical activity. Therefore, another formulation, called epicardial potential imaging, which aims at reconstructing epicardial potential from BSPMs, has been investigated by several groups (Barr et al., 1977; Franzone et al., 1978; Oster et al. 1997, Yamashita & Takahashi, 1984; Shahidi et al., 1994; Throne & Olson, 1994; Greensite & Huiskamp, 1998; MacLeod & Brooks, 1998). This approach makes no assumption about the nature of the electrical sources in the heart and builds a transfer matrix between epicardial and body surface potentials. This method has been previously investigated both via animal experiments and

in human subjects, under normal or abnormal cardiac electrophysiological conditions (Barr & Spach, 1978; MacLeod et al., 1995; Oster et al., 1997; Burnes et al., 2000; Ramanathan et al., 2004; Wang et al., 2011b). An alternative approach called heart surface activation imaging has been developed by several groups (Cuppen & van Oosterom, 1984; Huiskamp & Greensite, 1997; Pullan et al., 2001; Modre et al., 2002; Tilg et al., 2002; Greensite, 2004). In this kind of approach, the cardiac electrical source is modeled by an equivalent uniform dipole layer, lining the excited portions of the both epicardial and endocardial surfaces. Based on this model, the investigators were able to obtain an isochrone map over both epicardial and endocardial surfaces in human subjects (Berger et al., 2006; van Dam et al., 2009; Berger et al., 2011).

Another difficulty of solving ECG inverse problem lies in that the problem is mathematically ill-posed, so that small errors in the heart-torso geometry and in the measured body surface potentials result in severe instability of the solution. The techniques of regularization must therefore be used to suppress the effects of inevitable errors due to imposing constrains on the inverse solution. Many regularization techniques have been proposed to seek a reliable and physiologically meaningful solution (Tikhonov et al., 1977; Hansen & O'Leary, 1993; Johnston & Gulrajani, 1997; Brooks et al., 1999; Greensite, 2004).

It is important to image the cardiac electrical activity throughout the 3D myocardium, which may provide direct information for both basic cardiovascular research and clinical diagnosis and management of cardiac diseases. Much effort has been put in the past decades to extend the ECG inverse problem to achieve this goal (He

& Wu, 2001; Li & He, 2001; He et al., 2002, 2003; Ohyu et al., 2002; Skipa et al., 2002; Zhang et al., 2005; Liu et al., 2006a; Liu et al., 2006b; Nielsen et al., 2007; Liu et al., 2008; Han et al., 2008; Wang et al., 2011a; Han et al., 2011, 2012). Among these studies, a heart-model-based approach has been proposed to estimate the 3D cardiac electrical activity from BSPMs with the aid of a heart-excitation model and a nonlinear optimization algorithm (Li & He, 2001; He et al., 2002, 2003). Both the computer simulation study (Li & He, 2001; He et al., 2002) and the animal experiment (Zhang et al., 2005, Liu et al., 2006a; Liu et al., 2008) showed high consistence between the estimated activation sequence and "true" simulated activation sequence or the experimentally measured activation sequence. Furthermore, potential distributions are estimated throughout the 3D ventricles from BSPMs by this heart-model-based approach (He et al., 2003; Liu et al., 2012a). Most recently, a physical-model-based 3D cardiac electrical imaging approach (Liu et al., 2006b) has been proposed to mathematically model the cardiac electrical activity using equivalent current density (ECD) distribution (He & Wu, 2001), and therefore the 3D cardiac activation sequence could be extracted from the inverse solution of ECD distribution. This novel 3DCEI approach only uses the general biophysical relationships governing the cardiac electrical activity, and has a notable feature of minimal dependence on the physiological knowledge of cardiac electrical properties. Therefore, this physical-model-based 3DCEI approach is applicable to various cardiac electrophysiology conditions (Han et al., 2008; Han et al., 2011, 2012).

2.3. Intracavitary Potential-based Inverse Solution

In addition to body surface ECG-based inverse solutions, important advancements have been made to image and localize cardiac electrical activity from the potentials recorded within the blood cavities using catheter technology. In one of the formations, a cavitary noncontact multielectrode catheter-probe is used to record the beat-to-beat electrical potentials in the blood-filled cavity, which is used for the inverse reconstruction of the electrical potentials on the endocardial surface (Taccardi et al., 1987). This technique has been previously validated in both animal experiments and clinical research by several groups (Khoury et al., 1998; Liu et al., 1998; Gornick et al., 1999; Kadish et al., 1999; Jia et al., 2000; Ciaccio et al., 2004). There is one commercially available system (Ensite system) that is developed based on this technique. It is noted that while this endocardial approach shows promise of offering a minimally invasive means of localizing and mapping cardiac electrical activity over the endocardial surface, the approach is limited in where activation arises from the myocardial regions far from the endocardial surface. Therefore most recently, investigations have been made to extend the inverse solution from endocardium into 3D myocardium (He et al., 2007), and both the computer simulation (He et al., 2007) and animal experiments (Liu et al., 2012b) show the feasibility of this novel method. However, this novel method still requires the placement of the catheter with sophisticated clinical manipulations, and it may cause clinical complications to those hemodynamically unstable patients.

Chapter 3

Three-dimensional Cardiac Electrical Imaging

2.1. Biophysical Principles and Equivalent Source Model

The physical-model-based three-dimensional (3D) cardiac electrical imaging (3DCEI) approach is developed by mathematically modeling the cardiac electrical activity using equivalent source model, and the cardiac excitation information could thus be extracted based on fundamental biophysical principles (Liu et al., 2006b; Han et al., 2008). Most materials in this chapter have been previously published (Han et al., 2008).

During cardiac excitation, the activation time of each myocardial cell is the latency at which the trans-membrane potential (TMP) rises almost instantaneously from the resting potential of -90 mV to a plateau potential typically around 0 mV for a normal or an abnormal cell. Regardless of the regional difference of the action potential amplitude, the activation time is classically characterized by the maximum temporal derivative of the TMP waveform. Other than the temporal method for determining the activation time, the spatial method provides an alternative and equally effective feature for deriving the activation time (Punske et al., 2003). Cardiac excitation propagates as a moving wavefront separating the depolarized and non-depolarized myocardium. For a given myocardial cell, the activation time can be thought of as the latency at which the excitation wavefront passes through the cell. Since a considerable difference of the TMP amplitude only exists across the excitation wavefront, a cell at its activation time is also

characterized by the maximum TMP spatial gradient (Han et al., 2008). This concept is mathematically expressed as Eq. (3.1).

$$\tau(\mathbf{r}) = \arg\max_{t} \left| \nabla \phi_m(\mathbf{r}, t) \right| \tag{3.1}$$

where $\phi_m(\mathbf{r}, t)$ is the TMP at location $\mathbf{r}$ and time t.

Note that Eq. (3.1) also points to the biophysical principle of a well established intra-cardiac mapping technique based on intramural bipolar recordings (Han et al., 2008). The electrical potential difference between two closely spaced electrodes (i.e. the bipolar potential) is approximately a directional component (along the intramural needle) of the TMP spatial gradient. Therefore, the time instant with the peak value of the absolute bipolar potential precisely corresponds to the activation time with the maximum TMP spatial gradient, as defined in Eq. (3.1).

For any myocardial location $\mathbf{r}$ and any time t, we define the equivalent current density (ECD) $\vec{\mathbf{j}}_{eq}(\mathbf{r}, t)$ to be proportional to the local TMP spatial gradient, as expressed by Eq. (3.2)

$$\vec{\mathbf{j}}_{eq}(\mathbf{r}, t) = -\mathbf{G}_i(\mathbf{r}) \nabla \phi_m(\mathbf{r}, t) \tag{3.2}$$

where $\mathbf{G}_i(\mathbf{r})$ is the intracellular effective conductivity tensor.

By definition, we have Eq. (3.3) as a consequence of Eq. (3.1) and Eq. (3.2).

$$\tau(\mathbf{r}) = \arg\max_{t} \left| \vec{\mathbf{j}}_{eq}(\mathbf{r}, t) \right| \tag{3.3}$$

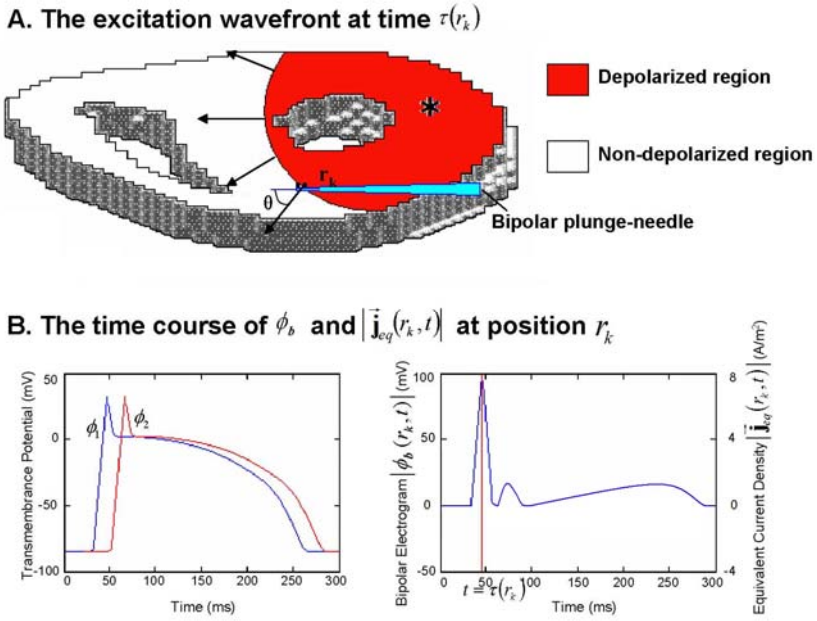

Fig. 2, (A) An axial slice of the ventricles, in which the cardiac cells are undergoing depolarization. The red region behind the excitation wavefront represents the depolarized muscle cells, while the local equivalent current density field over each point along this wavefront, indicated by black arrow, represents propagation direction of the wavefront at these points. A transmural needle is inserted in the ventricular myocardium. (B) The time course of the transmembrance potentials (left panel) and the time course of the magnitude of local equivalent current density. (From Ref. (Han et al., 2008) with permission © IEEE 2008)

Therefore, the activation time is also characterized by the maximum magnitude of the ECD (Liu et al., 2006b). The relationship among the activation time, the TMP and its spatial gradient, the ECD and the intramural bipolar potential is illustrated in Fig.2. The electrode 1 and electrode 2 record the potentials ϕ_1 and ϕ_2, and the recorded time course bipolar electrogram at point r_k is given as $|\phi_b(r_k,t)| = |\phi_1 - \phi_2|$. At the instant $t = \tau(r_k)$, the cardiac cell at point r_k is undergoing depolarization, which is represented by ECD $\vec{\mathbf{j}}_{eq}(r_k,t)$. The angle between the direction of the transmural needle and the direction of

ECD $\vec{\mathbf{j}}_{eq}(r_k,t)$ is θ. The relationship between the magnitude of local ECD and recorded bipolar electrogram can be mathematically described as

$$\left|\vec{\mathbf{j}}_{eq}(r_k,t)\right| = \frac{g(r_k)\left|\phi_b(r_k,t)\right|}{d\cos\theta} \tag{3.4}$$

where d is the distance between electrode 1 and electrode 2, and $g(r_k)$ is the conductivity at position r_k (Han et al., 2008).

3.2. Imaging Principles

3.2.1. Forward Problem

Based on the bidomain theory (Miller & Geselowitz, 1978; Tung, 1978), the 3D distributed ECD can be regarded as the electrical "source" model accounting for the extracellular potential "field", as shown in the following governing equation.

$$\nabla\cdot\left[\left(\mathbf{G}_i(\mathbf{r})+\mathbf{G}_e(\mathbf{r})\right)\nabla\phi_e(\mathbf{r},t)\right] = \nabla\cdot\vec{\mathbf{j}}_{eq}(\mathbf{r},t) \tag{3.5}$$

where $\mathbf{G}_i(\mathbf{r})$ and $\mathbf{G}_e(\mathbf{r})$ are the intracellular and extracellular effective conductivity tensors respectively, and $\phi_e(\mathbf{r},t)$ is the extracellular potential.

In 3DCEI, the distributed ECD model is used to represent the 3D cardiac electrical activity (Han et al., 2008). Given a tessellated geometrical heart-torso model and the prior knowledge of the electrical conductivity of relevant tissues and organs, the extracellular potentials measurable over the body surface is linearly related to the 3D ECD distribution. Boundary element method (BEM) is applied to discretize the above equation, and this

linear relationship can be expressed using a matrix-vector notation in Eq. (3.6)

$$\mathbf{\Phi}(t) = \mathbf{L}\mathbf{J}(t) \tag{3.6}$$

where $\mathbf{\Phi}(t)$ is the vector of body surface potential distribution at M electrode positions and $\mathbf{J}(t)$ is the vector of 3D ECD distribution at N know myocardial sites at instant t. $\mathbf{L}$ is the $M \times 3N$ source-to-sensor transfer matrix.

3.2.2. Inverse Problem

The concept of the ECD as well as its "source" interpretation according to the bidomain theory allows to relate the imaging contrast (i.e. activation time) to the measurement (i.e. body surface potentials) through well defined equations from Eq. (3.3) through Eq. (3.6). The linear inverse problem of Eq. (3.6) is solved instant by instant to estimate the spatiotemporal ECD distribution from the body surface potentials and then derive the activation time from the estimated ECD time course for each individual myocardial location (Han et al., 2008).

The inverse problem is solved using the generalized (Tikhonov et al., 1977) Tikhonov regularization method, which aims to search for the solution estimate that minimizes

$$\left\|\mathbf{\Phi}(t) - \mathbf{L}\mathbf{J}(t)\right\|_2^2 + \lambda\left\|\mathbf{W}\mathbf{J}(t)\right\|_2^2 \tag{3.7}$$

where $\mathbf{W}$ is a $3N \times 3N$ regularization matrix, and λ is the regularization parameter. The regularization matrix is chosen based on the lead-field normalized weighted minimum norm (LFN-WMN) estimation (Wang et al., 1992; Pascual-Marqui, 1995). In addition, a spatiotemporal regularization technique is applied to deal with the

noise perturbation (Greensite & Huiskamp, 1998). Briefly, the singular value decomposition (SVD) is employed to decompose the spatiotemporal ECG data matrix into orthogonal spatial and temporal components. The spatial components that do not satisfy the discrete Picard condition (Hansen, 1990) are assumed to be dominated by noise perturbation, and thereby are truncated. The LFN-WMN estimation is applied to each remaining spatial component and the regularization parameter λ can be determined by the "L-curve" method (Hansen & O'Leary, 1993) instant by instant. The LFN-WMN solutions multiplied with the corresponding singular values and temporal components are summed to obtain the spatiotemporal ECD estimates. The activation time at each myocardial site is then determined from the time course of the estimated local ECD, by finding the maximum ECD estimate according to Eq. (3.3) (Liu et al., 2006b).

3.2. Computer Simulation Study

In order to evaluate the performance of the 3DCEI technique comprehensively, compare the results obtained by different inverse algorithms, and help data interpretation of the *in vivo* experimental validation, computer simulations was conducted on a realistic rabbit geometry and piece-wise homogeneous heart-torso model (Han et al., 2008). The heart-torso model was built from computed tomography (CT) images of a rabbit, and it included myocardial tissue, intra-ventricular blood masses, lungs, and the rabbit torso. The conductivities were set to be 0.2, 0.67, 0.05, and 0.21 S/m, respectively. The whole 3D ventricular myocardial volume was discretized into 7625 grid points evenly spaced by

1 mm. There were 53 body surface electrode locations uniformly covering the anterior-lateral chest of the rabbit body surface, which fit the realistic geometry size of the rabbit torso, and simulated the *in vivo* experimental setting.

A cellular automaton heart model (Li & He, 2001; He et al., 2002, 2003) was employed to simulate the ventricular electrical activity using single-site pacing and dual-site pacing protocols. In the single-site pacing, nine representative pacing sites were selected throughout the 3D myocardium of ventricles, which include basal left wall (BLW), basal right wall (BRW), basal anterior (BA), basal posterior (BP), middle left wall (MLW), middle right wall (MRW), middle anterior (MA), middle posterior (MP),

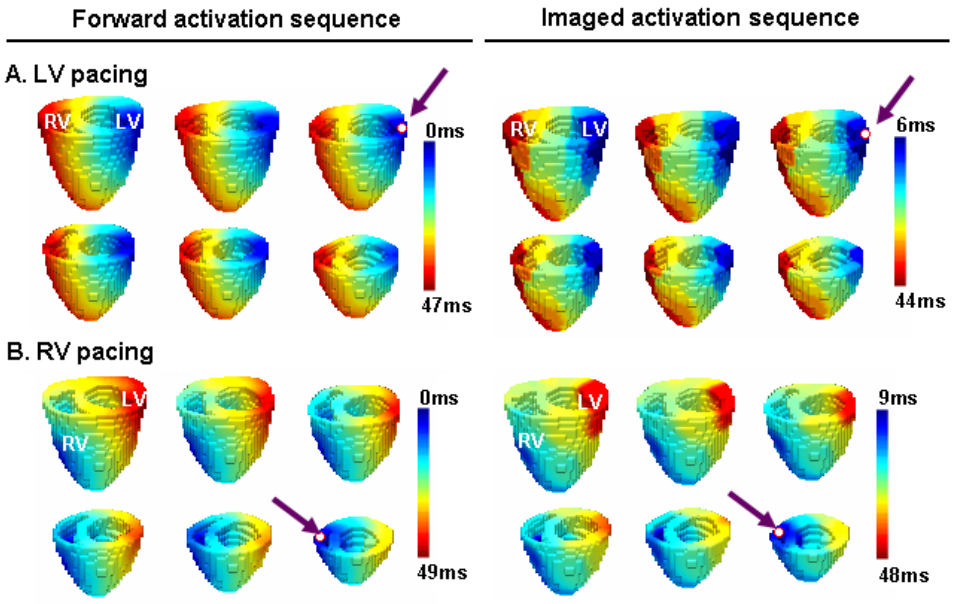

Fig. 3, Comparison between the forward simulation activation sequence and imaged activation sequence during the single-site pacing simulation in computer simulation study. (A) Activation was paced at basal lateral wall of the left ventricle (LV). (B) Activation was paced at middle lateral wall of right ventricle (RV). (From Ref. (Han et al., 2008) with permission © IEEE 2008)

and apex. A dual-site pacing protocol was used to simulate more complex excitation than that of the single-site pacing. Eight pairs of pacing sites were selected throughout the 3D myocardium of ventricles, which include basal right wall (BRW), basal posterior (BP), middle left wall (MLW), middle right wall (MRW), middle anterior (MA), and middle posterior (MP). With the setting that maximum peak-peak value is 3 mV determined from actual ECG data, Gaussian white noise (GWN) of 20 μV was added to the BSPMs generated by the BEM-based forward computation (Han et al., 2008).

In order to study the performance of 3DCEI under different noise levels and electrode numbers, GWN of various noise levels (0, 5, 10, 20, 40, and 60 μV) and different electrode numbers (197, 160, 120, 80, and 40 electrodes) were considered during the simulation study under single-site pacing.

Relative error (RE) was calculated to evaluate the dissimilarity between the imaged activation sequence and simulated "true" activation sequence. Localization error (LE) was calculated to measure the capability of localizing the origin of excitation during single-site pacing. RE is defined as

$$RE = \sqrt{\frac{\sum_{i=1}^{n}\left(AT_i^E - AT_i^T\right)^2}{\sum_{i=1}^{n}\left(AT_i^T\right)^2}} \tag{3.8}$$

where n is the number of grid points of the heart model, and AT_i^E and AT_i^T are the estimated activation time and simulated "true" activation time at the i-th myocardial grid point, respectively. The LE is defined as the distance between the simulated "true" pacing

site with earliest activation and the center of mass of the myocardial region with the earliest imaged activation time.

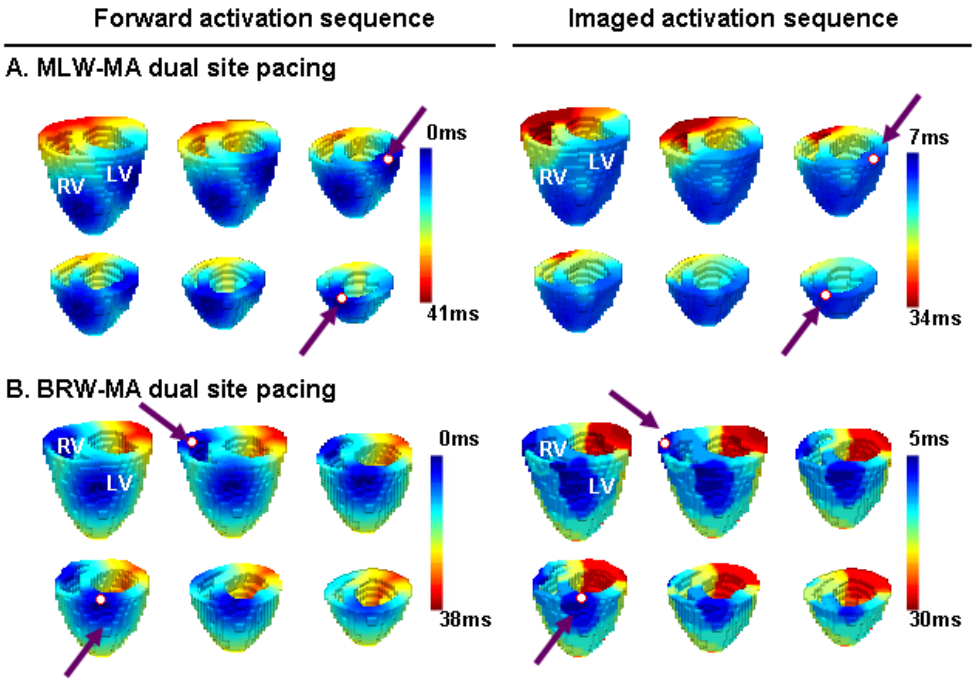

Fig. 4, Comparison between the forward simulation activation sequence and imaged activation sequence during the dual-site pacing simulation in computer simulation study. (A) Activation was simultaneously paced at middle left wall (MLW) and middle anterior (MA) of ventricles. (B) Activation was simultaneously paced at basal right wall (BRW) and middle anterior (MA) of ventricles. (From Ref. (Han et al., 2008) with permission © IEEE 2008)

3.2.1. Preliminary Results

Fig.3 shows examples of comparison between the imaged activation sequence and simulated "true" activation sequence during computer simulation under 20 μV GWN and 53 electrodes in a single-site pacing protocol. As shown in Fig.3.A, the imaged pattern coincided well with the simulated activation sequence, with RE = 0.16. The left ventricle

pacing site was localized with LE = 3.86 mm. Similar imaging performance was observed when the activation was induced by pacing at the middle lateral wall of the right ventricle, as shown in Fig.4.B, with RE = 0.19 and LE = 4.69 mm. Fig.4 shows examples of simultaneous dual-site pacing under 20 μV GWN and 53 electrodes. As shown in Fig.4.A, the imaged activation sequence is consistent with the simulated activation sequence, which is simultaneously paced at MLW and MA. The quantitative comparison gives an RE = 0.17 which shows that our 3DCEI can reconstruct the activation sequence throughout the ventricles for dual-site pacing at two separate locations Fig.4.B shows another example of simultaneous dual-site pacing at BRW and MA, with RE = 0.21. Quantitative comparison between imaged activation sequence and simulated "true" activation sequence under both single-site pacing and dual-site pacing with respect to the different location of the origin of the ventricular excitation are summarized in Table 1 and Table 2. On average, RE was 0.20±0.07 and LE was 4.56±1.12 mm for single-site pacing. For dual-site pacing, averaged RE was 0.25±0.06. However, it is also observed in simulation results that the imaged activation sequence is initialized later and ended earlier than the "true" activation sequence, and therefore, the total activation time (TAT) is smaller than the imaged activation sequence.

To evaluate the performance of 3DCEI under various disturbances, simulation work was also done under different noise level and different numbers of body surface electrodes via single-site pacing protocol. Fig.5 shows the dissimilarity of simulated "true" activation sequence and imaged activation sequence, quantified as RE, under various noise levels and numbers of electrodes. Fig.6 shows the error for localizing the

origin of activation. These results show that the performance of 3DCEI decreases during the increase of noise level and the decrease of electrode number. However, even under high noise level (e.g. 60 μV GWN) and low electrode number (40 electrodes), reasonable result was still obtained as RE of 0.25 and LE of 5.3 mm. Such results show the robustness of 3DCEI against measurement noise and effects of the electrode number.

3.2.2. Discussion

Computer simulation aims to assess the capability, accuracy, and limitation of 3DCEI under a realistic and well-controlled environment, and thus provides us the reference for understanding the *in vivo* experimental data. In the present preliminary study, we have evaluated the performance of the 3DCEI approach in a simulated rabbit

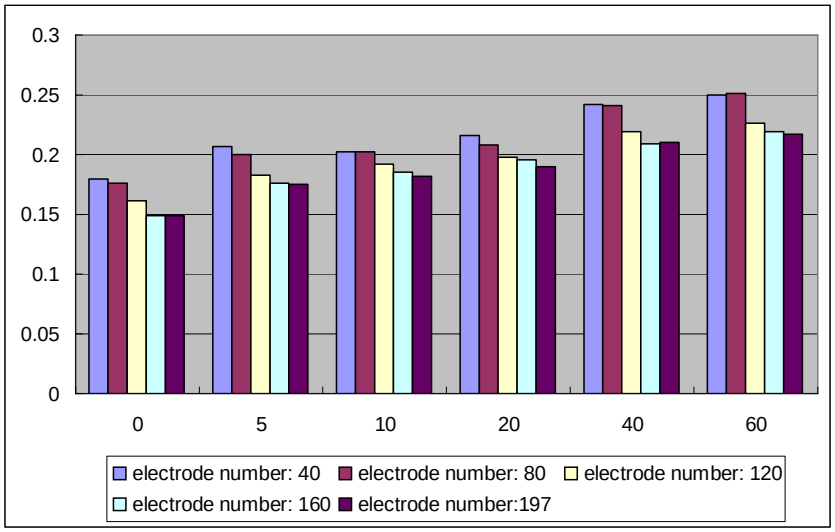

Fig. 5, Relative error under single-site pacing with varying electrode numbers and noise levels in computer simulation study.

model. A realistic geometry rabbit heart-torso volume conductor model was built from the CT images of a rabbit, and computer simulations were conducted to image the activation sequence under pacing protocol (Han et al., 2008). Under a 20 μV noise level and 53 body surface electrodes, the averaged RE and LE (over 9 pacing sites) were 0.20 and 4.56 mm for single-site pacing, and the average RE was 0.25 (over 8 pairs of dual-site) for dual-site pacing. Meanwhile, even under a high noise level (60 μV) and low electrode number, reasonable results were still obtained, which suggest the robustness of this approach against additive noise and effects of electrode number.

However, the need to solve a highly ill-posed linear inverse problem in order to estimate the ECD from body surface measurements poses a great challenge to 3DCEI (Han et al., 2008). Solving such an inverse problem is essentially a task of seeking a

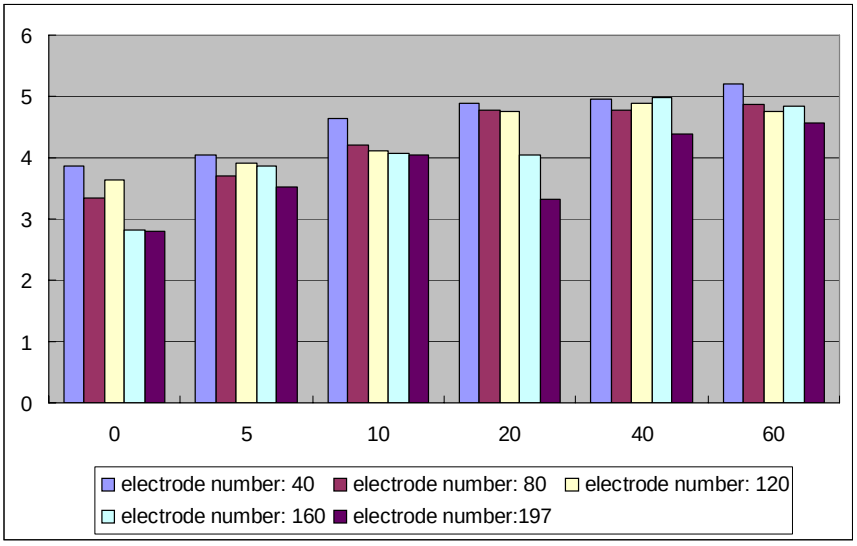

Fig. 6, Localization error under single-site pacing with varying electrode numbers and noise levels in computer simulation study.

spatial filter (or inverse operator) that projects the recorded data in the sensor space to the solution in the source space. It is often experienced in the ECG (as well as EEG/MEG) inverse problem that applying such a spatial filter cannot lead to a source reconstruction in perfect agreement with the true source distribution (Grave de Peralta-Menendez & Gonzalez-Andino, 1998). Instead, the source estimates may appear as a spatially blurred image, from which one may still resolve the true sources if they are distributed in a discrete or focal manner (He & Wu, 2001). But when the current sources are continuously distributed over a wavefront during the paced ventricular activation, the imaged ECD distribution at any specific time point is highly distinct from being a transmural surface as one may expect for the instantaneous excitation wavefront, and it is difficult to accurately reconstruct the instantaneous ECD distribution.

In 3DCEI, the activation time is determined exclusively from the time course of local

Table 1, Simulation results of imaging the 3D ventricular activation sequence induced by single-site pacing.

Pacing Site	RE	LE (mm)
BLW	0.16	3.86
BRW	0.20	4.32
BA	0.19	3.61
BP	0.32	6.40
MLW	0.18	3.61
MRW	0.19	4.69
MA	0.14	3.61
MP	0.31	6.40
Apex	0.15	4.58
Mean	0.20±0.07	4.56±1.12

Note: RE, relative error; LE, localization error; BLW, basal left wall; BRW, basal right wall; BA, basal anterior; BP, basal posterior; MLW, middle left wall; MRW, middle right wall; MA, middle anterior; MP, middle posterior. (From Ref. (Han et al., 2008) with permission © IEEE 2008)

ECD estimates. Surprisingly, we found that the ill-posed nature caused much less distortion to the normalized temporal waveform of ECD estimates than it did to the instantaneous ECD spatial distribution (Han et al., 2008). At a noisy condition, the ECD spatial distribution was found to be hardly interpretable, whereas the estimated ECD waveform at each individual myocardial site still demonstrated a clear peak instant that was determined as the activation time. Regarding this finding, our speculated explanation is twofold (Han et al., 2008). First, the activation time is a magnitude-independent temporal feature of local ECD estimates; therefore it is less sensitive to the spatial distortion of the inverse solution. It is true that the torso volume conductor behaves as a spatial filter and the estimation of the equivalent current density is essentially the de-convolution of this spatial filter. However, even though both forward and inverse procedures operate upon the spatial domain, the bias and blurring of the inverse solution

Table 2, Simulation results of imaging the 3D ventricular activation sequence induced by dual-site pacing

Pacing Site 1	Pacing Site 2	RE
BP	BLW	0.38
MRW	MLW	0.26
BP	MLW	0.28
BRW	MA	0.21
BP	MLW	0.24
MLW	MLW	0.23
MLW	MA	0.17
MP	MLW	0.25
Mean		0.25±0.06

Note: RE, relative error; BP, basal posterior; BLW, basal left wall; MRW, middle right wall; MLW, middle left wall; BRW, basal right wall; MA, middle anterior; MP, middle posterior. (From Ref. (Han et al., 2008) with permission © IEEE 2008)

in space also necessarily affects the time course of the source estimate. This effect may be well accounted for by a low-pass filter. Importantly, this effect does not significantly bias the peak instant which marks the activation time, since the "peak instant" of the source time course is a "low-frequency" feature. But this effect may cause the ambiguity and potential bias of other competitive methods based on determining the activation time from the maximum positive or minimum negative derivative, which is a "high-frequency" feature, of the estimated TMPs, or the estimated epicardial or endocardial potentials. In this sense, it represents another technical merit and robustness of 3DCEI. Second, the cardiac excitation process is typically continuous and smooth in nature and so is the point spread (or cross-talk) function of the 3D ECG inverse solution. In other words, the source estimates at any specific location are primarily affected by the source activities at neighboring sites with similar activation times.

The ill-posed problem of the ECD estimation is still the primary source of the activation imaging bias of 3DCEI (Liu et al., 2006b; Han et al., 2008). Because of the spatial blurring and bias of the inverse solution, the estimated ECD time course was also smooth over time, as compared with the theoretical delta function at the same site. This distinction accounted for the reduced specificity of activation time estimation. As a consequence, different myocardial locations within an extended region, particularly those that are activated around the middle of the QRS interval, often had the identical activation time, although they were actually activated progressively. In addition, it also caused the total activation time (TAT) obtained from the imaged activation sequence to be shorter than the TAT determined from the intra-cardiac data (Han et al., 2008).

In summary, the computer simulation work provides a comprehensive evaluation of the performance of the 3DCEI. The present results show that 3DCEI is in general capable of localizing the origin of activation and reconstructing the overall activation pattern under single-site pacing and dual-site pacing. However, we have also observed that the present 3DCEI algorithm has limitation in relatively lower spatial resolution when comparing with the simulated "true" activation sequence, which is reflected in shorter TAT and smoother time course of estimated current density.

Chapter 4

Experimental Investigation in Normal Rabbit Heart

4.1. Introduction

Ventricular tachycardia (VT) is a malignant arrhythmia that may degenerate to ventricular fibrillation and cause sudden cardiac death. In treatment of this arrhythmia, catheter ablation procedures require extensive invasive electrophysiological mapping (Dong et al., 2006) to determine the arrhythmogenic substrate, and thus keep patients in the electrophysiology laboratory for prolonged periods. Noninvasive cardiac electrical imaging techniques offer the potential to help define the underlying electrophysiological mechanisms and facilitate therapeutic treatments of cardiac disorders on a beat-to-beat basis.

In the previous chapter, we presented a novel three-dimensional (3D) cardiac electrical imaging (3DCEI) approach to image ventricular activation sequence from the inversely reconstructed equivalent current densities (ECDs) and evaluated the performance of this approach through computer simulation (Han et al., 2008). In this chapter, we presented our experimental investigation to rigorously evaluate the imaging performance of this novel 3DCEI approach using a well-established 3D intra-cardiac mapping procedure (Pogwizd & Corr, 1987; Pogwizd, 1994, 1995; Chung et al., 1997; Pogwizd et al., 1998) during paced rhythms and during VT induced by norepinephrine (NE) in the rabbit heart (Han et al., 2011). The 3DCEI imaged results were quantitatively

compared with simultaneous intra-cardiac mapping results and imaging performance was assessed. This study advances our previous experimental work (Zhang et al., 2005; Han et al., 2008) in four important ways: 1) Single-site pacing from a large number of subendocardial or subepicardial sites in left ventricle (LV) and right ventricle (RV) simulates more realistic single cardiac sources originating from the subendocardium and subepicardium, while septal pacing simulates intramural cardiac activation originating from the interventricular septum; 2) Simultaneous dual-site pacing was induced to evaluate the capability of 3DCEI to image more complex cardiac excitation processes; 3) The realistic geometry heart-torso model was constructed from computed tomography (CT) scans after the mapping experiment to account for the potential geometrical errors related to the preceding open-chest surgery and plunge electrode placement; 4) 3DCEI was applied to imaging the activation sequence of clinically-relevant NE-induced VTs. Materials in this chapter have been previously published (Han et al., 2011).

4.2. Study Design

4.2.1. Simultaneous Body Surface Potential Mapping and 3D Intra-cardiac Mapping

Thirteen healthy New Zealand white rabbits of either sex (3.6 to 4.3 kg) were studied under a protocol approved by the Institutional Animal Care and Use Committees of the University of Minnesota and the University of Alabama at Birmingham (Han et al., 2011). The protocol has been modified from our previous animal experiments (Zhang et

al., 2005). Fig.7 shows the schematic diagram of the experimental protocol. For each rabbit, simultaneous body surface potential mapping and 3D intra-cardiac mapping of ventricular electrical activities were performed during the experiment. Rabbit was sedated with ketamine (35 mg/kg), intubated with a size 3 ET tude, and anesthetized using 2% isoflurance. Oxygen and mechanical ventilation were administered as needed. Heart rate, blood pressure, and lead electrocardiograms (ECGs) were monitored to ensure the stability of hemodynamic during whole mapping study. The torso and limbs of rabbit were shaved for placement of surface ECG electrodes. 57-64 repositionable body surface potential maps (BSPM) electrodes (3M, St. Paul, MN) were uniformly placed to fully

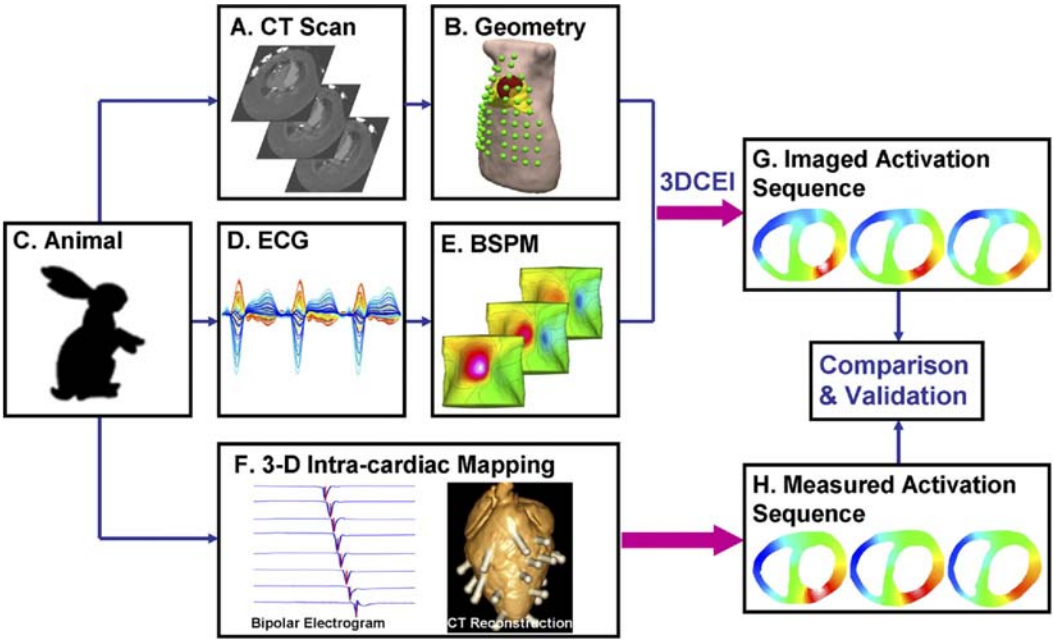

Fig. 7. Schematic diagram of the experimental protocol for validating the 3D cardiac electrical imaging (3DCEI) technique with simultaneous measurements from 3D intra-cardiac mapping in the rabbit heart. (From Ref. (Han et al., 2011) with permission)

cover the anterior-lateral chest up to the mid-axillary line. The number of BSPM electrodes depends on the surface area of the anterior chest. The heart was exposed via median sternotomy, and 20-27 transmural plunge-needle electrodes were inserted in the left and right ventricles of the rabbits. Each plunge-needle electrode contained 8 bipolar electrode-pairs with an inter-electrode distance of 500 μm (160-216 to intramural sites) (Pogwizd & Corr, 1987; Pogwizd, 1995). Septal electrodes were inserted into the anterior and posterior intraventricular septum of three rabbits (total of 16 interventricular sites for each rabbit). The septal electrode contained 4 bipolar electrode-pairs each separated by 2.5mm (Pogwizd, 1994). The chest and skin were then carefully closed with silk suture, and the mapping electrode wires were externalized above and below the sternotomy incision. Rapid single-site and simultaneous dual-site pacing were performed via bipolar electrode-pairs on selected plunge-needle electrodes in nine rabbits (rabbits P1-P9). NE was infused at 25-100 μg/kg/min (3 minutes at each dose) to induce premature ventricular complexes (PVCs) and VTs in another four rabbits (rabbits V1-V4) (Han et al., 2011). Bipolar electrograms were continuously recorded from all electrode-pairs together with body surface potentials from surface electrodes. Bipolar electrogram data were acquired at 1 kHz, using a 256 channels cardiac mapping system (Crescent Electronics, Salt Lake City, UT), and stored on a Dell laptop using specifically-designed software. Body surface potentials were simultaneously recorded using a 128 channels mapping system (Compumedics, Charlotte, NC) at a sampling rate of 1 kHz. The cardiac mapping and body surface potential mapping were performed simultaneously on two separate recording systems. The time alignment was performed during post data analysis. For each

run, the two datasets were synchronized by identifying the first pacing spike for pacing data or the first PVC beat for arrhythmia data (Han et al., 2011).

4.2.2. Ultra Fast Computed Tomography

At the completion of simultaneous mapping study, two sets of ultra fast CT (UFCT) (Philips, Amsterdam, NH, Netherlands) images were obtained on the living rabbit to obtain needed anatomical geometry information (Han et al., 2011). One without intravenous (IV) contrast (a continuous volume scan with slice thickness of 3 mm from the level of the mid neck down to the lower abdomen) was used to construct the rabbit torso model and extract the location of BSPM electrodes. Another one with IV contrast (from the great vessel level down to the diaphragm with slice thickness of 0.33 mm) was obtained for construction of a detailed heart model and 3D localization of plunge-needle electrodes. The in-plane resolution of CT images was 512*512 pixels. Ten cc to 12 cc of IV contrast (Ominipaque^{TM}) was administered at 1.5 cc/sec to visualize the heart chambers. The respiration of rabbit was held during the scan in order to minimize respiratory artifact. Continuous ECG was monitored and used for gating CT scanner. Fig.7.B shows a realistic geometry heart-torso model and BSPM electrodes configuration constructed from UFCT images. At the completion of the above procedures, the rabbit was euthanized. Then the chest was re-opened and the plunge-needle electrodes were carefully localized as described in (Pogwizd, 1994, 1995) by replacing each with a labeled pin. The heart was then excised and fixed in formalin. At a later date, photographs and post-operative UFCT scans (Han et al., 2011) were obtained on the

formalin-fixed heart with labeled pins to further facilitate precise 3D localization of the transmural electrodes (See Fig.7.F). It is noted that while some scatters caused by the needles were observed on CT images, we were still able to reconstruct the geometry of the ventricular cavities (which were brightly visualized by IV contrast) and localize the needles (shown as very bright dot spots).

4.2.3. 3D Intra-cardiac Mapping

The measured activation sequence within the 3D ventricular myocardium was constructed in a way that was slightly different from the previous method (Zhang et al., 2005; Han et al., 2008). The intersection between each transmural needle and the heart surface, and the orientation of each needle within the 3D ventricular myocardium was determined directly from the same CT images used for constructing the detailed heart model after the mapping study (Han et al., 2011). Each needle was represented by several bright dot points on CT slices. The needle was described as a line, whose parameters were best-fitting the orientation of the needle in the 3D space. Based on the determined coordinate for the intersection between the needle and the epicardial surface, and the prior structure information (e.g., inter-distance between bipolar electrode-pairs) of the needle, the coordinates of each eight bipolar electrode-pairs on the plunge needle within the heart model were calculated precisely from epicardium to endocardium using a linear equation and uniquely determined. An alternative heart surface model was built from the post-operative CT images of the isolated heart with labeled pins (representing the sites of transmural needles), and the location of each needle within this heart surface model was

determined from photographs of the isolated heart. This alternative heart surface model was carefully compared with the previous detailed heart model so that the identification and localization of the needles in that detailed heart model could be determined exclusively and precisely. The corresponding activation time of each recording electrode was assigned on the basis of peak criteria (Durrer & van der Tweel, 1954; Durrer et al., 1970; Pogwizd, 1994, 1995), and then a weighted average interpolation algorithm as described in (Zhang et al., 2005) was applied to obtain the complete 3D measured activation sequence throughout the ventricular myocardium.

4.2.4. Data Analysis and Statistical Analysis

For each rabbit, a commercial software package Curry 6.0 (Compumedics, Charlotte, NC) was used for contour detection and segmentation to build the subject-specific realistic geometry heart-torso model from UFCT images. This computer model includes heart, lungs, blood cavities, and chest surface. This heart-torso model was exported for further forward and inverse computation (Han et al., 2011) in a software package we developed in MATLAB2007a (MathWorks, Natick, MA). The 3D ventricular myocardium was discretized into thousands of grid points. The spatial resolution of the ventricular models was 1mm. A distributed ECD model was used to represent the cardiac electrical sources within the 3D ventricular myocardium. Given a tessellated geometrical heart-torso model and the prior knowledge of the electrical conductivity of relevant tissues and organs, the extracellular potentials measurable over the body surface is linearly related to the 3D ECD distribution by using the boundary element method.

The inverse problem is solved by using the algorithm presented in the previous chapter (Han et al., 2008). Briefly, the ECDs are reconstructed by the lead-field normalized weighted minimum norm (LFN-WMN) estimation (Wang et al., 1992) in combination with a spatiotemporal regularization. The singular value decomposition (SVD) is employed to decompose the spatiotemporal ECG data matrix into orthogonal spatial and temporal components. The spatial components that do not satisfy the discrete Picard condition (Hansen, 1990) are assumed to be dominated by noise perturbation, and thereby are truncated. The LFN-WMN estimation is applied to each remaining spatial component. The LFN-WMN solutions multiplied with the corresponding singular values and temporal components are summed to obtain the spatiotemporal ECD estimates. The activation time at each myocardial site is then determined from the time course of the estimated local ECD, by finding the maximum ECD estimate according to Eq. (3.3).

The correlation coefficient (CC), relative error (RE), and localization error (LE) were computed to quantify the overall agreement and disagreement between the invasively measured activation sequence and the non-invasively imaged activation sequence. LE was defined in the previous chapter. The CC and RE are defined as

$$CC = \frac{\sum_{i=1}^{n}\left(AT_i^E - \overline{AT^E}\right)\left(AT_i^M - \overline{AT^M}\right)}{\sqrt{\sum_{i=1}^{n}\left(AT_i^E - \overline{AT^E}\right)^2} \times \sqrt{\sum_{i=1}^{n}\left(AT_i^M - \overline{AT^M}\right)^2}}, \tag{4.1}$$

$$RE = \sqrt{\frac{\sum_{i=1}^{n}\left(AT_i^E - AT_i^M\right)^2}{\sum_{i=1}^{n}\left(AT_i^M\right)^2}} \tag{4.2}$$

where n is the number of grid points of the heart model, AT_i^E and AT_i^M are the estimated activation time and measurement constructed activation time at the i-th myocardial grid point, and $\overline{AT^E}$ and $\overline{AT^M}$ are the averaged estimated and measured activation time over all n myocardial grid points, respectively.

4.3. Results

After insertion of plunge electrodes, closure of the chest did not alter heart rate or mean arterial blood pressure (232 ± 6 vs 238 ±6 bpm and 62±4 vs 62±3 mm Hg, P=NS vs pre-closure) or total activation times of sinus beats (31±1ms vs 29±1ms, P=NS vs pre-closure), which were consistent with previously published data in control rabbits (Pogwizd, 1995; Zhang et al., 2005). The ventricular myocardium was tessellated into 6250±1137 evenly-spaced grid points. The spatial resolution of the ventricle models was 1 mm. There were 178±25 intramural bipolar electrodes during 3D intra-cardiac mapping and 60±2 BSPM electrodes.

4.3.1. Validation during Pacing

Single-site pacing was performed in rabbits P1-P9 (Han et al., 2011). The pacing sites were chosen to include multiple regions of LV, RV, and septum. Fig.8.A and Fig.8.B show the representative example of the comparison between the measured and imaged activation sequence when rabbit P6 was paced respectively at subendocardium (Fig.8.A) or subepicardium (Fig.8.B) via a plunge-needle electrode located at anterior

basal wall of LV. From the measured activation sequence of the endocardial-paced beat in Fig.8.A, the earliest activation was observed at the subendocardium. When the wavefront arrived at the epicardium, a relatively large breakthrough was noticed on the

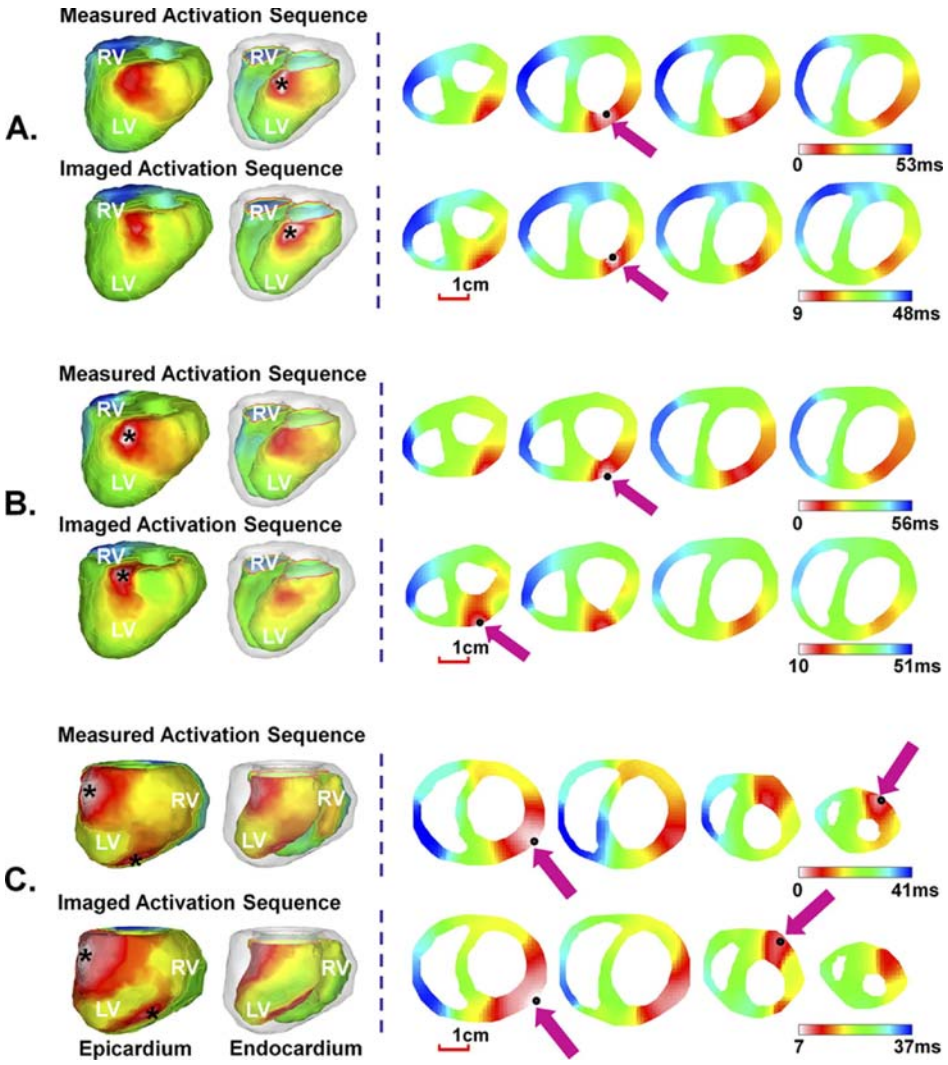

Fig. 8, Comparison between the 3D activation sequence measured via 3D intra-cardiac mapping and the 3D activation sequence imaged by 3DCEI when a rabbit was paced respectively at the endocardium (A) and epicardium (B) of LV basal anterior wall and when another rabbit was simultaneously paced at epicardium of LV apex and anterior basal left wall (C). (From Ref. (Han et al., 2011) with permission)

epicardial surface. The wavefront then propagated over the septum, and ended at the basal lateral wall of RV. The spatial activation pattern for the epicardial-paced beat in Fig.8.B is similar to that of endocardial-paced beat, but the major difference is that the origin of the activation from both the measured and the imaged activation sequences is located at the subepicardium rather than the subendocardium. For both cases, the imaged activation sequence closely approximated the measured activation sequence, with a CC of 0.76 and an RE of 0.29 for endocardial-paced beat, and a CC of 0.77 and an RE of 0.30

Table 3, Quantitative comparison between measured and imaged activation sequences in single-site LV pacing in the rabbit heart.

Rabbit No.	Pacing Needle Location	Endocardial LV Pacing			Epicardial LV Pacing		
		CC	RE	LE (mm)	CC	RE	LE (mm)
P1	LVA	0.71	0.25	4.7	0.67	0.23	3.2
P2	BLW	0.73	0.33	6.2	0.75	0.31	5.7
P3	Anterior BLW	0.78	0.30	7.6	0.79	0.32	7.1
	LVA	0.65	0.27	5.2	0.69	0.27	4.1
P4	BLW	0.81	0.29	4.6	0.86	0.27	2.7
	Posterior BLW	0.73	0.34	3.9	0.71	0.33	4.2
P5	Posterior MLW	0.74	0.34	3.9	0.73	0.32	4.8
	LVA	0.74	0.32	7.4	0.75	0.29	7.4
	Anterior BLW	0.63	0.30	4.9	0.61	0.33	4.1
P6	Anterior BLW	0.71	0.30	3.8	0.75	0.31	2.3
P7	Anterior MLW	0.79	0.28	3.7	0.81	0.27	3.4
	Posterior MLW	0.69	0.29	5.1	0.68	0.31	5.0
P8	MLW	0.72	0.33	4.7	0.73	0.32	5.1
	BLW	0.75	0.26	3.8	0.74	0.27	3.2
P9	MLW	0.76	0.31	4.6	0.77	0.32	4.5
	Mean	0.73±0.05	0.30±0.03	4.9±1.2	0.74±0.06	0.29±0.03	4.5±1.5

Note: LV, left ventricle; CC, correlation coefficient; RE, relative error; LE, localization error; BLW, basal left wall; LVA, left ventricle apex; MLW, middle left wall. (From Ref. (Han et al., 2011) with permission)

for epicardial-paced beat. The origin of activation was visually localized at the

subendocardium or subepicardium, with a low LE of 3.6mm and 3.0mm for these two cases respectively.

Septal pacing was performed via the selected plunge-needle electrodes placed in the interventricular septum for rabbits P7-P9 (Han et al., 2011). Fig.9 shows a representative example when rabbit P9 was paced at base septum via a septal electrode inserted from the anterior rabbit ventricles. From the measured map, the activation initiated at the intramural septum slightly closer to LV. The wavefront then propagated to the rest of the ventricles and terminated at the RV apex. The overall pattern of the imaged activation

Table 4, Quantitative comparison between measured and imaged activation sequences in single-site RV and septal pacing in rabbit heart.

Rabbit No.	Pacing Needle Location	CC	RE	LE (mm)
P1	MRW	0.75	0.30	3.2
P2	Posterior MRW	0.68	0.31	7.8
	MRW	0.74	0.29	4.0
P3	BRW	0.78	0.30	5.6
P4	Anterior BRW	0.73	0.26	4.3
	Posterior MRW	0.68	0.36	5.2
P5	BRW	0.80	0.32	6.3
	RVA	0.78	0.28	4.9
P6	Posterior MRW	0.74	0.27	5.5
	MRW	0.69	0.32	4.7
P7	Posterior MS	0.67	0.30	5.3
	Posterior AS	0.72	0.33	7.2
P8	Posterior AS	0.71	0.29	5.0
P9	Anterior BS	0.69	0.31	4.7
	Anterior MS	0.68	0.32	5.8
	Mean	0.72±0.04	0.30±0.03	5.3±1.2

Note: RV, right ventricle; CC, correlation coefficient; RE, relative error; LE, localization error; AS, apex septum; BRW, basal right wall; BS, basal septum; MRW, middle right wall; MS, middle septum; RVA, right ventricle apex. (From Ref. (Han et al., 2011) with permission)

sequence resembled the measured one, with a CC of 0.68, and an RE of 0.29. The initiation site was well localized at the septum with an LE of 4.4 mm for this beat.

A total of 300 beats of LV pacing from 15 selected plunge-needle electrodes were analyzed (10 endocardial paced beats and 10 epicardial paced beats for each plunge-needle electrode). The ability of 3DCEI in reconstructing the overall activation pattern and localizing the pacing site during LV pacing in quantitative comparison is summarized in Table 3. A slightly better performance of imaging epicardial pacing was observed in terms of LE. Another 150 beats of single-site pacing at 10 RV epicardial sites and 5 septal sites (10 paced beats for each pacing) were analyzed and the quantitative comparison is summarized in Table 4. A slight increase of LE was observed during septal pacing, as compared to LV pacing. The averaged CC and averaged RE for the combination of LV pacing, RV pacing, and septal pacing were 0.73±0.04 and 0.30±0.02

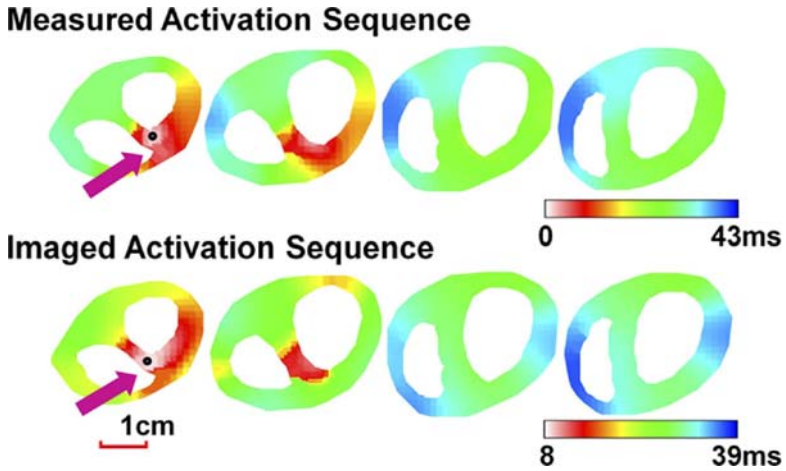

Fig. 9, Comparison between the 3D measured activation and the 3D imaged activation sequence during septum pacing in rabbit heart. (From Ref. (Han et al., 2011) with permission)

respectively, suggesting excellent agreement between the measured and imaged activation sequence. Furthermore, the pacing sites were estimated to be 4.9±1.3mm away from the measured ones, suggesting reasonable localization accuracy of this approach (Han et al., 2011).

Dual-site pacing was performed in rabbits P1-P5 (Han et al., 2011). Fig.8.C shows the representative comparison when rabbit P3 was simultaneously paced at an LV epicardial site in the basal lateral wall and at an LV epicardial site in the posterior apex. The two pacing sites were 21mm apart within the heart. The activation ended in the RV basal lateral wall. The non-invasively reconstructed activation sequence closely resembled the measured one, with a CC of 0.72 and an RE of 0.30. The double origins of the activation were clearly resolved from the imaged result. A total of 70 beats of simultaneous dual-site pacing from 7 pairs of epicardial pacing sites (10 beats for each dual-site pacing) were analyzed. The performance of 3DCEI in imaging dual-site pacing

Table 5, Quantitative comparison between measured and imaged activation sequence in simultaneous dual-site pacing in rabbit heart.

Rabbit No.	Pacing Needle Locations	CC	RE
P1	LVA, MRW	0.65	0.34
P2	BLW, Posterior MRW	0.59	0.39
P3	Anterior BLW, LVA	0.71	0.33
P4	Anterior BRW, Posterior BLW	0.72	0.33
P5	BRW, LVA	0.69	0.31
	RVA, LVA	0.71	0.32
	Anterior BLW, LVA	0.73	0.34
	Mean	0.69±0.05	0.33±0.05

Note: CC, correlation coefficient; RE, relative error; BLW, basal left wall; BRW, basal right wall; LVA, left ventricle apex; MRW, middle right wall; RVA, right ventricle apex. (From Ref. (Han et al., 2011) with permission)

in quantitative comparison is summarized in Table 5. The inter-site distance for the two pacing sites ranged from 10-27mm. The double origins were identified when they were located at contralateral sides of ventricles or at the ventricular lateral wall and the apex, respectively. The averaged CC and RE were 0.69±0.05 and 0.33±0.05 respectively, suggesting excellent agreement between measured and estimated activation sequences when imaging more complex activation pattern other than single-site pacing.

4.3.2. Norepinephrine-induced Ventricular Arrhythmias

Isolated PVCs and nonsustained monomorphic VTs were obtained during the infusion of NE in rabbits V1-V4. A total of 28 PVCs and 45 beats of VTs were analyzed

Table 6, Quantitative comparison between measured and imaged activation sequence in norepinephrine induced VT in rabbit heart.

Rabbit No.	Arrhythmia Type	Origin	CC	RE	LE (mm)
V1	PVC	LVA	0.61	0.31	7.4
	Monomorphic VT	BLW	0.70	0.33	5.4
V2	PVC	MRW	0.71	0.30	5.0
	PVC	Posterior MRW	0.69	0.31	3.8
	Monomorphic VT	Anterior MRW	0.77	0.31	6.0
V3	PVC	MRW	0.75	0.32	4.8
	PVC	BLW	0.70	0.30	4.8
	PVC	BRW	0.69	0.31	4.7
	Monomorphic VT	BRW	0.73	0.29	7.1
V4	PVC	BRW	0.69	0.31	4.9
	PVC	Posterior MRW	0.65	0.27	7.1
	Monomorphic VT	BRW	0.68	0.32	4.0
	Mean		0.70±0.04	0.31±0.02	5.4±1.2

Note: VT, ventricular tachycardia; CC, correlation coefficient; RE, relative error; PVC, premature ventricular complex; BLW, basal left wall; BRW, basal right wall; LVA, left ventricle apex; MRW, middle right wall. (From Ref. (Han et al., 2011) with permission)

and the mechanism of the arrhythmia was defined for all these ectopic beats from intra-cardiac mapping. All these PVC and VT beats initiated in the subendocardium and did so by a focal, and what we believe to be a nonreentrant mechanism (Han et al., 2011), based on the lack of intervening electrical activity between the preceding beat and the initiation of the ectopic beat in intramural recordings (Pogwizd, 1995; Pogwizd et al., 1998). PVCs in each rabbit demonstrated different initial sites of activation, except rabbit V1 which had PVCs only initiated from a single site. Seven PVCs initiated in the LV and 21 in the RV. PVCs initiated with a coupling interval of 279±39ms and conducted with a total activation time of 46±9ms. The averaged coupling interval among all maintained VT beats was 216±11ms, and the averaged total activation time was 48±7ms. The quantitative comparison for PVCs and VTs beats is summarized in Table 6.

Fig.10.A-Fig.10.C show the comparison between the measured and imaged activation sequences for three PVC beats in rabbit V3. Different activation patterns were observed, with different initiation sites at subendocardium of basal right wall, basal left wall, and middle right wall respectively. The imaged results resembled the measured counterparts, with a CC of 0.69 and an RE of 0.31 for PVC in Fig.10.A, a CC of 0.71 and an RE of 0.29 for PVC in Fig.10.B, and a CC of 0.78 and an RE of 0.28 for PVC in Fig.10.C. The initiation sites were estimated to be 4.8mm, 3.6mm, and 4.5mm from the measured sites respectively.

An example of a representative VT beat in a six-beat monomorphic VT in rabbit V1 is shown in Fig.10.D. After initiation, all VT beats looked similar. As shown in the measured activation sequence, the VT beat initiated within subendocardium by a focal

(nonreentrant) mechanism at the basal lateral wall of LV. After initiation, activation propagated to the RV and terminated at base of RV with a total activation time of 42ms.

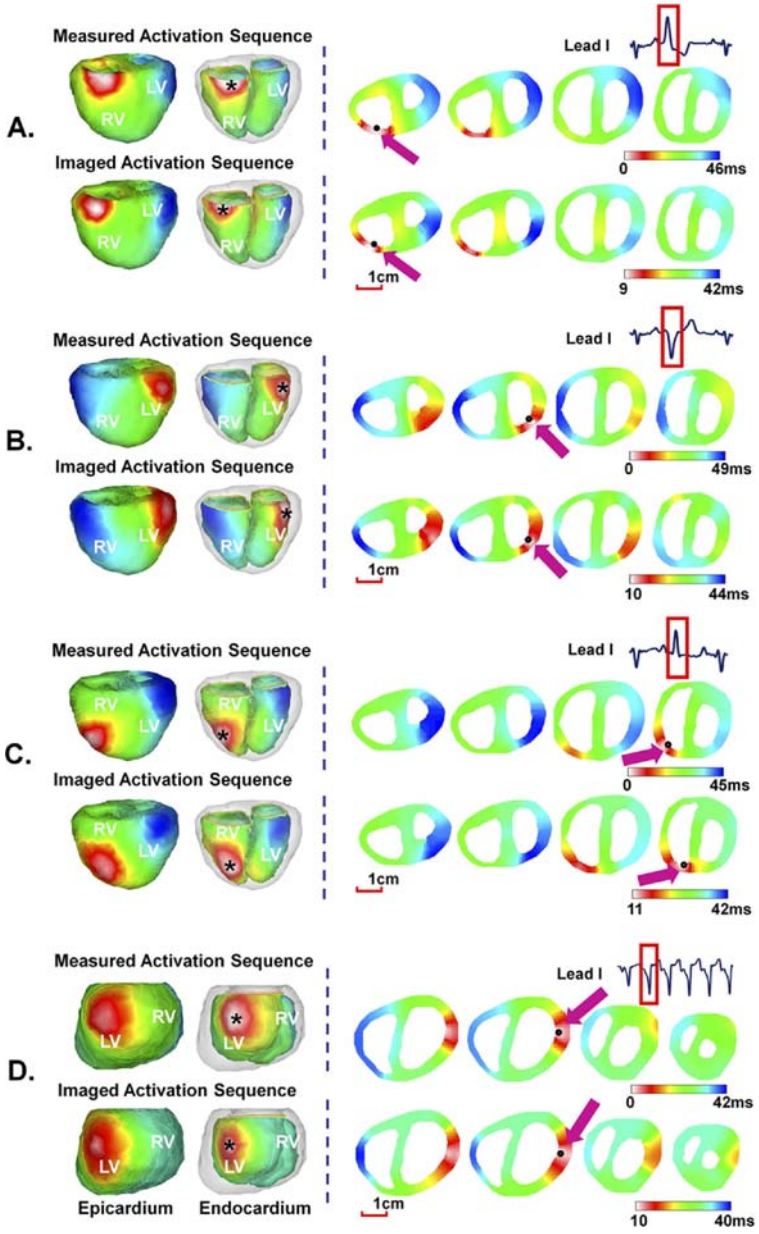

Fig. 10, Comparison between the 3D measured activation sequence and the 3D imaged activation sequence during premature ventricular complex and ventricular tachycardia induced by norepinephrine in the rabbit heart. (From Ref. (Han et al., 2011) with permission)

The imaged activation sequence matched measured one, with a CC of 0.76 and an RE of 0.30. The initiation of the activation was well localized with an LE of 4.8mm.

4.4. Discussion

The present study in this chapter aims to assess the performance of the 3DCEI technique in non-invasively reconstructing the 3D ventricular activation sequence and localizing the origin of activation in the *in vivo* rabbit heart (Han et al., 2011). By comparing the imaged results with simultaneous measurements through 3D intra-cardiac mapping from up to 216 intramural sites, this study validated the ability of 3DCEI to identify, locate and resolve single and double electric events during single-site and dual-site paced rhythms, as well as NE-induced nonsustained monomorphic VTs and PVCs. Our results showed an excellent agreement of the spatial activation pattern between the non-invasively imaged activation sequence and its directly measured counterparts, as quantified by a CC of 0.72 and an RE of 0.30 averaged over all paced and ectopic beats. The origins of the activation in imaged results had an averaged distance of ~5mm from the pacing sites for the single-site paced beats (450 beats at 45 pacing locations in 9 animals) and site of initiation for ventricular ectopic beats determined by intra-cardiac mapping (73 beats in 4 animals). These findings imply that 3DCEI is feasible in reconstructing the spatial patterns of 3D ventricular activation sequences, localizing the focal or multiple arrhythmogenic foci, and imaging dynamically changing arrhythmia on a beat-to-beat basis (Han et al., 2011).

Rigorous validation studies in biological systems are crucial for establishing any imaging methods. Compared with other animal experiments and human studies (Oster et al., 1997; Berger et al., 2006; Ghosh et al., 2008) in validating epicardial potential and heart surface activation imaging techniques, the present study has used a novel *in vivo* experimental design in which BSPMs were obtained simultaneously with intramural electrical recordings from plunge-needle electrodes in a closed-chest condition, and thus provided quantitative assessments of the 3DCEI approach. The experimental protocol has been refined from our previous studies (Zhang et al., 2005; Han et al., 2008) in using CT images obtained on the anesthetized animals immediately following the mapping studies. Such improvements could more accurately model the heart-torso geometry by considering certain effects related to the procedures of open-chest surgery (e.g., rotation of the heart orientation and position-shift of BSPM electrodes) and more accurately determine the location of the plunge-needle electrodes within the detailed heart model, as compared with previous studies (Han et al., 2011).

The present physical-model based 3DCEI approach only uses the general biophysical relationships governing the cardiac electrical activity, without incorporating any physiological assumptions. The activation sequence throughout 3D ventricular myocardium was estimated based on the inversely reconstructed ECDs from the BSPMs. Like other studies (Oster et al., 1997; Tilg et al., 2002), we experience smoothing effects when we solve the inverse problem, especially at the earliest and latest activation times, when body surface potentials are of relatively small magnitudes compared to noise. The resultant solution may lead to spatially smoothed images, and thus cause the delayed

initiation and premature termination. Nevertheless, the imaged activation sequence still provided a close match to the direct measurements, suggesting that significant information regarding ventricular excitation has been preserved in imaged results. Such information revealed the activation pattern within a single map and helped identify the initiation sites in the endocardium, epicardium or intramural septum (Han et al., 2011).

For the first time, the 3DCEI approach was applied in imaging ventricular arrhythmias and validated with the aid of 3D intra-cardiac mapping (Han et al., 2011). NE simulated the activation of the sympathetic nervous system and induced PVCs and VTs. The measured activation sequence also showed that these arrhythmias usually originated within the subendocardium and may arise from Purkinje cells or subendocardial myocardium. The origins have been well localized by the noninvasive 3DCEI approach with good accuracy, implying that this approach may be valuable for imaging focal ventricular arrhythmias arising in the deeper myocardium. For the earliest activation onset, it is possible that PVCs and VT beats may initiate close to the plunge electrode that records earliest electrical activity. However, mapping at the resolution that we employed in this study (recording from 200 intramural sites in the rabbit heart is equivalent to recording from up to 2600 intramural sites in the canine heart) (Pogwizd, 1995) and having each bipolar initiation site surrounded by several dozen intramural recording sites that recorded later activity, we minimized the effects of extrapolation so that we anticipated earliest onset to be immediately adjacent to the earliest recording site (Pogwizd, 1995).

Our results indicated that the site of earliest activation was always in close proximity to the measured initiation site, with an averaged distance from imaged and measured sites to be ~5mm (Han et al., 2011). While the noninvasive imaging approach would enable the clinical electrophysiologist to localize to within ~5 mm of the myocardium region from which focal activation is arising, additional catheter mapping would certainly be required to more precisely localize this focal site for the ensuing ablation. The key values of this approach would be to shorten the ablation time and, perhaps more importantly, to help determine whether initiation is arising in the endocardium or the epicardium (which would also shorten ablation time since epicardial ablation requires a pericardial approach, and this is often initiated after endocardial catheter mapping suggests an epicardial site of origin). This study also extended the evaluation in imaging relatively more complex activation pattern, as simulated by dual-site pacing (Han et al., 2011). This has specific clinical relevance when more than one arrhythmogenic activity (e.g., two pre-excitation sites or fusion beat) are taking place simultaneously, and it would then be imperative to know the locations of these electric events before ablation. Furthermore, dual-site pacing simulates the cardiac resynchronization therapy (Abraham et al., 2002), which is an important clinical procedure in treatment of heart failure patient and may have potential clinical applications in this area.

In conclusion, the present study suggests that the 3DCEI approach can reconstruct 3D ventricular activation sequence and localize the origin of activation during pacing and focal ventricular arrhythmias, as validated by 3D intra-cardiac mapping in the rabbit heart. It also implies the potential application of 3DCEI as a clinically useful tool to aid

in localizing the origins of ventricular arrhythmias and understanding the mechanism of these arrhythmias.

Chapter 5

Experimental Investigation in Normal Canine Heart

5.1. Introduction

In the previous chapter, we have rigorously validated the three-dimensional (3D) cardiac electrical imaging (3DCEI) approach using 3D intra-cardiac mapping in the normal rabbit heart during pacing and ventricular tachycardia (VT) (Han et al., 2011). The present study extends the validation of this novel 3DCEI approach using the well-established 3D intra-cardiac mapping procedure (Pogwizd & Corr, 1987; Pogwizd, 1994, 1995; Pogwizd et al., 1998; Han et al., 2008; Han et al., 2011) in the canine heart which is closer to the human heart in cardiac size and electrophysiological characteristics (Han et al., 2012). Plunge-needle electrodes were placed in the left ventricle (LV) and right ventricle (RV), and the body surface potentials and intramural bipolar recordings were measured simultaneously in a closed-chest condition. Pacing was performed at the subendocardium and subepicardium of the canine ventricles. Furthermore, norepinephrine (NE) was infused to induce ventricular ectopic activities including multiform premature ventricular complexes (PVCs), couplets, and runs of nonsustained monomorphic VTs (MVTs) and polymorphic VTs (PVTs). The 3DCEI imaging results were quantitatively compared with the intra-cardiac mapping results to assess the imaging performance. Materials in this chapter have been previously published (Han et al., 2012).

5.2. Study Design

5.2.1. Canine Model and Experimental Procedures

Five healthy control canines (of either sex) were studied under a protocol of simultaneous body surface potential mapping and 3D intra-cardiac mapping of ventricular electrical activity (Han et al., 2012). The protocol was approved by the Institutional Animal Care and Use Committees of the University of Minnesota and the University of Alabama at Birmingham. Fig.11 shows the schematic paradigm of the experiment. Each canine was anesthetized using 0.04 mg/kg intramuscular atropine and ~20 mg/kg intravenous (IV) pentothal. The animal was then intubated and placed on a ventilator. Anesthesia was maintained with 2-3% isoflurane delivered in 100% oxygen. Up to 124 repositionable BSPM electrodes (3M, St. Paul, MN) were uniformly placed to cover both the anterior and posterior chest, and up to 42 transmural plunge-needle electrodes were inserted in the LV and RV (up to 216 intramural sites). Each LV plunge-needle electrode contains 4 bipolar electrode-pairs (inter-electrode distance of 500 μm) each separated by 2.5mm (Pogwizd, 1994; Pogwizd et al., 1998), and each RV electrode contains 8 bipolar electrode-pairs with an inter-electrode distance of 500 μm (Pogwizd, 1995). The chest and skin were then carefully closed with silk suture, and the mapping electrode wires were externalized above and below the sternotomy incision. Bipolar electrograms were continuously recorded from all electrode-pairs together with body surface potentials from surface electrodes. Bipolar electrograms were acquired at 1 kHz, using a 256 channels cardiac mapping system (Crescent Electronics, Salt Lake City, UT).

Body surface potentials were simultaneously recorded using a 128 channels mapping system (Compumedics, Charlotte, NC) at a sampling rate of 1 kHz.

During pacing study, rapid pacing were performed (for 10-20 secs) in canines C1-C5 via bipolar electrode-pairs on selected plunge-needle electrodes located at subendocardium and subepicardium of the ventricles using a specially-designed junction box. Furthermore, NE was infused to induce ventricular arrhythmias including PVCs, couplets, nonsustained MVTs, and PVTs in canines C3-C5 after the pacing study (Han et al., 2012).

At the completion of simultaneous mapping study, two sets of ultra fast computed tomography (UFCT) (Philips, Amsterdam, NH, Netherlands) images were obtained on

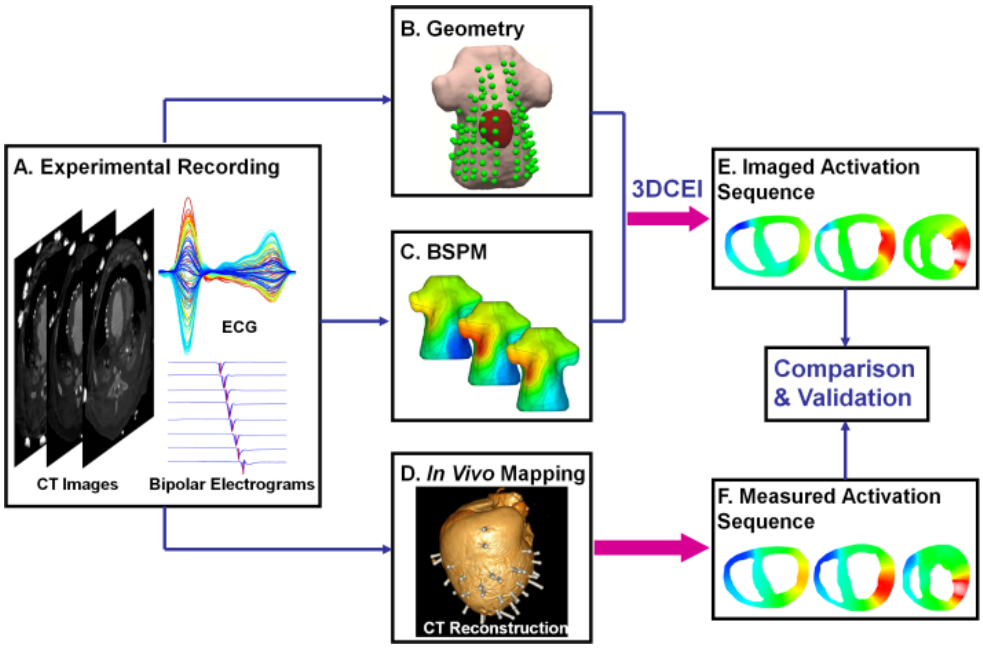

Fig. 11, Schematic diagram of the experimental protocol for validating the 3D cardiac electrical imaging (3DCEI) technique with simultaneous measurements from 3D intra-cardiac mapping in the canine heart. (From Ref. (Han et al., 2012))

the living animal to obtain the anatomical information (Han et al., 2012). One without IV contrast (a continuous volume scan with slice thickness of 3mm from the level of the mid neck down to the lower abdomen) was used to construct the torso model and extract the location of BSPM electrodes. Another one with IV contrast (from the great vessel level down to the diaphragm with slice thickness of 0.33mm) was obtained for construction of a detailed heart model and 3D localization of plunge-needle electrodes. The in-plane resolution of UFCT images was 512*512 pixels. 30 cc of IV contrast was administered at 3.0cc/sec to visualize the heart chambers during the cardiac UFCT scan. The plunge-needle electrodes were then carefully localized as previously described in (Han et al., 2011) by replacing each with a labeled pin. A post-operative UFCT scan of the formalin-fixed canine heart was subsequently performed to further facilitate precise 3D localization of the transmural electrodes.

5.2.2. Data Analysis

The physical-model-based 3DCEI approach was used to non-invasively reconstruct the activation sequence throughout the 3D ventricular myocardium. The forward modeling and inverse computation of the 3DCEI approach were described in the previous chapters. Briefly, the realistic geometry heart-torso model was constructed from UFCT images for each animal, using a commercial software package CURRY 6.0 (Compumedics, Charlotte, NC). This heart-torso model was exported for further forward and inverse computation (Han et al., 2011, 2012). The electrical conductivities were set to 0.2, 0.67, 0.05, and 0.21 S/m respectively. The algorithm presented in the previous

chapters was used to solve the inverse problem and reconstruct the 3D activation sequence.

The performance of 3DCEI was evaluated by comparing the non-invasively imaged activation sequence with the simultaneously direct measurements obtained from 3D intra-cardiac mapping. The measured activation sequence within the 3D ventricular myocardium was constructed to allow for a quantitative comparison. The orientation and location of each needle within the 3D ventricular myocardium was determined directly from the same UFCT images used for constructing the detailed heart model after the mapping study and therefore the 3D measured activation sequence was reconstructed (Han et al., 2011, 2012).

Numerical data are presented as mean ± SD. The correlation coefficient (CC) and relative error (RE) were computed respectively to quantify the agreement of overall activation pattern and the consistency of the activation time between the invasively measured activation sequence and the non-invasively imaged activation sequence. CC and RE were defined in Eq. (4.1) and Eq. (4.2) respectively. The root mean square error (RMSE) was computed to quantify the timing difference between measured and imaged activation sequences. The RMSE is defined as

$$RMSE = \sqrt{\frac{\sum_{i=1}^{n}\left(AT_i^E - AT_i^M\right)^2}{n}} \tag{5.1}$$

where n is the number of grid points of the heart model, AT_i^E and AT_i^M are the non-invasively estimated activation time and measurement constructed activation time at the

i-th myocardial grid point. $\overline{AT^E}$ and $\overline{AT^M}$ are their respective mean values. The localization error (LE), was computed to evaluate the performance of 3DCEI in localizing the origin of activation. Statistical significance of differences was evaluated by Student's t-test (paired or unpaired) and ANOVA test, and a p value < 0.05 was considered statistically significant (Han et al., 2012).

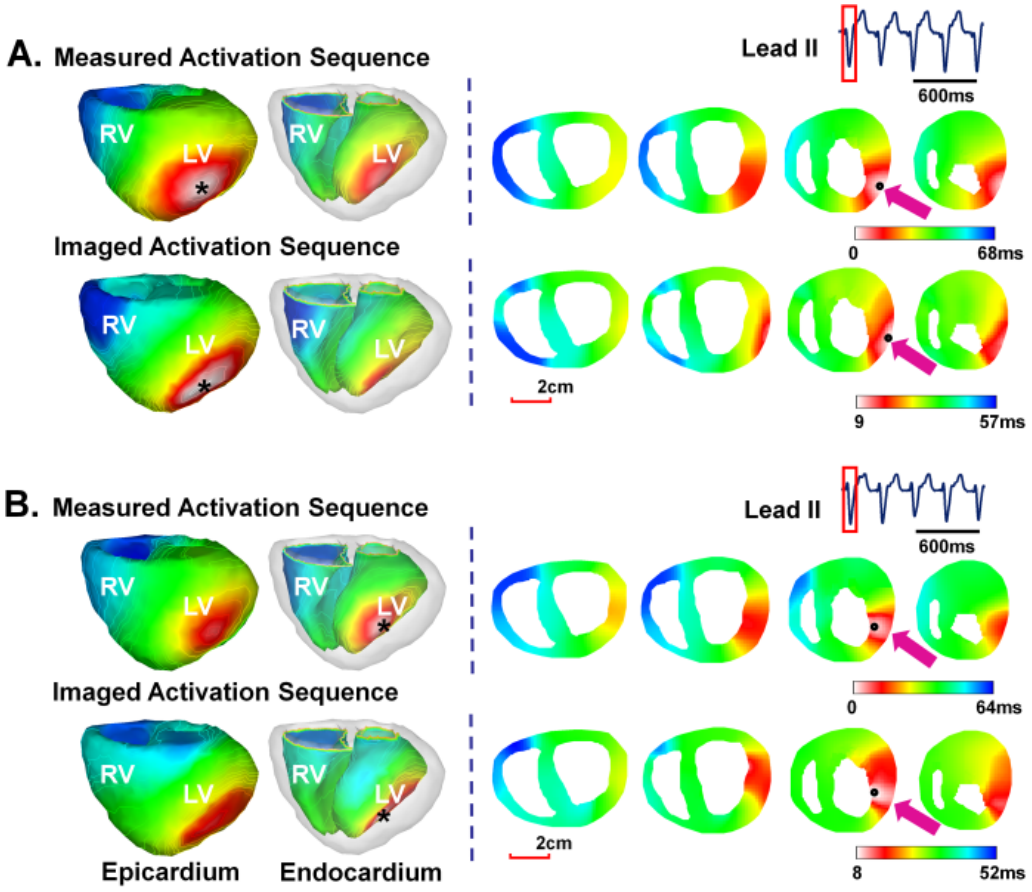

Fig. 12, Comparison between the 3D measured activation sequence and the 3D imaged activation sequence when canine was paced at the subepicardium (A) and subendocardium (B) of middle lateral wall of left ventricle. (From Ref. (Han et al., 2012))

5.3. Results

5.3.1. Experimentation and Modeling

Five canines were studied during the *in vivo* experiments. After insertion of plunge-needle electrodes, closure of the chest did not alter heart rate or mean arterial blood pressure (115±15 versus 120±20 bpm, $p>0.05$, paired t-test, and 60±3 versus 57±6 mm Hg, $p>0.05$, paired t-test) or total activation times of sinus beats (43±2ms versus 44±2ms, $p>0.05$, paired t-test) for each canine (Han et al., 2012). The realistic geometry heart-torso model was constructed for each animal from two sets of UFCT images obtained after the mapping study. The ventricular myocardium was tessellated into 21332±7036 evenly-spaced grid points. The spatial resolution of the ventricle models was 1.5 mm. There were 200±10 intramural bipolar electrodes during 3D intra-cardiac mapping and 114±7 BSPM electrodes on the canine body surface.

5.3.2. Pacing in the Canine Heart

Simultaneous body surface potential mapping and 3D intra-cardiac mapping were performed under single-site pacing in canine C1-C5 (Han et al., 2012). The pacing sites were chosen to include multiple regions of the LV and RV. Fig.12 shows a representative example of the comparison between the measured and imaged activation sequences when canine C2 was paced respectively at subepicardium and subendocardium via a plunge-needle electrode located in the left lateral free wall midway between the base and the apex. The spatial distribution of the activation time within the ventricular myocardium is color-coded. The white corresponds to early activation, while blue corresponds to late

activation. The left column shows the comparison of the activation sequence on the epicardial and endocardial surfaces. The right column shows four axial slices starting from ventricular base. The subendocardial and the subepicardial sites of origin were identified for these two cases respectively from the imaged activation sequence. The overall pattern of the imaged activation sequence closely approximated the measured one during early and middle activation, while a slight difference was observed during late activation. The quantitative comparison gave a CC of 0.72, an RE of 0.25, and an RMSE

Table 7, Quantitative comparison between measured activation sequence and imaged activation sequence during single-site LV pacing in the canine heart.

Canine	Pacing Needle Location	Endocardial LV Pacing				Epicardial LV Pacing			
		CC	RE	LE (mm)	RMSE (ms)	CC	RE	LE (mm)	RMSE (ms)
C1	BLW	0.75	0.36	7.9	13	0.79	0.38	7.6	8
	Posterior MLW	0.79	0.28	5.3	7	0.81	0.22	4.2	5
	LVA	0.80	0.37	7.6	9	0.83	0.39	8.2	10
C2	Posterior MLW	0.70	0.29	8.2	11	0.71	0.32	7.8	14
	MLW	0.73	0.26	6.9	10	0.72	0.25	6.7	8
	LVA	0.69	0.21	5.1	9	0.72	0.24	5.7	6
C3	MLW	0.65	0.31	7.4	11	0.67	0.32	6.4	12
	LVA	0.62	0.25	9.1	8	0.68	0.36	8.8	7
C4	BLW	0.70	0.24	10.2	8	0.77	0.18	9.1	6
	Anterior MLW	0.78	0.32	8.1	7	0.86	0.31	8.3	7
	MLW	0.68	0.24	6.3	12	0.69	0.20	5.2	9
C5	BLW	0.72	0.25	6.5	8	0.74	0.26	6.1	7
	MLW	0.78	0.23	5.7	7	0.79	0.27	5.3	6
	LVA	0.68	0.33	7.3	11	0.69	0.34	7.2	12
	Mean	0.72±0.06	0.28±0.05	7.3±1.4	9±2	0.75±0.06	0.29±0.07	6.9±1.5	8±3

Note: CC, correlation coefficient; RE, relative error; LE, localization error; RMSE, root mean square error; BLW, basal left wall; MLW, middle left wall; LVA, left ventricle apex. (From Ref. (Han et al., 2012))

of 8ms for the subepicardial-paced beat, and a CC of 0.71, an RE of 0.26, and an RMSE of 9ms for the subendocardial-paced beat. The origin of activation was localized to be 6.6mm and 6.2mm for these two cases respectively.

A total of 280 beats of single-site LV pacing from 14 subendocardial sites and 14 subepicardial sites (10 beats for each single site) were analyzed. The performance of 3DCEI in imaging ventricular activation during LV pacing is summarized in Table 7. A slightly better performance of imaging epicardial pacing was observed in terms of CC

Table 8, Quantitative comparison between measured activation sequence and imaged activation sequence during single-site RV pacing in the canine heart.

Canine	Pacing Site	CC	RE	LE (mm)	RMSE (ms)
C1	Anterior BRW	0.77	0.28	7.4	11
	MRW	0.78	0.31	7.7	12
	RVA	0.68	0.33	7.5	8
C2	RVA	0.66	0.33	7.4	9
	MRW	0.79	0.24	10.3	4
	Anterior MRW	0.80	0.29	6.3	11
	Posterior MRW	0.76	0.28	7.9	11
	Anterior BRW	0.79	0.25	5.7	12
C3	Posterior RVA	0.74	0.24	8.6	10
	RVA	0.75	0.34	6.3	9
	BRW	0.73	0.39	7.4	10
	MRW	0.84	0.34	8.2	9
C4	MRW	0.84	0.33	10.7	11
	Posterior MRW	0.77	0.33	6.2	12
	RVA	0.68	0.38	6.3	5
C5	Posterior MRW	0.68	0.23	7.3	12
	BRW	0.77	0.28	6.7	11
	MRW	0.79	0.31	6.1	14
	Mean	0.76±0.05	0.30±0.05	7.4±1.4	10±2

Note: CC, correlation coefficient; RE, relative error; LE, localization error; RMSE, root mean square error; BRW, basal right wall; MRW, middle right wall; RVA, right ventricle apex. (From Ref. (Han et al., 2012))

(0.75±0.06 versus 0.72±0.06, $p<0.05$, paired t-test) and LE (6.9±1.5mm versus 7.3±1.4mm, $p<0.05$, paired t-test). The 3DCEI approach was able to identify the subendocardial origins for 10 subendocardial pacing sites, and subepicardial origins for 12 subepicardial pacing sites (Han et al., 2012). Table 8 summarizes the performance of 3DCEI in imaging ventricular activation during RV pacing (18 subepicardial pacing sites). For each animal, the imaging performance varied among difference anatomical pacing locations. In general, slightly decreased performance when imaging the global activation pattern during apical pacing in term of CC (0.76±0.05 versus 0.71±0.06, $p<0.05$, unpaired t-test) was observed averaging all animals. The averaged CC, RE, and RMSE over both LV and RV pacing were 0.74±0.06, 0.29±0.05, and 9±3ms respectively, suggesting good agreement between measured and estimated activation sequences. The averaged LE was 7.2±1.4mm, suggesting reasonable localization accuracy when imaging subjects with larger cardiac size.

5.3.3. Ventricular Arrhythmias in the Canine Heart

Frequent multiform PVCs and runs of nonsustained MVTs and PVTs were demonstrated during the infusion of NE (Han et al., 2012). A total of 96 ventricular ectopic beats including 26 PVCs, 5 couplets, 4 runs of MVTs and 6 runs of PVTs were analyzed. PVCs in each canine demonstrated different initial sites of activation. Twelve PVCs initiated in the LV and 14 in the RV. The PVC and VT beats were observed to initiate by a focal mechanism from a single site or sequentially from multiple sites in the subendocardium of ventricles, including lateral walls and apex. Quantitative comparisons

were made between non-invasively imaged activation sequence and invasively measured activation sequence for these PVCs and VTs beats in the canine heart. The comparison results are summarized in Table 9. The methods to image 96 PVC and VT beats are similar to those to image 460 beats paced from the LV or RV ($p>0.05$ for CC, RE, LE, and RMSE respectively, ANOVA test).

Fig.13 shows examples of two nonsustained MVT beats in canine C3. As shown in Fig.13.A for a representative MVT beat, this VT beat initiated at a subendocardial site at

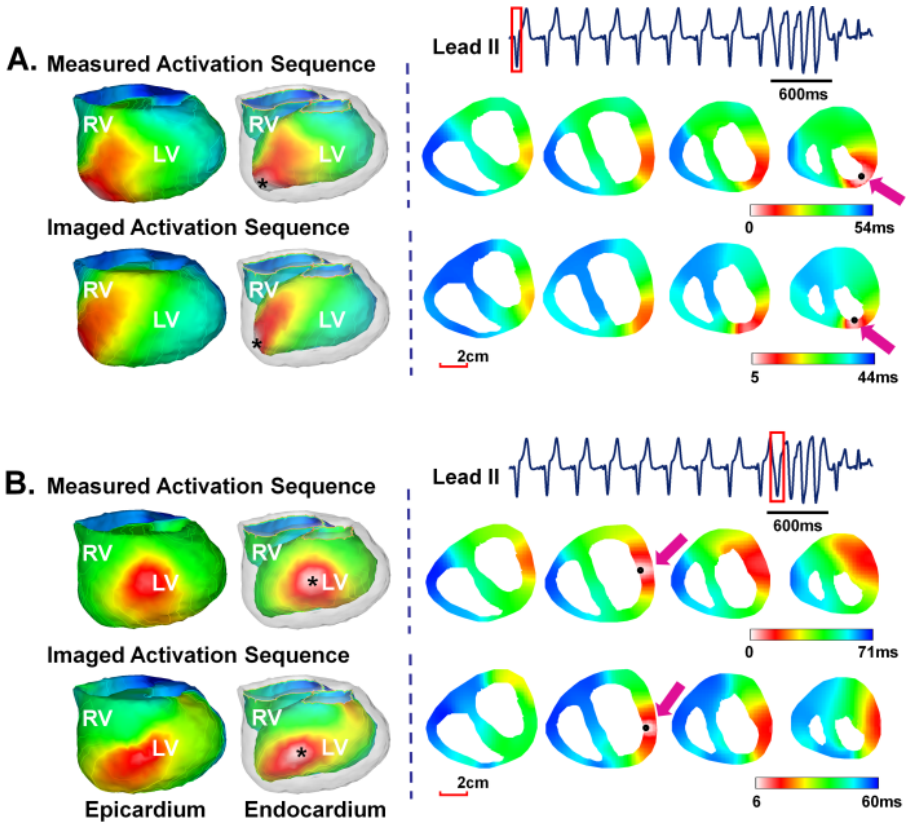

Fig. 13, Comparison between the 3D measured activation sequence and the 3D imaged activation sequence for two monomorphic ventricular tachycardia beats in the canine heart. (From Ref. (Han et al., 2012))

anterior LV apex by a focal mechanism and propagated to the RV basal wall. The subsequent eight VT beats demonstrated focal initiation at the same LV site and similar global activation pattern. The averaged coupling interval of these maintained VT beats was 329±9ms. The imaged activation sequence matched measured activation sequence in its overall activation pattern, with a CC of 0.72, an RE of 0.28, and an RMSE of 8ms for this beat. The initiation of the activation was well localized with an LE of 7.2mm. The VT then accelerated into a fast four-beat episode, as shown in Fig.13.B. The activation pattern of these four beats looked similar and the initiation site of the activation moved to LV lateral wall. The averaged coupling interval for these four VT beats was 140±10ms. The imaged activation sequence was consistent with the direct measurement, with a CC of 0.78, an RE of 0.24, and an RMSE of 9ms. The initiation of the activation was well localized with an LE of 6.8mm for the fast VT beat shown in the red box of ECG in Fig.13.B.

Another example is shown in Fig.14 for a four-beat PVT in canine C3. As shown in measured activation sequence in Fig.14.A, the first VT beat initiated at a RV site close to apex by a focal mechanism and propagated to the LV basal wall. The second beat initiated at anterior LV apex and activation pattern was similar to the beat shown in Fig.14.A. Beat 3 and beat 4 demonstrated the focal initiation at the same RV site close to posterior middle wall and similar global activation pattern, as shown in Fig.14.B. The coupling interval for this VT was 271±33ms. The imaged activation sequence matched the measured activation sequence in its overall activation pattern, with a CC of 0.73, an RE of 0.26, and an RMSE of 5ms for the beat in Fig.14.A, and a CC of 0.79, an RE of

0.25, and an RMSE of 10ms for the beat in Fig.14.B. The initiation of the activation was well localized with an LE of 7.4mm and 7.8mm respectively.

5.4. Discussion

In this chapter, we extended our validation of a physical-model-based 3DCEI technique in non-invasively reconstructing the 3D ventricular activation sequence and localizing the origin of activation in the canine heart with the aid of simultaneous 3D

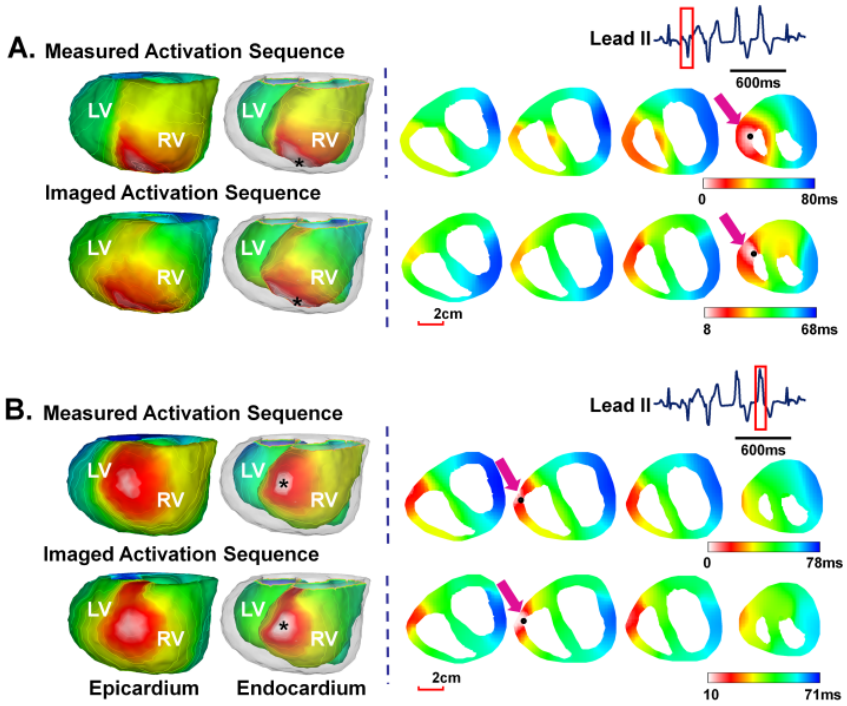

Fig. 14, Comparison between the 3D measured activation sequence and the 3D imaged activation sequence for two polymorphic ventricular tachycardia beats in the canine heart. (From Ref. (Han et al., 2012))

intra-cardiac mapping from up to 216 intramural sites (Han et al., 2012). The quantitative comparison showed a good agreement between the non-invasively imaged activation sequence and its directly measured counterparts, as quantified by a CC of 0.74, an RE of 0.29, and an RMSE of 9ms averaged over all paced and ectopic beats. The origins of the activation were reasonably estimated to be ~7mm from the initiation sites determined from intra-cardiac mapping. These findings imply that 3DCEI is feasible in reconstructing spatial pattern of 3D ventricular activation sequence and localizing the arrhythmogenic foci on a beat-to-beat basis (Han et al., 2012).

The current imaging technique has a notable feature of imaging the cardiac activation

Table 9, Quantitative comparison between measured activation sequence and imaged activation sequence in norepinephrine induced ventricular tachycardia in the canine heart.

Canine	Origin Site	Arrhythmia Type	No. of Ectopic beats	CC	RE	LE (mm)	RMSE (ms)
C3	BRW	PVT	1	0.67	0.30	8.7	10
	MLW	PVC, Couplet, MVT, PVT	18	0.71	0.26	5.8	9
	Posterior MRW	PVC, Couplet, PVT	11	0.78	0.23	7.5	9
	LVA	MVT, PVT	17	0.73	0.28	7.1	5
C4	LVA	MVT	16	0.72	0.33	10.6	10
	MRW	PVC	3	0.74	0.29	6.8	13
	BRW	PVC	1	0.64	0.35	8.0	14
C5	MLW	PVC, Couplet, MVT, PVT	16	0.73	0.23	7.6	7
	BRW	PVC, Couplet, PVT	9	0.68	0.33	10.8	12
	LVA	PVT	4	0.74	0.33	6.8	11
		Mean		0.72±0.03	0.28±0.04	7.9±1.8	10±3

Note: CC, correlation coefficient; RE, relative error; LE, localization error; RMSE, root mean square error; BRW, basal right wall; MLW, middle left wall; MRW, middle right wall; LVA, left ventricle apex; RVA, right ventricle apex; PVC, premature ventricular complex; PVT, polymorphic ventricular tachycardia; MVT, monomorphic ventricular tachycardia. (From Ref. (Han et al., 2012))

sequence throughout the 3D ventricular myocardium, which represents an important alternative to other heart surface based imaging techniques. It is also noted that this physical-model-based 3DCEI approach only uses the general biophysical relationships governing the cardiac electrical activity and does not need to build a sophisticated cardiac electrophysiological model (Han et al., 2012). By solving the spatial-temporal linear inverse problem, the 3DCEI approach estimated the instantaneous current density at each grid point and then estimate the local activation time as the time instant at peak of current density magnitude (Liu et al., 2006b) throughout the ventricular myocardium. It is challenging to estimate the "spatial" distribution of ECD distribution from BSPM at a given time point, but the activation time as determined from the peak of the ECD time course is not distorted substantially by such spatial relationship between ECD distribution and BSPM, as we have demonstrated in previous computer simulation (Han et al., 2008) and in animal experiments in rabbits (Han et al., 2011) and dogs (Han et al., 2012). Therefore, this physical-model-based 3DCEI approach is minimally dependent on the physiological knowledge of cardiac electrical properties and has the potential to image various cardiac arrhythmias. Note that our imaging approach involves solving a linear inverse problem and no initialization is needed (Liu et al., 2006b).

Rigorous validation studies in biological systems are critical for any imaging approaches. The present study has used a novel *in vivo* experimental design in which BSPMs were obtained simultaneously with intramural electrical recordings from plunge-needle electrodes in a closed-chest condition, and thus provided quantitative assessments of the 3DCEI approach. The present work extended our validation study of the canine

heart (Han et al., 2012). Compared with previous validation study in the rabbit heart (Han et al., 2011), the canine model provides larger heart-torso geometry and closer approximation to humans in cardiac size and electrophysiological characteristics. As we experienced in the rabbit heart, we also observed that there was a slight discrepancy in timing between the measured and computed activation times. This was due to the intrinsic smoothing effects when we solved the inverse problem, especially at the earliest and latest activation times, when body surface potentials are of relatively small magnitudes compared with noise (Han et al., 2012). As such, the resultant solution may lead to spatially smoothed images, and thus caused the slightly delayed initiation and premature termination. Nevertheless, the imaged activation sequence still provided a close match to the direct measurements, suggesting that important information regarding ventricular excitation (e.g., global activation pattern, regions of early and late activation) has been preserved in imaged results. Furthermore, the initiation sites were estimated to be ~7mm from the measured sites, suggesting that resolution in the canine heart (12-times greater mass than rabbit heart) is associated with only a small (40%) change in resolution (versus ~5mm in rabbit heart) (Han et al., 2012). The present study suggests that the imaging accuracy does not necessarily scale linearly to the geometric size of the subject, but rather mainly determined by experimental procedures. It could be expected that in a clinical setting when human subjects are studied and different procedures involved (e.g., more BSPM electrodes would be used, and there would be no sternotomy), the imaging and localization errors would not increase further.

It is noted that two sets of UFCT images with and without IV contrast images were obtained on the anesthetized animals immediately after the mapping studies to accurately model the heart-torso geometry and localize the plunge-needle electrodes within the heart (Han et al., 2012). However, it was difficult to determine the exact name and label for each needle directly from the IV contrasted UFCT images for constructing the detailed heart model. Therefore, these needles were carefully replaced with labeled pins after the mapping study and the isolated heart was fixed in formalin. A third UFCT scan was performed on the formalin-fixed isolated heart to build the isolated heart model with 3D localization of plunge-needle electrodes, and the label for each needle in this isolated heart model was determined by photographs taken on the formalin-fixed isolated heart. This isolated heart model was carefully compared with the previously constructed detailed heart model from the heart-torso model so that the label of each needle within that detailed heart model could be identified.

It has been shown from direct intra-cardiac mapping techniques (Pogwizd & Corr, 1987; Pogwizd, 1994, 1995; Chung et al., 1997; Pogwizd et al., 1998; Zhang et al., 2000) that ventricular arrhythmias could arise from either subendocardium or subepicardium. Computational modeling of cardiac excitation plays an important role in dissecting the arrhythmia mechanisms throughout the 3D myocardium (Wei et al., 1995; Winslow et al., 2000; Hunter et al., 2003; Kerckhoffs et al., 2006; Deo et al., 2010; Trayanova, 2011). The 3DCEI approach represents an important and novel means, which offers the potentials to provide the additional noninvasive assessments of the underlying arrhythmia mechanisms throughout the ventricular myocardium and may facilitate interventional

therapeutic procedures (e.g., catheter ablation) by using a more targeted approach and shortening the procedure time (Han et al., 2012).

Single-beat noninvasive imaging of myocardial activation is important for the clinical diagnosis and management of hemodynamically unstable arrhythmias. Considering that not all arrhythmogenic substrates are accessible from endocardium, the necessity of applying epicardial ablation needs to be determined in some cases (Sosa et al., 2000). Being able to non-invasively assess the transmural location of the arrhythmogenic site prior to the procedure is likely to translate into a shortened time for the ablation procedure and potentially a reduction in risk to the patient by using a more targeted approach (Han et al., 2012). In the present study, we have infused NE in the canine heart to simulate the activation of the sympathetic nervous system and highly arrhythmic activities were induced including multiform PVCs and runs of nonsustained MVTs and PVTs. The measured activation sequence also showed that these arrhythmias usually originated within the subendocardium and may arise continuously from a single site or consecutively from multiple sites located at Purkinje cells or subendocardial myocardium (Han et al., 2012). The focal activation with NE induced VT resembles idiopathic VT in the human heart (Doppalapudi et al., 2009; Yamada et al., 2009). The origins have been well localized by the noninvasive 3DCEI approach with reasonably good accuracy. The performance is also consistent with those when imaging LV and RV pacing both in term of global pattern and timing difference. Furthermore, the beat-to-beat difference in activation pattern for the PVTs has been well characterized from the imaged activation maps. These results imply that this approach may be valuable for single-beat

imaging of focal ventricular arrhythmias arising in the deeper myocardium and facilitating the selection of clinical treatment options for these arrhythmias.

It is noted that the current experimental protocol (e.g., median sternotomy) may affect the imaging accuracy due to the change of the torso volume conductor property. However, with careful surgery procedure (e.g., multilayer-suture chest closing) and CT images after the mapping study to accurately model the heart-torso geometry, we minimized such changes on the volume conductor (Han et al., 2012). Besides, in order to perform a quantitative comparison for the global pattern between the imaged and measured activation sequences, an interpolation algorithm was used in the intra-cardiac mapping procedure to obtain the measured activation sequence throughout the 3D ventricular myocardium. However, we found that this yielded only a very slight decrease in performance by comparing the CC and RE in one dog with and without interpolation (Han et al., 2012).

In conclusion, the present study suggests that the 3DCEI approach can reconstruct 3D ventricular activation sequence and localize the origin of activation during pacing and focal ventricular arrhythmias, as validated by 3D intra-cardiac mapping procedure in the canine heart. It also implies the potential application of 3DCEI as a clinically complimentary tool to aid in localizing the origins of ventricular arrhythmias and understanding the mechanism of these arrhythmias.

Chapter 6

Experimental Investigation of Ventricular Arrhythmia Mechanisms

6.1. Ventricular Arrhythmias during Drug-induced QT Prolongation in the Rabbit Heart

6.1.1. Introduction

Torsades de pointes (TdP) is a life-threatening arrhythmia that might degenerate into ventricular fibrillation and cause sudden cardiac death. TdP can occur during the prolongation of QT interval, as a consequence of a genetic alteration in ion channel behavior or because of the administration of certain drugs. Various investigations have been made to examine the potential of drugs to prolong QT interval and cause TdP, which usually exhibits a characteristic twisting of QRS complexes around the isoelectric axis (Dessertenne, 1966). TdP has a continuously changing QRS morphology and thus requires single-beat mapping techniques to characterize the dynamic activation pattern within the heart. Three-dimensional (3D) intra-cardiac mapping technique emerges as an important tool to investigate the electrophysiological mechanism underlying the ventricular arrhythmias associated with QT prolongation in *in vivo* animal models (El-Sherif et al., 1996; Murakawa et al., 1997; Schreiner et al., 2004; Boulaksil et al., 2011).

Noninvasive cardiac electrical imaging techniques represent a novel means which offer the potential to help define the underlying arrhythmia mechanisms and may be used

to study the proarrhythmic effects of drug infusion and characterize the activation patterns of the associated arrhythmias. In this study, we investigate the 3D cardiac electrical imaging (3DCEI) technique to image TdP during drug-induced QT prolongation. The class III antiarrhythmic drug clofilium (Carlsson et al., 1992) and phenylephrine were infused in the *in vivo* rabbit model to prolong QT interval and induce ventricular arrhythmias (Batey & Coker, 2002) including premature ventricular complexes (PVCs), couplets, and TdPs. We performed simultaneous body surface potential mapping and 3D intra-cardiac mapping in a closed-chest condition in rabbits. The 3DCEI technique was applied to characterize the dynamic activation patterns of the induced arrhythmias. The imaged activation sequence was also compared with the simultaneously measured activation sequence from 3D intra-cardiac mapping.

6.1.2. Study Design

Eight healthy New Zealand white rabbits of either sex (3.6 to 4.3 kg) were studied under a protocol approved by the Institutional Animal Care and Use Committees of the University of Minnesota and the University of Alabama at Birmingham. The animal preparation and surgical procedure were as described in Chapter 4 (Han et al., 2011). Each rabbit was sedated with ketamine (35 mg/kg), intubated, and anesthetized using 2% isoflurane. Up to 64 repositionable BSPM electrodes were uniformly placed to cover the anterior-lateral chest up to the mid-axillary line. The heart was exposed via median sternotomy, and up to 27 transmural plunge-needle electrodes were inserted in the left ventricle (LV) and right ventricle (RV) of the rabbits. Each LV plunge-needle electrode

contains 8 bipolar electrode-pairs with an inter-electrode distance of 500 μm, while each RV electrode contains 2 bipolar electrode-pairs with an inter-electrode distance of 500 μm. The chest and skin were then carefully closed with silk suture. Bipolar electrograms were continuously recorded from all electrode-pairs together with body surface potentials from surface electrodes. At the completion of the mapping study, ultra fast computed tomography (UFCT) scans were performed on the living rabbit to obtain the heart-torso anatomical information and extract the location of BSPM electrodes on the chest and plunge-needle electrodes within the myocardium (Han et al., 2011). When UFCT scans after mapping study were unavailable in three rabbits, the pre-operative UFCT images obtained before the open-chest surgery and mapping study were used for constructing the heart-torso geometrical model. The rabbit was then euthanized and the plunge-needle electrodes were carefully localized by replacing each with a labeled pin. The heart was fixed in formalin and underwent a UFCT scan to further facilitate precise 3D localization of the transmural electrodes.

Ventricular arrhythmias including premature ventricular complexes (PVCs), couplets, and TdPs were induced by i.v. administration of clofilium and phenylephrine in combinations of various infusion rates and doses in the *in vivo* normal rabbit heart using an established protocol (Batey & Coker, 2002). Fig.15.A shows the protocol for drug infusion. For the first dose cycle, the phenylephrine infusion rate was begun at 75 nmol kg^{-1} min^{-1}, and gradually increased to 150, 225 and 300 nmol kg^{-1} min^{-1} for every 3 min, while clofilium was infused at 20 nmol kg^{-1} min^{-1} 5 min after the infusion of phenylephrine. This protocol was repeated at higher doses of clofilium at 60 and 200

nmol kg^{-1} min^{-1} with the same infusion rate for phenylephrine for the second and third dose cycle. There were 10 min intervals between different dose cycles (Batey & Coker, 2002).

Post-experiment data analysis was performed for the recorded ECG data. The QT interval was manually annotated from the beginning of Q wave to the end of the T wave.

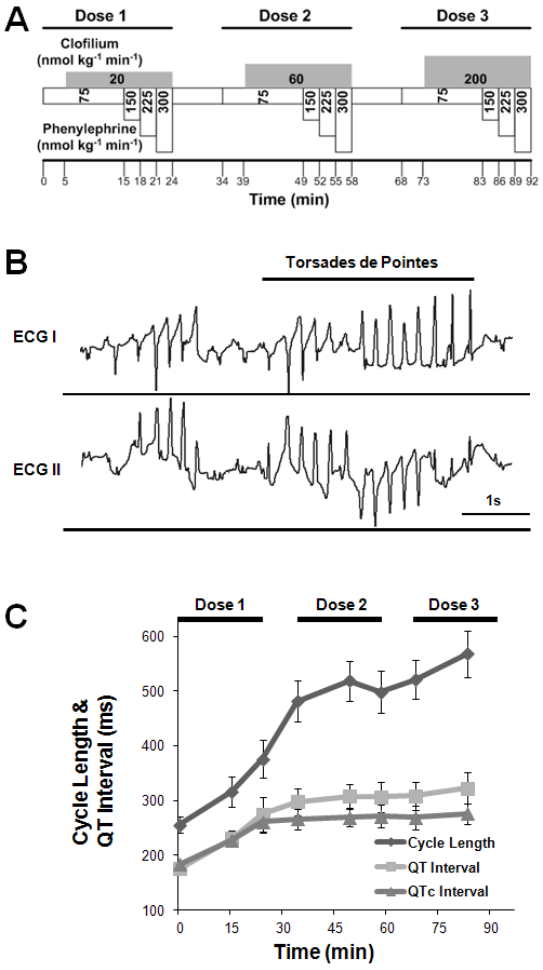

Fig. 15, (A) The drug infusion protocol for inducing torsade de pointes in the rabbit heart. (B) Example of an episode of torsades de pointes, where the twisting of the QRS complexes around the isoelectric line can be seen clearly. (C) The change of cycle length, QT interval, and rated-corrected QT (QTc) interval during the drug infusion for the three dose cycles.

The rate-corrected QT (QTc) interval was calculated according to Carlsson's formula: QTc = QT – 0.175(RR - 300) (Carlsson et al., 1992).

Subject-specific realistic geometry heart-torso model was built from UFCT images and 3DCEI was applied to image the activation sequence for each rabbit. The imaged activation sequence was compared with the simultaneously direct measurements obtained from 3D intra-cardiac mapping. The measured activation sequence within the 3D ventricular myocardium was constructed in the method described in Chapter 4 when the heart and torso UFCT scans after mapping study were available (Han et al., 2011). In three rabbits, when heart and torso UFCT scans after mapping study were unavailable, an alternative isolated heart surface model was built from the post-operative UFCT images of the isolated heart with labeled pins (representing the sites of transmural needles), and this heart surface model has been carefully co-registered with the detailed heart model built from pre-operative UFCT images using anatomical landmarks (e.g., apex, outflow tract, and atria appendages). The orientation and location of each needle could then be projected to the detailed heart model. The 3D measured activation sequence could then be reconstructed throughout the ventricular myocardium.

Numerical data are presented as mean ± SEM. The correlation coefficient (CC) was computed to quantify the agreement of overall activation pattern between the invasively measured activation sequence and the non-invasively imaged activation sequence. The localization error (LE) was computed to evaluate the performance of 3DCEI in localizing the origin of activation. Statistical significance of differences was evaluated by Student's t-test, and a P value < 0.05 was considered statistically significant.

6.1.3. Results

Eight healthy rabbits were studied in the present *in vivo* experiments. After insertion of plunge electrodes, closure of the chest did not alter heart rate or mean arterial blood pressure (232 ± 6 vs 238 ±6 bpm and 62±4 vs 62±3 mm Hg, respectively, P=NS vs pre-closure) or total activation times of sinus beats (31±1ms vs 29±1ms, P=NS vs pre-closure), which were consistent with previously published data in control rabbits in Chapter 4 and in (Pogwizd, 1995; Zhang et al., 2005; Han et al., 2011). The infusion of clofilium and phenylephrine led to the significant increase of the RR interval (255±14ms

Table 10, Summary of data analysis for ventricular arrhythmias induced during the infusion of clofilium and phenylephrine in rabbit heart.

Rabbit No.	Sex	PVC	Couplet	TdP	Sites of Initiation	
					RVOT	LV
1	F	+	+	+	Basal anterior.	Basal anterior.
2	F	+	+	+	Basal inferior, basal lateral.	Basal anterior, apical inferior.
3	M	+	+	+	Basal lateral, basal anterior.	Basal anterior, middle inferior.
4	F	+	+	-	Basal anterior.	Middle ante-lateral, apical inferior.
5	F	+	+	+	Middle anterior, middle septum.	Apical lateral.
6	F	+	+	-	Middle anterior.	Middle ante-septal, apical anterior.
7	F	+	+	-	Basal lateral.	Basal ante-septal, basal anterior, basal infe-lateral.
8	F	+	-	-	Basal lateral.	Apex.

Note: PVC, premature ventricular complex; TdP, torsades de pointes; RVOT, right ventricle outflow tract; LV, left ventricle.

to 376±34ms, P<0.05), the QT interval (175±7ms to 274±31ms, P<0.05), and the QTc interval (183±5ms to 262±21ms, P<0.05) during the first dose cycle, as shown in Fig.15.C. The change of QT intervals was greater in the first dose cycle, as compared to the other two cycles. Table 10 summarizes the ventricular arrhythmias induced during the

drug infusion. Ectopic activities in terms of multiform PVCs were observed in all animals during the infusion of clofilium and phenylephrine. TdPs were induced in four rabbits (See Figure 15.B for an example of TdP on ECG). One rabbit degenerated into ventricular fibrillation. Another two rabbits degenerated into asystole without ventricular fibrillation during the last dose cycle.

The realistic geometry rabbit heart-torso model was constructed for each animal from the UFCT images. The rabbit ventricular myocardium was tessellated into 6987±330 evenly-spaced grid points. The spatial resolution of the ventricle models was 1 mm.

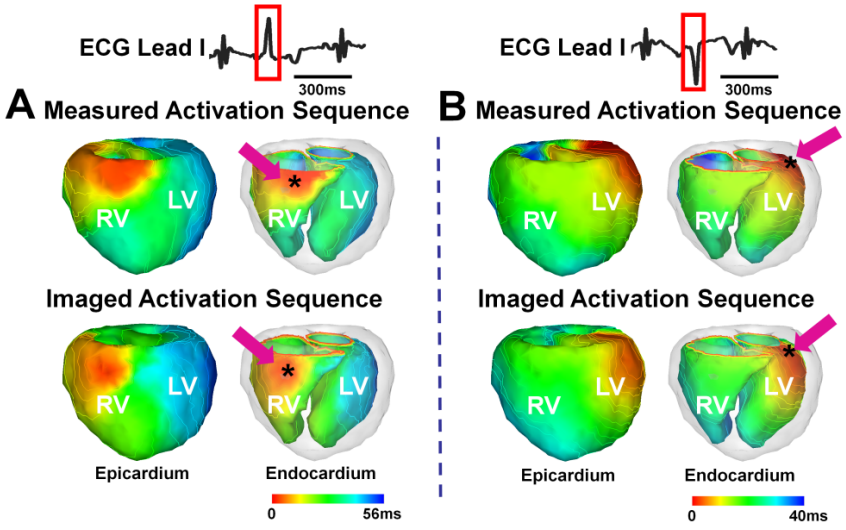

Fig. 16, Comparison between the measured activation sequence and the imaged activation sequence for two premature ventricular contractions with different activation patterns in (A) and (B) during the infusion of phenylephrine and clofilium in rabbit.

There were 151±7 intramural bipolar electrodes during 3D intra-cardiac mapping and 59±1 BSPM electrodes on the rabbit body surface.

Data analysis using 3DCEI and 3D intra-cardiac mapping performed on a total of 31 isolated PVCs and 7 couplets from all rabbits suggests that these ectopic beats initiated in the subendocardium by focal activation. For each rabbits, the PVCs were observed to continuously initiate at several myocardial sites. The initiation sites covered both LV and RV outflow tract (RVOT). PVCs initiated with a coupling interval of 407±18ms and conducted with a total activation time of 53±2ms, while the coupling interval and total activation time for couplets were 387±32ms and 56±2ms respectively. Fig.16.A and Fig.16.B show the comparison between the measured and imaged activation sequences

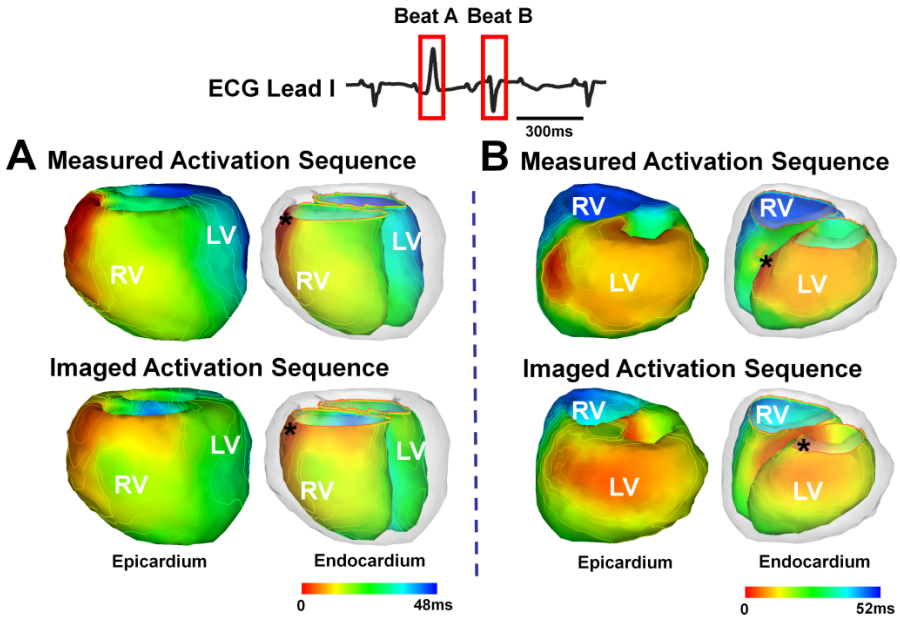

Fig. 17, Comparison between the measured activation sequence and the imaged activation sequence for a couplet with different activation patterns (A) and (B) during the infusion of phenylephrine and clofilium in rabbit.

for two PVC beats in rabbit 1 during the first dose cycle. The first PVC initiated at basal anterior RVOT, and the wavefront then propagated over the septum and terminated at middle lateral LV. The second PVC initiated at the basal anterior LV and terminated at

posterior RV. The imaged results resembled the measured counterparts with respect to the overall activation patterns. Furthermore, the initiation sites were reconstructed at basal anterior RVOT and basal anterior LV respectively. Multiple PVCs and beats from TdPs in rabbit 1 were observed to be continuously firing at these two sites. Fig.17 shows an example of a couplet from rabbit 7. The first beat in Fig.17.A initiated at basal lateral wall of RVOT, and then the wavefront propagated over the septum and terminated at middle left wall. The second beat of this couplet initiated at the basal anterior septum of LV and terminated at RV lateral wall, as shown in Fig.17.B. The imaged results captured the overall activation patterns for this couplet and the initial sites were identified at basal lateral wall of RVOT and basal anterior septum of LV respectively.

TdPs were induced in four rabbits. The QT interval and QTc interval of sinus beats right before the onset of first TdPs were increased as compared with those of sinus beats before drug infusion (285±29ms vs 180±14ms, $P<0.05$ for QT interval and 258±22ms vs 188±9ms, $P<0.05$ for QTc interval). Data analysis was performed on a total of 73 beats from 10 episodes of TdPs (three to twenty-two beats for each episode). The averaged cycle length was 263±10ms and the activation time was 52±1ms. All these ectopic beats had focal initiation. Fig.18 shows an example of a ten-beat TdP in rabbit 2. The ECG morphology exhibited TdP form with twisted QRS complexes around the isoelectric axis in ECG lead I. More negative QRS-complexes turned into more positive complexes with an intervening transition zone. The averaged cycle length was 195±8ms and the total activation time was 52±5ms for this TdP. Fig.18.A and Fig.18.B demonstrate the activation patterns during beat 2 and 9 respectively. At the beginning of this TdP,

activation initiated from a subendocardial site of the basal LV. From there, it spread to the basal lateral wall of RVOT. This activation pattern did not change significantly for the first 6 ectopic beats and the site of latest activation during an ectopic beat was far from the site of earliest activation of the following beat. Beat 9 and beat 10 demonstrated another typical activation pattern, with initiation located at the RV base, as shown in Fig.18.B. The mapping results further suggested that in the middle of this TdP, there was simultaneous early activation at two sites, with one site located at basal lateral RVOT and another site located at basal LV, indicating the fusion beats with two completing foci. The imaged activation sequences clearly captured such dynamic transition of activation

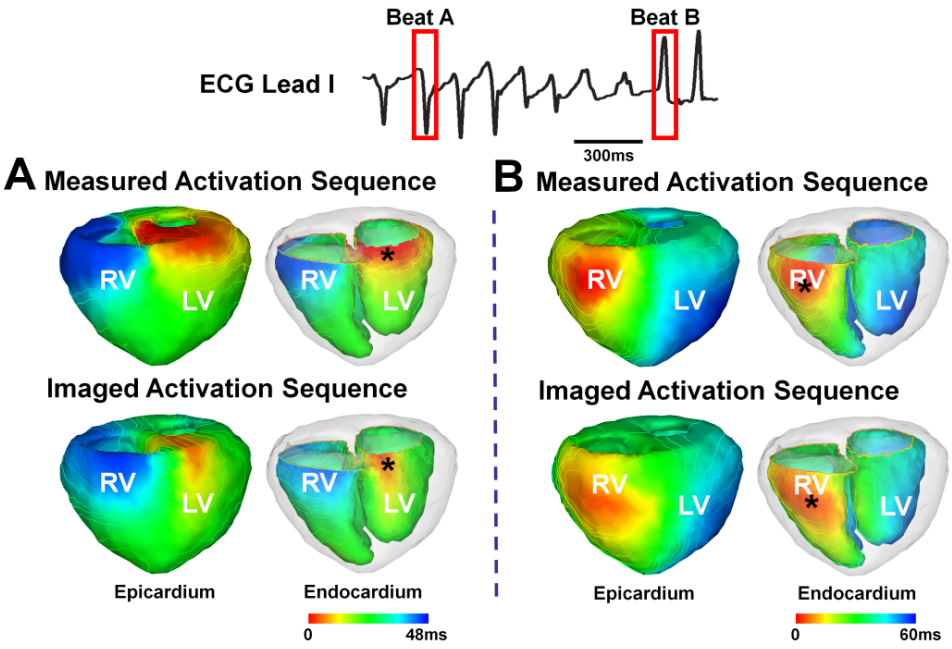

Fig. 18, Comparison between the measured activation sequence and the imaged activation sequence for ten-beat torsades de pointes during the infusion of phenylephrine and clofilium in rabbit.

patterns for this TdP. Besides, the two initiation sites of this TdP were well localized from the imaged activation maps. Fig.19 shows another example of a 6-beat TdP in rabbit 3. In this TdP, three different activation patterns were observed as shown in Fig.19.A, Fig.19.B, and Fig.19.C. In Fig.19.A, the first ectopic beat had an initiation site at anterior RVOT, and then the initiation site shifted to anterior middle wall of LV for the second ectopic beat (Fig.19.B). The last four ectopic beats had continuously been firing at the same site at post-lateral wall of middle RV (Fig.19.C). The averaged cycle length was 220±8ms and the activation time was 48±2ms for this TdP. The imaged activation sequence clearly captured such shift of initial activation sites and the overall activation patterns were in good agreement with the measurements.

Averaging 111 ectopic beats from PVCs, couplets, and TdPs with single focal initiation site, the CC was 0.65±0.02, suggesting good agreement between the imaged

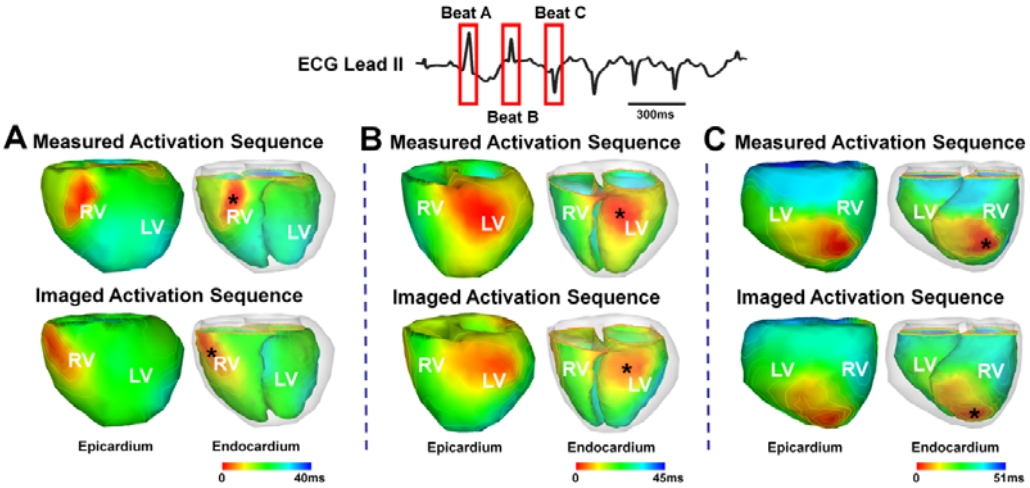

Fig. 19, Comparison between the measured activation sequence and the imaged activation sequence for a six-beat torsades de pointes in rabbit 3. Panels (A), (B), and (C) show the activation sequence for the first three beats respectively.

activations sequence with the simultaneous measurements. Furthermore, the origin of arrhythmias was estimated to be 5.9±0.3 mm from the measured site, implying the reasonably good localization accuracy.

6.1.4. Discussion

The present study reports the use of a novel 3DCEI technique to non-invasively investigate the global activation pattern of cardiac arrhythmias during drug-induced QT-prolongation in the *in vivo* rabbit heart. We showed that the infusion of clofilium and phenylephrine led to QT prolongation and induced different forms of ventricular arrhythmias during simultaneous body surface potential mapping and 3D intra-cardiac mapping. The data analysis suggested that the ectopic beats including PVCs, couplets, and TdPs were all initiated by a focal mechanism and the TdPs were initiated at focal sites and maintained with the dynamical shift of initiation sites or two completing foci. The non-invasively imaged activation sequences were in good correlation with the simultaneous intra-cardiac measurements with an averaged CC of 0.65±0.02 and LE of ~5mm over 111 ectopic beats with single initiation site. These findings imply that 3DCEI is feasible in reconstructing global activation pattern and imaging dynamically changing arrhythmias on a beat-to-beat basis.

This work extended our previous study in the control rabbits into investigating the 3DCEI technique for imaging activation sequence in the setting of drug-induced prolongation of action potential and QT interval in rabbits. The imaging performance was consistent to our previous findings in the control rabbits in terms of CC and LE. The

close match between the imaged activation sequence and the direct measurement suggests that significant information regarding ventricular excitation (e.g., global activation pattern and regions with earliest and latest activation) has been preserved in the imaged activation maps in this animal model of human disease.

The results suggest the potential clinical role of 3DCEI in diagnosing arrhythmia mechanisms and complementing cardiac mapping techniques. In this study, different ventricular arrhythmias including PVCs, couplets, and TdPs were induced during the infusion of clofilium and phenylephrine in the *in vivo* rabbit heart. We also observed short episodes of TdP that had a clear twisting of QRS complexes around the isoelectric line. The mechanism of TdP perpetuation is still not clear. Two possible mechanisms have been suggested: focal activity due to triggered activity and reentry. Both arrhythmogenic mechanisms have been documented during cardiac mapping studies (El-Sherif et al., 1996; Murakawa et al., 1997; Asano et al., 1997; Akar et al., 2002; Schreiner et al., 2004; Boulaksil et al., 2011). In the present study, both the 3D intra-cardiac mapping results and the noninvasive imaging results suggested the focal mechanism for these TdPs that were recorded during the study. The results further suggested the two competing foci which provided the underlying electrophysiological mechanism for the twisted QRS morphology in ECG for the episodes of TdP. While the current study cannot provide a clear cut answer to explain the discrepancies between focal and reentry mechanisms for TdP, the findings imply the potential role of 3DCEI for characterizing the activation patterns of dynamically-changing polymorphic ventricular arrhythmias and studying the proarrhythmic effects during drug infusion.

In conclusion, the present study suggests the capability of the 3DCEI technique to dynamically characterize the 3D ventricular activation patterns and localize the origin of activation during polymorphic ventricular arrhythmias with drug-induced QT prolongation, as evaluated by 3D intra-cardiac mapping procedure in the rabbit heart. The findings imply the potential application of 3DCEI to aid in studying the proarrhythmic effects of drug infusion and understanding the arrhythmia mechanisms associated with QT prolongation in the clinical setting.

6.2. Ventricular Arrhythmias in a Canine Model of Nonischemic Heart Failure

6.2.1. Introduction

Congestive heart failure (HF) afflicts approximately 5 million individuals in the United States alone and is responsible for ~200,000 deaths per year, primarily from ventricular tachycardia (VT) degenerating to ventricular fibrillation (Packer, 1985). Noninvasive cardiac electric imaging techniques provide a much needed means which offers the potential to help with delineation of the underlying arrhythmia mechanisms related to HF and to facilitate corresponding selections of treatment options for HF and its related arrhythmias (e.g., guiding catheter ablation (Wood & Morady, 1999) or implantation of cardiac resynchronization therapy (Spragg et al., 2010)). In previous chapters, we have rigorously and extensively validated the 3DCEI technique in rabbit heart (Han et al., 2011) and canine heart (Han et al., 2012) without structure diseases. In

this study, we investigate the activation patterns of spontaneously occurring and induced VTs in a newly-developed arrhythmogenic canine model of nonischemic HF by using noninvasive 3DCEI and 3D intra-cardiac mapping in a close-chest condition.

6.2.2. Study Design

The experimental protocol, approved by the Institutional Animal Care and Use Committees of the University of Minnesota and the University of Alabama at Birmingham, was performed on two canines. HF in each dog was produced by induction of aortic insufficiency, which was later followed by constriction of the abdominal aorta. Aortic insufficiency was created via the carotid artery, in which a small catheter was pushed through the aortic valve between the LV and the aorta. Aortic constriction was created through an abdominal incision in which a suture was placed around the aorta and/or one renal artery to decrease the vessel diameter by ~50%. The dogs survived for up to a maximum of 24 months after which a terminal mapping study was performed. Progression of HF was assessed by LV end-diastolic dimension, LV end-systolic dimension and LV fractional shortening using Doppler echocardiography.

Simultaneous body surface potential mapping and 3D intra-cardiac mapping was performed on the dogs when severe HF was developed for the terminal study. The animal preparation and surgical procedure were similar to the normal canine experiment in Chapter 5. There were 128 repositionable BSPM electrodes uniformly placed to cover both the anterior-lateral chest up to the mid-axillary line and the posterior chest. The heart was exposed via median sternotomy, and up to 47 transmural plunge-needle

electrodes were inserted in the LV and right ventricle (RV). Spontaneously occurring ventricular arrhythmias including PVC, couplet, and VT were recorded during the mapping study. Norepinephrine (NE) was later infused at 1.6-3.2μg/kg/min to further induce ventricular arrhythmias. At the completion of the mapping study, UFCT scans were performed on the living HF dog to obtain the needed anatomical information. The plunge-needle electrodes were then carefully localized by replacing each with a labeled pin (Han et al., 2012). A post-operative UFCT scan of the formalin-fixed isolated heart was subsequently performed to further facilitate precise 3D localization of the transmural electrodes.

For each HF dog, the 3DCEI approach was applied to non-invasively reconstruct the activation sequence throughout the ventricular myocardium. The realistic geometry heart-torso model was constructed from UFCT images. This heart-torso model was exported for further forward and inverse computation. The performance of 3DCEI was evaluated by comparing the non-invasively imaged activation sequence with the simultaneously direct measurements obtained from 3D intra-cardiac mapping. The measured activation sequence within the 3D ventricular myocardium was constructed as we did for control canine in Chapter 5. Data are expressed as mean ± SD. The CC was computed to quantify the agreement of overall activation pattern between the invasively measured activation sequence and the non-invasively imaged activation sequence. LE was calculated to evaluate the performance of 3DCEI in localizing the origin of activation. Statistical significance of differences was evaluated by Student's t-test (paired or unpaired), and a P value < 0.05 was considered statistically significant.

6.2.3. Results

With HF, LV end diastolic dimension increased by 39% (average of 3.72 cm to 5.18 cm), and LV fraction shortening decreased by 14% (average of 44% to 37%). The realistic geometry canine heart-torso model was constructed from UFCT images obtained after the mapping study. The canine ventricular myocardium was tessellated into 27853±5560 evenly-spaced grid points. The spatial resolution of the ventricle models was 2 mm.

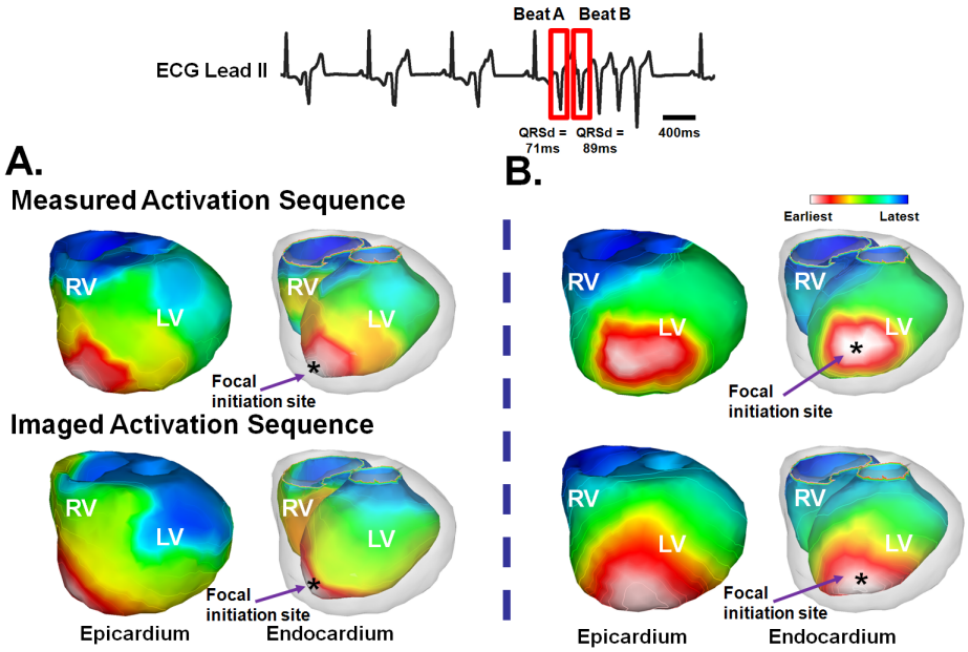

Fig. 20, Comparison between measured activation sequence and imaged activation sequence for a five-beat spontaneously occurring ventricular tachycardia in a heart failure canine.

Data analysis was performed on spontaneously occurring and NE-induced arrhythmias including 10 PVCs, 3 couplets, and 13 episodes of VTs. The NE-induced VTs (n=10) were longer than the spontaneously occurring VTs (n=3) (12±11 vs 4±1

beats long, $p<0.05$), and the NE-induced VTs were also more rapid than the spontaneously occurring VTs (cycle length of 240±46 vs 394±35 ms, $p<0.05$). Good correlation was obtained between imaged activation sequence and direct measurements (averaged CC of 0.70). Initiation sites were reconstructed to be ~10mm from measured sites, suggesting good localization in a large animal model with cardiac size similar to human.

Fig.20 shows an example of a five-beat polymorphic VT spontaneously occurring without any drug intervention during the mapping study. The ECG shows that this VT was preceded by ventricular bigeminy, which was generated by the interaction between a sinus beat and a PVC beat. As shown in Fig.20.A, the first VT beat initiated at subendocardium of LV apex and the wavefront then terminated at the basal posterior ventricles. Both the 3DCEI-imaged results and direct invasive measurements showed that this VT beat had the same activation pattern with the PVCs in the preceding bigeminy. Fig.20.B shows the second VT beat, where the initiation site has shifted to the middle lateral wall of LV. This VT was maintained by shifting the initiation site within the two sites (in Fig.20.A and Fig.20.B) for the following three beats. The non-invasively imaged activation sequence showed good agreement with the measured activation sequence, and the shift of initiation site was well captured from the imaged maps.

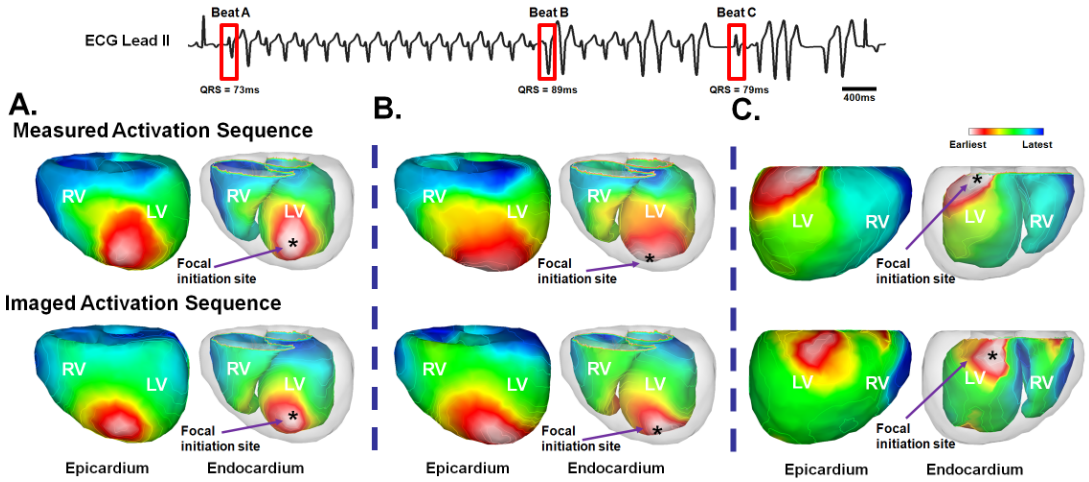

Fig. 21, Comparison between measured activation sequence and imaged activation sequence for a thirty one-beat ventricular tachycardia induced by norepinephrine in a heart failure canine.

Another example of a thirty one-beat polymorphic VT induced by NE is shown in Fig.21. All the ectopic beats in this VT had focal activation pattern. As shown in Fig.21.A, the beginning of this VT has been continuously firing at a high LV apex site slightly closer to anterior wall. However, starting from middle stage of this VT, other initiation sites were also observed among different ectopic beats. Fig.21.B shows that VT beat B (indicated in the red box of ECG lead II in the figure) had a slightly different activation pattern where the initiation site has shifted to the low LV apex. Fig.21.C shows another activation pattern for the VT beat C (also indicated in the red box of ECG lead II in the figure), where the initiation site moved to posterior base of LV. Such dynamic shift of initiation site has been well captured in the non-invasively imaged activation sequence.

6.2.4. Discussion

In this study, we investigated the 3DCEI approach for characterizing the global activation pattern and localizing origin of activation during both the spontaneously occurring and NE-induced ventricular arrhythmias in a novel arrhythmogenic model of nonischemic HF. We showed that both the spontaneously occurring VTs and NE-induced VTs were initiated and maintained by a focal mechanism. Good agreement was obtained between the non-invasively imaged activation sequence and its directly measured counterpart, as quantified by a CC of ~0.70 and an LE of ~10mm averaged over 135 ectopic beats. These findings imply that 3DCEI is feasible in non-invasively characterizing the spatial patterns of ventricular activation sequences, and localizing the arrhythmogenic foci on a beat-to-beat basis in the setting of nonischemic HF.

This present work extended our previous study in the normal animals in evaluating the 3DCEI technique in the setting of diseased heart by using an arrhythmogenic canine model with nonischemic HF. The imaging performance was consistent to our previous findings in the control canines in terms of CC. The close match between the imaged activation sequence and the direct measurement suggests that significant information regarding ventricular excitation (e.g., global activation pattern and regions with earliest and latest activation) has been preserved in the imaged activation maps in such animal model with diseased heart. Considering the large increase of cardiac volume size, the slight increase of localization accuracy is reasonable, indicating the good localization of 3DCEI in a large animal model with cardiac size similar to human.

Previous invasive 3D intra-cardiac mapping showed that spontaneously occurring PVCs and VTs in a nonischemic HF rabbit model were initiated in the subendocardium by a nonreentrant mechanism (Pogwizd, 1995). Focal mechanism was also observed in patients with idiopathic dilated cardiomyopathy (Pogwizd et al., 1998). In the present study, the findings for the mechanism of spontaneously occurring arrhythmias were consistent with the previous invasive mapping results. Similar to the spontaneously occurring VTs, the NE-induced VTs arose by a similar mechanism. However, the NE-induced VTs were faster and longer than the spontaneously occurring VTs. The good correlation between the imaged activation sequence and the measured activation sequence implies that 3DCEI may become a noninvasive and important alternative to the direct intra-cardiac mapping. It could potentially improve clinical diagnosis and understanding of the arrhythmias mechanisms in patients and thus facilitate developing mechanism-based therapy and patient specific treatments.

Another innovation of the present study is that we did not assume any a priori properties of the HF heart tissue. Rather, our model is based on the fundamental cardiac biophysics with regard to the myocardial excitation. With such basic assumption, our results demonstrate the feasibility of noninvasive activation imaging throughout the 3D myocardium in the HF canine, as validated from simultaneous intra-cardiac mapping. The present study suggests the potential application of 3DCEI as a clinically useful tool to aid diagnosis of ventricular arrhythmias associated with HF patients and to facilitate the selection of the corresponding mechanism-based treatment options for HF patients.

Chapter 7
Conclusions and Future Work

7.1. Conclusions

Noninvasive imaging of the cardiac electrical activity is of great importance for both basic cardiovascular research and clinical medicine. In this dissertation, the recently developed physical-model-based three-dimensional cardiac electrical imaging (3DCEI) approach is rigorously investigated.

The computer simulation provides a rigorous evaluation of the physical-model-based 3DCEI under a realistic and well-controlled environment, and thus provides us the reference for understanding the experimental data. The present computer simulation study in a simulated rabbit model in single-site pacing and dual-site pacing demonstrates that the physical-model-based 3DCEI can localize the initial site of cardiac activation and image the cardiac activation sequences throughout the three-dimensional ventricular myocardium with reasonable accuracy. These promising results represent a significant step toward the potential clinical establishment of the 3DCEI approach and demonstrate the feasibility for experimentally validating this approach in animals.

The performance of 3DCEI is experimentally and rigorously evaluated through well-controlled animal validation studies in both the small animal model (thirteen rabbits) and large animal model (five canines). By comparing the 3DCEI-imaged results with

simultaneous measurements through intra-cardiac mapping with plunge-needle electrodes inserted throughout the myocardium, the experimental investigations validate the ability of 3DCEI to image cardiac activation sequence and localize the origin of activation during single-site and dual-site paced rhythms, as well as norepinephrine-induced ventricular arrhythmnias. The consistent agreement between the non-invasively imaged activation sequence and its directly measured counterparts in both the rabbit heart and canine heart, implies that 3DCEI is feasible in reconstructing the spatial patterns of ventricular activation sequences, localizing the focal or multiple arrhythmogenic foci, and imaging dynamically changing arrhythmia on a beat-to-beat basis. It also implies the potential application of 3DCEI as a clinically useful tool to aid in localizing the origins of ventricular arrhythmias and understanding the mechanism of these arrhythmias.

The clinical relevance and the potential clinical role of 3DCEI are further demonstrated by investigating 3DCEI in the animal models simulating cardiovascular diseases in human. In one group, the QT prolongation is induced in eight rabbits using a novel protocol of drug infusion and 3DCEI is used to characterize the activation pattern for the ventricular arrhythmias accociated with QT prolongation. The promising results imply the potential application of 3DCEI to aid in studying the proarrhythmic effects of drug infusion and understanding the arrhythmia mechanisms associated with QT prolongation in the clinical setting. In another group, 3DCEI is used to investigate the activation patterns of spontaneously occurring and induced ventricular tachycardia in a newly-developed arrhythmogenic canine model of nonischemic heart failure in two canines. The promising results suggest the potential application of 3DCEI as a clinically

useful tool to aid diagnosis of ventricular arrhythmias associated with heart failure patients.

In summary, the present dissertation study investigates a novel physical-model-based 3DCEI approach through both computer simulation and animal experiments with difference electrophysiological conditions. The promising results presented in this dissertation study suggest that this cardiac electrical imaging approach may provide an important alternative for non-invasively imaging cardiac electrical activity throughout ventricular myocardium and may potentially become an important tool to facilitate clinical diagnosis and treatments of malignant ventricular arrhythmias.

7.2. Future Work

The present dissertation study provides promising results on the physical-model-based 3DCEI approach. On the other hand, there are some works that can be made for the further improvement of 3DCEI.

In the present dissertation study, we focus on investigating 3DCEI in imaging ventricular electrical activity during both the computer simulation study and animal experiments, without investigating the electrical activity in both atria. It is noted that cardiac electrical activities are distributed throughout the whole heart, and there are interactions between atria and ventricles. Besides, atrial arrhythmias account for a very large patient population. Therefore in the future study, it would be important to extend

the development of 3DCEI methodology in atrial arrhythmias, such as atrial tachycardia, atrial flutter, and atrial fibrillation.

The significance of this dissertation study lies in that the 3DCEI technique would facilitate clinical diagnosis and management of various cardiac arrhythmias. While in this dissertation study we demonstrate that 3DCEI is capable of imaging experimentally-induced ventricular arrhythmias, the present dissertation study is limited in animal experiments. Besides, some human arrhythmias can be much more complex than those we have induced and investigated in animals. Under certain conditions, the arrhythmias in human may be very different from those in animal models. Therefore, to further develop and improve the 3DCEI approach, it would be very important to validate the approach in human subjects, to quantify its capability of imaging human arrhythmias, and to establish its clinical role in facilitating clinical treatment of those cardiac diseases.

The fundamental basis of the 3DCEI lies in mathematically modeling the cardiac electrical activity using equivalent cardiac source models and extracting the cardiac excitation information from the inverse solution of the equivalent source model. In this dissertation project, we mainly focus on extracting cardiac activation sequence from the reconstructed equivalent current densities. On the other hand, other clinically important information can also be extracted from the equivalent source models. For example, the myocardial infarction substrate may be identified directly from equivalent current densities. Therefore, in the future study, it would be important to extend the 3DCEI in extracting other clinically useful features (e.g., localization of myocardium infarction) from the inverse solution of equivalent source models.

In the present dissertation study, we report the localization accuracy of the 3DCEI technique to be between 5-10 mm for localizing origin of activation, varying among the size of the heart. Such localization accuracy is reasonable and promising, since it is also consistent with the outcome of cardiac catheter ablation (ablation usually creates a lesion of 5-10mm (Simmons et al., 1996)) and thus the results have clinical values in facilitating management of cardiac arrhythmias. However, there is also room for further development of the method and improving accuracy of the imaging algorithms by applying additional physical constraints or physiologically meaningful constraints.

In conclusion, despite many challenges, with the integrated efforts of methodology development, experimental investigation, and clinical validation, it can be foreseen that the physical-model-based 3DCEI approach will become an important clinical tool for noninvasive diagnosis of cardiac abnormalities, and may also improve our understanding of the basic physiological mechanisms underlying the cardiac electrical activity.

Literature Cited

Abboud, S., Eshel, Y., Levy, S. & Rosenfeld, M. 1994, "Numerical calculation of the potential distribution due to dipole sources in a spherical model of the head", *Computers and Biomedical Research,* vol. 27, no. 6, pp. 441-455.

Abildskov, J., Burgess, M., Lux, R.L. & Wyatt, R.F. 1976, "Experimental evidence for regional cardiac influence in body surface isopotential maps of dogs", *Circulation research,* vol. 38, no. 5, pp. 386-391.

Abraham, W.T., Fisher, W.G., Smith, A.L., Delurgio, D.B., Leon, A.R., Loh, E., Kocovic, D.Z., Packer, M., Clavell, A.L. & Hayes, D.L. 2002, "Cardiac resynchronization in chronic heart failure", *New England Journal of Medicine,* vol. 346, no. 24, pp. 1845-1853.

Akahoshi, M., Hirai, M., Inden, Y., Sano, H., Shimizu, A., Kondo, T., Makino, M., Horiba, M., Yoshida, Y. & Tsuboi, N. 1997, "Body-surface distribution of changes in activation-recovery intervals before and after catheter ablation in patients with Wolff-Parkinson-White syndrome: clinical evidence for ventricular 'electrical remodeling' with prolongation of action-potential duration over a preexcited area", *Circulation,* vol. 96, no. 5, pp. 1566-1574.

Akar, F.G., Yan, G.X., Antzelevitch, C. & Rosenbaum, D.S. 2002, "Unique topographical distribution of M cells underlies reentrant mechanism of torsade de pointes in the long-QT syndrome", *Circulation,* vol. 105, no. 10, pp. 1247-1253.

Armoundas, A.A., Feldman, A.B., Mukkamala, R. & Cohen, R.J. 2003, "A single equivalent moving dipole model: An efficient approach for localizing sites of origin of ventricular electrical activation", *Annals of Biomedical Engineering,* vol. 31, no. 5, pp. 564-576.

Asano, M., Davidenko, M., Jorge, M., Baxter, M., William, T., Gray PhD, R.A. & Jalife, M. 1997, "Optical mapping of drug-induced polymorphic arrhythmias and torsade de pointes in the isolated rabbit heart", *Journal of the American College of Cardiology,* vol. 29, no. 4, pp. 831-842.

Barr, R.C. & Spach, M. 1978, "Inverse calculation of QRS-T epicardial potentials from body surface potential distributions for normal and ectopic beats in the intact dog", *Circulation Research,* vol. 42, no. 5, pp. 661-675.

Barr, R.C., Pilkington, T.C., Boineau, J.P. & Spach, M.S. 1966, "Determining surface potentials from current dipoles, with application to electrocardiography", *IEEE Transactions on Biomedical Engineering,* vol. 13, no. 2, pp. 88-92.

Barr, R.C., Ramsey, M., & Spach, M.S. 1977, "Relating epicardial to body surface potential distributions by means of transfer coefficients based on geometry measurements", *IEEE Transactions on Biomedical Engineering,* vol. 24, no. 1, pp. 1-11.

Batey, A.J. & Coker, S.J. 2002, "Proarrhythmic potential of halofantrine, terfenadine and clofilium in a modified in vivo model of torsade de pointes", *British Journal of Pharmacology,* vol. 135, no. 4, pp. 1003-1012.

Berger, T., Fischer, G., Pfeifer, B., Modre, R., Hanser, F., Trieb, T., Roithinger, F.X., Stuehlinger, M., Pachinger, O. & Tilg, B. 2006, "Single-beat noninvasive imaging of cardiac electrophysiology of ventricular pre-excitation", *Journal of the American College of Cardiology,* vol. 48, no. 10, pp. 2045-2052.

Berger, T., Pfeifer, B., Hanser, F.F., Hintringer, F., Fischer, G., Netzer, M., Trieb, T., Stuehlinger, M., Dichtl, W. & Baumgartner, C. 2011, "Single-beat noninvasive imaging of ventricular endocardial and epicardial activation in patients undergoing CRT", *PLoS One,* vol. 6, no. 1, pp. e16255.

Boulaksil, M., Jungschleger, J.G., Antoons, G., Houtman, M.J.C., de Boer, T.P., Wilders, R., Beekman, J.D., Maessen, J.G., van der Hulst, F.F. & van der Heyden, M.A.G. 2011, "Drug-induced torsade de pointes arrhythmias in the chronic AV block dog are perpetuated by focal activity ", *Circulation: Arrhythmia and Electrophysiology,* vol. 4, no. 4, pp. 566-576.

Brooks, D.H., Ahmad, G.F., MacLeod, R.S. & Maratos, G.M. 1999, "Inverse electrocardiography by simultaneous imposition of multiple constraints", *IEEE Transactions on Biomedical Engineering,* vol. 46, no. 1, pp. 3-18.

Burnes, J.E., Taccardi, B., MacLeod, R.S. & Rudy, Y. 2000, "Noninvasive ECG imaging of electrophysiologically abnormal substrates in infarcted hearts: A model study", *Circulation,* vol. 101, no. 5, pp. 533-540.

Carlsson, L., Abrahamsson, C., Drews, L. & Duker, G. 1992, "Antiarrhythmic effects of potassium channel openers in rhythm abnormalities related to delayed repolarization", *Circulation,* vol. 85, no. 4, pp. 1491-1500.

Chung, M.K., Pogwizd, S.M., Miller, D.P. & Cain, M.E. 1997, "Three-dimensional mapping of the initiation of nonsustained ventricular tachycardia in the human heart", *Circulation,* vol. 95, no. 11, pp. 2517-2527.

Ciaccio, E.J., Chow, A.W., Davies, D.W., Wit, A.L. & Peters, N.S. 2004, "Localization of the isthmus in reentrant circuits by analysis of electrograms derived from clinical noncontact mapping during sinus rhythm and ventricular tachycardia", *Journal of Cardiovascular Electrophysiology,* vol. 15, no. 1, pp. 27-36.

Cuppen, J.J.M. & van Oosterom, A. 1984, "Model studies with the inversely calculated lsochrones of ventricular depolarization", *IEEE Transactions on Biomedical engineering,* vol. 31, no. 10, pp. 652-659.

Deo, M., Boyle, P.M., Kim, A.M. & Vigmond, E.J. 2010, "Arrhythmogenesis by single ectopic beats originating in the Purkinje system", *American Journal of Physiology-Heart and Circulatory Physiology,* vol. 299, no. 4, pp. H1002-H1011.

Dessertenne, F. 1966, "La tachycardie ventriculaire a deux foyers opposes variables", *Arch Mal Coeur,* vol. 59, pp. 263-272.

DiMarco, J.P. 2003, "Implantable cardioverter–defibrillators", *New England Journal of Medicine,* vol. 349, no. 19, pp. 1836-1847.

Dong, J., Calkins, H., Solomon, S.B., Lai, S., Dalal, D., Lardo, A., Brem, E., Preiss, A., Berger, R.D. & Halperin, H. 2006, "Integrated electroanatomic mapping with three-dimensional computed tomographic images for real-time guided ablations", *Circulation,* vol. 113, no. 2, pp. 186-194.

Doppalapudi, H., Yamada, T., Ramaswamy, K., Ahn, J. & Kay, G.N. 2009, "Idiopathic focal epicardial ventricular tachycardia originating from the crux of the heart", *Heart Rhythm,* vol. 6, no. 1, pp. 44-50.

Durrer, D., Van Dam, R., Freud, G., Janse, M., Meijler, F. & Arzbaecher, R. 1970, "Total excitation of the isolated human heart", *Circulation,* vol. 41, no. 6, pp. 899-912.

Durrer, D. & van der Tweel, L.H. 1954, "Spread of activation in the left ventricular wall of the dog. II. Activation conditions at the epicardial surface", *American Heart Journal,* vol. 47, no. 2, pp. 192-203.

Einthoven, W. 1906, "Le telecardiogramme", *Archives Internationales de Physiologie,* vol. 4, pp. 132-164.

El-Sherif, N., Caref, E.B., Yin, H. & Restivo, M. 1996, "The electrophysiological mechanism of ventricular arrhythmias in the long QT syndrome: tridimensional mapping of activation and recovery patterns", *Circulation Research,* vol. 79, no. 3, pp. 474-492.

Fischer, G., Tilg, B., Modre, R., Huiskamp, G., Fetzer, J., Rucker, W. & Wach, P. 2000, "A bidomain model based BEM-FEM coupling formulation for anisotropic cardiac tissue", *Annals of Biomedical Engineering,* vol. 28, no. 10, pp. 1229-1243.

Flowers, N. & Horan, L. 1995, "Body surface potential mapping" in *Cardiac Electrophysiology: From Cell to Bedside*, 2th edn, ed. D.P. Zipes & J. Jalife, W.B. Saunder Company, Philadelphia, pp. 1049-1067.

Franzone, P.C., Guerri, L., Taccardi, B. & Viganotti, C. 1985, "Finite element approximation of regularized solutions of the inverse potential problem of electrocardiography and applications to experimental data", *Calcolo,* vol. 22, no. 1, pp. 91-186.

Franzone, P.C., Taccardi, B. & Viganotti, C. 1978, "An approach to inverse calculation of epicardial potentials from body surface maps", *Advances in Cardiology,* vol. 21, pp. 50-54.

Gelernter, H. & Swihart, J. 1964, "A mathematical-physical model of the genesis of the electrocardiogram", *Biophysical Journal,* vol. 4, no. 4, pp. 285-301.

Gepstein, L., Hayam, G. & Ben-Haim, S.A. 1997, "A novel method for nonfluoroscopic catheter-based electroanatomical mapping of the heart: in vitro and in vivo accuracy results", *Circulation,* vol. 95, no. 6, pp. 1611-1622.

Ghosh, S., Rhee, E.K., Avari, J.N., Woodard, P.K. & Rudy, Y. 2008, "Cardiac memory in patients with Wolff-Parkinson-White syndrome: Noninvasive imaging of activation and repolarization before and after catheter ablation", *Circulation,* vol. 118, no. 9, pp. 907-915.

Goldberger, E. 1942, "The aVL, aVR, and aVF leads; A simplification of standard lead electrocardiography", *American Heart Journal,* vol. 24, no. 3, pp. 378-396.

Gornick, C.C., Adler, S.W., Pederson, B., Hauck, J., Budd, J. & Schweitzer, J. 1999, "Validation of a new noncontact catheter system for electroanatomic mapping of left ventricular endocardium", *Circulation,* vol. 99, no. 6, pp. 829-835.

Grave de Peralta-Menendez, R. & Gonzalez-Andino, S.L. 1998, "A critical analysis of linear inverse solutions to the neuroelectromagnetic inverse problem", *IEEE Transactions on Biomedical Engineering,* vol. 45, no. 4, pp. 440-448.

Greensite, F. 2004, "Heart surface electrocardiographic inverse solutions" in *Modeling and Imaging of Bioelectric Activity-Principles and Applications*, ed. B. He, Kluwer Academic/Plenum, New York, pp. 119-160.

Greensite, F. & Huiskamp, G. 1998, "An improved method for estimating epicardial potentials from the body surface", *IEEE Transactions on Biomedical Engineering,* vol. 45, no. 1, pp. 98-104.

Gulrajani, R.M. 2005, "The forward problem of electrocardiography: Theoretical underpinnings and applications" in *Modeling and Imaging of Bioelectric Activity-Principles and Applications*, ed. B. He, Kluwer Academic/Plenum, New York, pp. 43-79.

Gulrajani, R.M. 1998a, "The forward and inverse problems of electrocardiography", *IEEE Engineering in Medicine and Biology Magazine,* vol. 17, no. 5, pp. 84-101.

Gulrajani, R.M. 1998b, *Bioelectricity and Biomagnetism,* Wiley, New York.

Gulrajani, R.M., Roberge, F.A. & Savard, P. 1984, "Moving dipole inverse ECG and EEG solutions", *IEEE Transactions on Biomedical Engineering,* vol. 21, no. 12, pp. 903-910.

Han, C., Liu, Z., Zhang, X., Pogwizd, S. & He, B. 2008, "Noninvasive three-dimensional cardiac activation imaging from body surface potential maps: a computational and experimental study on a rabbit model", *IEEE Transactions on Medical Imaging,* vol. 27, no. 11, pp. 1622-1630.

Han, C., Pogwizd, S.M., Killingsworth, C.R. & He, B. 2011, "Noninvasive imaging of three-dimensional cardiac activation sequence during pacing and ventricular tachycardia", *Heart Rhythm,* vol. 9, no. 9, pp. 1266-1272.

Han, C., Pogwizd, S.M., Killingsworth, C.R. & He, B. 2012, "Noninvasive reconstruction of the three-dimensional ventricular activation sequence during pacing and ventricular tachycardia in the canine heart", *American Journal of Physiology-Heart and Circulatory Physiology,* vol. 302, no. 1, pp. H244-H252.

Hansen, P.C. 1990, "The discrete Picard condition of discrete ill-posed problems", *BIT,* vol. 30, pp. 658-672.

Hansen, P.C. & O'Leary, D.P. 1993, "The use of the L-curve in the regularization of discrete ill-posed problems", *SIAM Journal on Scientific Computing,* vol. 14, no. 6, pp. 1487-1503.

Hayes, D.L., Lloyd, M.A. & Friedman, P.A. 2000, *Cardiac Pacing and Defibrillation: A Clinical Approach,* Wiley-Blackwell, New York.

He, B. & Cohen, R.J. 1992, "Body surface Laplacian ECG mapping", *IEEE Transactions on Biomedical Engineering,* vol. 39, no. 11, pp. 1179-1191.

He, B. & Liu, C. 2010, "Cardiac Electrophysiological Imaging: Solving the Inverse Problem of Electrocardiography", in *Cardiac Electrophysiology Methods and Models,* ed. D. Sigg, Springer, New York, pp. 357-373.

He, B., Liu, C. & Zhang, Y. 2007, "Three-dimensional cardiac electrical imaging from intracavity recordings", *IEEE Transactions on Biomedical Engineering,* vol. 54, no. 8, pp. 1454-1460.

He, B., Li, G. & Zhang, X. 2003, "Noninvasive imaging of cardiac transmembrane potentials within three-dimensional myocardium by means of a realistic geometry anisotropic heart model", *IEEE Transactions on Biomedical Engineering,* vol. 50, no. 10, pp. 1190-1202.

He, B., Li, G. & Zhang, X. 2002, "Noninvasive three-dimensional activation time imaging of ventricular excitation by means of a heart-excitation model", *Physics in Medicine and Biology,* vol. 47, no. 22, pp. 4063-4078.

He, B. & Wu, D. 2001, "Imaging and visualization of 3-D cardiac electric activity", *IEEE Transactions on Information Technology in Biomedicine,* vol. 5, no. 3, pp. 181-186.

Hsia, H.H., Callans, D.J. & Marchlinski, F.E. 2003, "Characterization of endocardial electrophysiological substrate in patients with nonischemic cardiomyopathy and monomorphic ventricular tachycardia", *Circulation,* vol. 108, no. 6, pp. 704-710.

Huiskamp, G. & Greensite, F. 1997, "A new method for myocardial activation imaging", *IEEE Transactions on Biomedical Engineering,* vol. 44, no. 6, pp. 433-446.

Hunter, P.J., Pullan, A.J. & Smaill, B.H. 2003, "Modeling total heart function", *Annual Review of Biomedical Engineering,* vol. 5, no. 1, pp. 147-177.

Jia, P., Punske, B., Taccardi, B. & Rudy, Y. 2000, "Electrophysiologic endocardial mapping from a noncontact nonexpandable catheter: A validation study of a

geometry-based concept", *Journal of Cardiovascular Electrophysiology,* vol. 11, no. 11, pp. 1238-1251.

Johnston, P.R. & Gulrajani, R.M. 1997, "A new method for regularization parameter determination in the inverse problem of electrocardiography", *IEEE Transactions on Biomedical Engineering,* vol. 44, no. 1, pp. 19-39.

Kadish, A., Hauck, J., Pederson, B., Beatty, G. & Gornick, C. 1999, "Mapping of atrial activation with a noncontact, multielectrode catheter in dogs", *Circulation,* vol. 99, no. 14, pp. 1906-1913.

Kerber, R. 2000, "Transthoracic cardioversion and defibrillation" in *Cardiac Electrophysiology: From Cell to Bedside,* 3rd edn, ed. D.P. Zipes & J. Jalife, W.B. Saunder Company, Philadelphia, pp. 944-948.

Kerckhoffs, R.C.P., Healy, S.N., Usyk, T.P. & McCulloch, A.D. 2006, "Computational methods for cardiac electromechanics", *Proceedings of the IEEE,* vol. 94, no. 4, pp. 769-783.

Khoury, D.S., Berrier, K.L., Badruddin, S.M. & Zoghbi, W.A. 1998, "Three-dimensional electrophysiological imaging of the intact canine left ventricle using a noncontact multielectrode cavitary probe: study of sinus, paced, and spontaneous premature beats", *Circulation,* vol. 97, no. 4, pp. 399-409.

Kuck, K.H., Cappato, R., Siebels, J. & Rüppel, R. 2000, "Randomized comparison of antiarrhythmic drug therapy with implantable defibrillators in patients resuscitated from cardiac arrest: the Cardiac Arrest Study Hamburg (CASH)", *Circulation,* vol. 102, no. 7, pp. 748-754.

Lai, D., Liu, C., Eggen, M.D., Iaizzo, P.A. & He, B. 2010, "Equivalent moving dipole localization of cardiac ectopic activity in a swine model during pacing", *IEEE Transactions on Information Technology in Biomedicine,* vol. 14, no. 6, pp. 1318-1326.

Li, G. & He, B. 2001, "Localization of the site of origin of cardiac activation by means of a heart-model-based electrocardiographic imaging approach", *IEEE Transactions on Biomedical Engineering,* vol. 48, no. 6, pp. 660-669.

Li, Z., Hertervig, E., Kongstad, O., Holm, M., Grins, E., Olsson, S.B. & Yuan, S. 2003, "Global repolarization sequence of the right atrium: monphasic action potential mapping in health pigs", *PACE,* vol. 26, no. 9, pp. 1803-1808.

Liu, C., Eggen, M., Swingen, C.M., Iaizzo, P.A. & He, B. 2012a, "Noninvasive mapping of transmural potentials during activation in swine hearts from body surface electrocardiograms", *IEEE Transactions on Medical Imaging,* in press.

Liu, C., Iaizzo, P.A. & He, B. 2012b, "Three-dimensional imaging of ventricular activation and electrograms from intracavitary recordings", *IEEE Transactions on Biomedical Engineering,* vol. 58, no. 4, pp. 868-875.

Liu, C., Skadsberg, N.D., Ahlberg, S.E., Swingen, C.M., Iaizzo, P.A. & He, B. 2008, "Estimation of global ventricular activation sequences by noninvasive three-dimensional electrical imaging: Validation sudies in a swine model during pacing", *Journal of Cardiovascular Electrophysiology,* vol. 19, no. 5, pp. 535-540.

Liu, C., Zhang, X., Liu, Z., Pogwizd, S.M. & He, B. 2006a, "Three-dimensional myocardial activation imaging in a rabbit model", *IEEE Transactions on Biomedical Engineering,* vol. 53, no. 9, pp. 1813-1820.

Liu, Z., Liu, C. & He, B. 2006b, "Noninvasive reconstruction of three-dimensional ventricular activation sequence from the inverse solution of distributed equivalent current density", *IEEE Transactions on Medical Imaging,* vol. 25, no. 10, pp. 1307-1318.

Liu, Z.W., Jia, P., Biblo, L.A., Taccardi, B. & Rudy, Y. 1998, "Endocardial potential mapping from a noncontact nonexpandable catheter: a feasibility study", *Annals of Biomedical Engineering,* vol. 26, no. 6, pp. 994-1009.

MacLeod, R.S. & Brooks, D.H. 1998, "Recent progress in inverse problems in electrocardiology", *IEEE Engineering in Medicine and Biology Magazine,* vol. 17, no. 1, pp. 73-83.

MacLeod, R.S., Gardner, M., Miller, R.M. & Horacek, B.M. 1995, "Application of an electrocardiographic inverse solution to localize ischemia during coronary angioplasty", *Journal of Cardiovascular Electrophysiology,* vol. 6, no. 1, pp. 2-18.

Malmivuo, J. & Plonsey, R. 1995, *Bioelectromagnetism: Principles and Applications of Bioelectric and Biomagnetic Fields,* Oxford University Press, USA.

Mehra, R., Zeiler, R.H., Gough, W.B. & El-Sherif, N. 1983, "Reentrant ventricular arrhythmias in the late myocardial infarction period. Electrophysiologic-anatomic correlation of reentrant circuits", *Circulation,* vol. 67, no. 1, pp. 11-24.

Miller, W. & Geselowitz, D.B. 1978, "Simulation studies of the electrocardiogram. I. The normal heart", *Circulation Research,* vol. 43, no. 2, pp. 301-315.

Mirvis, D.M. 1988, *Body Surface Electrocardiographic Mapping,* Kluwer Academic, New York.

Mirvis, D.M., Keller, F.W., Ideker, R.E., Cox Jr, J.W., Dowdie, R.F. & Zettergren, D.G. 1977, "Detection and localization of multiple epicardial electrical generators by a two-dipole ranging technique", *Circulation Research,* vol. 41, no. 4, pp. 551-557.

Modre, R., Tilg, B., Fischer, G. & Wach, P. 2002, "Noninvasive myocardial activation time imaging: a novel inverse algorithm applied to clinical ECG mapping data", *IEEE Transactions on Biomedical Engineering,* vol. 49, no. 10, pp. 1153-1161.

Murakawa, Y., Sezaki, K., Yamashita, T., Kanese, Y. & Omata, M. 1997, "Three-dimensional activation sequence of cesium-induced ventricular arrhythmias", *American Journal of Physiology-Heart and Circulatory Physiology,* vol. 273, no. 3, pp. H1377-H1385.

Myerburg, R.J., Kessler, K.M. & Castellanos, A. 1993, "Sudden cardiac death: epidemiology, transient risk, and intervention assessment", *Annals of Internal Medicine,* vol. 119, no. 12, pp. 1187-1197.

Nash, M.P. & Pullan, A.J. 2005, "Challenges facing validation of noninvasive electrical imaging of the heart", *Annals of Noninvasive Electrocardiology,* vol. 10, no. 1, pp. 73-82.

Nielsen, B.F., Cai, X. & Lysaker, M. 2007, "On the possibility for computing the transmembrane potential in the heart with a one shot method: An inverse problem", *Mathematical Biosciences,* vol. 210, no. 2, pp. 523-553.

Ohyu, S., Okamoto, Y. & Kuriki, S. 2002, "Use of the ventricular propagated excitation model in the magnetocardiographic inverse problem for reconstruction of electrophysiological properties", *IEEE Transactions on Biomedical Engineering,* vol. 49, no. 6, pp. 509-519.

Okamoto, Y., Teramachi, Y. & Musha, T. 1983, "Limitation of the inverse problem in body surface potential mapping", *IEEE Transactions on Biomedical Engineering,* vol. 30, no. 11, pp. 749-754.

Oster, H.S., Taccardi, B., Lux, R.L., Ershler, P.R. & Rudy, Y. 1997, "Noninvasive electrocardiographic imaging: reconstruction of epicardial potentials, electrograms, and isochrones and localization of single and multiple electrocardiac events", *Circulation,* vol. 96, no. 3, pp. 1012-1024.

Packer, M. 1985, "Sudden unexpected death in patients with congestive heart failure: a second frontier", *Circulation,* vol. 72, no. 4, pp. 681-685.

Pascual-Marqui, R.D. 1995, "Reply to comments by Hämäläinen, Ilmoniemi and Nunez", *ISBET Newsletter,* vol. 6, pp. 16-28.

Pilkington, T.C., Morrow, M.N. & Stanley, P.C. 1985, "A comparison of finite element and integral equation formulations for the calculation of electrocardiographic potentials", *IEEE Transactions on Biomedical Engineering,* vol. 32, no. 2, pp. 166-173.

Pogwizd, S.M. 1994, "Focal mechanisms underlying ventricular tachycardia during prolonged ischemic cardiomyopathy", *Circulation,* vol. 90, no. 3, pp. 1441-1458.

Pogwizd, S.M. 1995, "Nonreentrant mechanisms underlying spontaneous ventricular arrhythmias in a model of nonischemic heart failure in rabbits", *Circulation,* vol. 92, no. 4, pp. 1034-1048.

Pogwizd, S.M. & Corr, P.B. 1987, "Reentrant and nonreentrant mechanisms contribute to arrhythmogenesis during early myocardial ischemia: results using three-dimensional mapping", *Circulation Research,* vol. 61, no. 3, pp. 352-371.

Pogwizd, S.M., McKenzie, J.P. & Cain, M.E. 1998, "Mechanisms underlying spontaneous and induced ventricular arrhythmias in patients with idiopathic dilated cardiomyopathy", *Circulation,* vol. 98, no. 22, pp. 2404-2414.

Pullan, A. 1996, "A high-order coupled finite element/boundary element torso model", *IEEE Transactions on Biomedical Engineering,* vol. 43, no. 3, pp. 292-298.

Pullan, A., Cheng, L., Nash, M., Bradley, C. & Paterson, D. 2001, "Noninvasive electrical imaging of the heart: theory and model development", *Annals of Biomedical Engineering,* vol. 29, no. 10, pp. 817-836.

Punske, B.B., Ni, Q., Lux, R.L., MacLeod, R.S., Ershler, P.R., Dustman, T.J., Allison, M.J. & Taccardi, B. 2003, "Spatial methods of epicardial activation time determination in normal hearts", *Annals of Biomedical Engineering,* vol. 31, no. 7, pp. 781-792.

Ramanathan, C., Ghanem, R.N., Jia, P., Ryu, K. & Rudy, Y. 2004, "Noninvasive electrocardiographic imaging for cardiac electrophysiology and arrhythmia", *Nature Medicine,* vol. 10, no. 4, pp. 422-428.

Reithmann, C., Hahnefeld, A., Remp, T., Dorwarth, U., Dugas, M., Steinbeck, G. & Hoffmann, E. 2003, "Electroanatomic mapping of endocardial right ventricular

activation as a guide for catheter ablation in patients with arrhythmogenic right ventricular dysplasia", *PACE,* vol. 26, no. 6, pp. 1308-1316.

Rosenfeld, M., Tanami, R. & Abboud, S. 1996, "Numerical solution of the potential due to dipole sources in volume conductors with arbitrary geometry and conductivity", *IEEE Transactions on Biomedical Engineering,* vol. 43, no. 7, pp. 679-689.

Schalij, M.J., van Rugge, F.P., Siezenga, M. & van der Velde, E.T. 1998, "Endocardial activation mapping of ventricular tachycardia in patients: first application of a 32-site bipolar mapping electrode catheter", *Circulation,* vol. 98, no. 20, pp. 2168-2179.

Schreiner, K.D., Kelemen, K., Zehelein, J., Becker, R., Senges, J.C., Bauer, A., Voss, F., Kraft, P., Katus, H.A. & Schoels, W. 2004, "Biventricular hypertrophy in dogs with chronic AV block: effects of cyclosporin A on morphology and electrophysiology", *American Journal of Physiology-Heart and Circulatory Physiology,* vol. 287, no. 6, pp. H2891-H2898.

Shahidi, A.V., Savard, P. & Nadeau, R. 1994, "Forward and inverse problems of electrocardiography: Modeling and recovery of epicardial potentials in humans", *IEEE Transactions on Biomedical Engineering,* vol. 41, no. 3, pp. 249-256.

Simmons, W.N., Mackey, S., He, D.S. & Marcus, F.I. 1996, "Comparison of gold versus platinum electrodes on myocardial lesion size using radiofrequency energy", *PACE,* vol. 19, no. 4 Pt 1, pp. 398-402.

Skipa, O., Nalbach, M., Sachse, F., Werner, C. & Dössel, O. 2002, "Transmembrane potential reconstruction in anisotropic heart model", *International Journal of Bioelectromagnetism,* vol. 4, no. 2, pp. 17-18.

Sosa, E., Scanavacca, M., d'Avila, A., Oliveira, F. & Ramires, J.A.F. 2000, "Nonsurgical transthoracic epicardial catheter ablation to treat recurrent ventricular tachycardia occurring late after myocardial infarction", *Journal of the American College of Cardiology,* vol. 35, no. 6, pp. 1442-1449.

Spragg, D.D., Dong, J., Fetics, B.J., Helm, R., Marine, J.E., Cheng, A., Henrikson, C.A., Kass, D.A. & Berger, R.D. 2010, "Optimal left ventricular endocardial pacing sites for cardiac resynchronization therapy in patients with ischemic cardiomyopathy", *Journal of the American College of Cardiology,* vol. 56, no. 10, pp. 774-781.

Stevenson, W.G. & Delacretaz, E. 2000, "Radiofrequency catheter ablation of ventricular tachycardia", *Heart,* vol. 84, no. 5, pp. 553-559.

Taccardi, B. 1963, "Distribution of heart potentials on the thoracic surface of normal human subjects", *Circulation Research,* vol. 12, no. 4, pp. 341-352.

Taccardi, B., Arisi, G., Macchi, E., Baruffi, S. & Spaggiari, S. 1987, "A new intracavitary probe for detecting the site of origin of ectopic ventricular beats during one cardiac cycle.", *Circulation,* vol. 75, no. 1, pp. 272.

Throne, R.D. & Olson, L.G. 1994, "A generalized eigensystem approach to the inverse problem of electrocardiography", *IEEE Transactions on Biomedical Engineering,* vol. 41, no. 6, pp. 592-600.

Tikhonov, A.N., Arsenin, V.I.A. & John, F. 1977, *Solutions of Ill-posed Problems,* Winston, New York.

Tilg, B., Fischer, G., Modre, R., Hanser, F., Messnarz, B., Schocke, M., Kremser, C., Berger, T., Hintringer, F. & Roithinger, F.X. 2002, "Model-based imaging of cardiac electrical excitation in humans", *IEEE Transactions on Medical Imaging,* vol. 21, no. 9, pp. 1031-1039.

Trayanova, N.A. 2011, "Whole-Heart Modeling", *Circulation Research,* vol. 108, no. 1, pp. 113-128.

Tung, L. 1978, *A Bidomain Model for Describing Ischemic Myocardial D.C. Potentials*, Ph.D. dissertation. Massachusettes Institute of Technology, Cambridge, MA,.

van Dam, P.M., Oostendorp, T.F., Linnenbank, A.C. & Van Oosterom, A. 2009, "Non-invasive imaging of cardiac activation and recovery", *Annals of Biomedical Engineering,* vol. 37, no. 9, pp. 1739-1756.

Walker, S.J. & Kilpatrick, D. 1987, "Forward and inverse electrocardiographic calculations using resistor network models of the human torso", *Circulation Research,* vol. 61, no. 4, pp. 504-513.

Wang, J.Z., Williamson, S.J. & Kaufman, L. 1992, "Magnetic source images determined by a lead-field analysis: the unique minimum-norm least-squares estimation", *IEEE Transactions on Biomedical Engineering,* vol. 39, no. 7, pp. 665-675.

Wang, L., Wong, K.C.L., Zhang, H., Liu, H. & Shi, P. 2011a, "Noninvasive computational imaging of cardiac electrophysiology for 3-d infarct", *IEEE Transactions on Biomedical Engineering,* vol. 58, no. 4, pp. 1033-1043.

Wang, Y., Cuculich, P.S., Zhang, J., Desouza, K.A., Vijayakumar, R., Chen, J., Faddis, M.N., Lindsay, B.D., Smith, T.W. & Rudy, Y. 2011b, "Noninvasive electroanatomic

mapping of human ventricular arrhythmias with electrocardiographic imaging", *Science Translational Medicine,* vol. 3, no. 98, pp. 98ra84.

Wei, D., Okazaki, O., Harumi, K., Harasawa, E. & Hosaka, H. 1995, "Comparative simulation of excitation and body surface electrocardiogram with isotropic and anisotropic computer heart models", *IEEE Transactions on Biomedical Engineering,* vol. 42, no. 4, pp. 343-357.

Widmaier, E., Raff, H. & Strang, K. 2005, *Vander's Human Physiology: The Mechanisms of Human Body Function*, 10th edn, McGraw-Hill, New York.

Wilson, F.N., Johnston, F.D., Macleod, A.G. & Barker, P.S. 1934, "Electrocardiograms that represent the potential variations of a single electrode", *American Heart Journal,* vol. 9, no. 4, pp. 447-458.

Wilson, F.N., Johnston, F.D., Rosenbaum, F.F., Erlanger, H., Kossmann, C.E., Hecht, H., Cotrim, N., de Oliveira, R.M., Scarsi, R. & Barker, P.S. 1944, "The precordial electrocardiogram", *American Heart Journal,* vol. 27, no. 1, pp. 19-85.

Winslow, R., Scollan, D., Holmes, A., Yung, C., Zhang, J. & Jafri, M. 2000, "Electrophysiological modeling of cardiac ventricular function: from cell to organ", *Annual Review of Biomedical Engineering,* vol. 2, pp. 119-155.

Wood, A.J.J. & Morady, F. 1999, "Radio-frequency ablation as treatment for cardiac arrhythmias", *New England Journal of Medicine,* vol. 340, no. 7, pp. 534-544.

Yamada, T., Mcelderry, H.T., Okada, T., Murakami, Y., Doppalapudi H., Yoshida N., Allred J.D., Murohara T. & Kay G.N. 2009, "Idiopathic focal ventricular arrhythmias originating from the anterior papillary muscle in the left ventricle", *Journal of Cardiovascular Electrophysiology,* vol. 20, no. 8, pp. 866-872.

Yamashita, Y. & Takahashi, T. 1984, "Use of the finite element method to determine epicardial from body surface potentials under a realistic torso model", *IEEE Transactions on Biomedical Engineering,* vol. 31, no. 9, pp. 611-621.

Zeppenfeld, K., Schalij, M.J., Bartelings, M.M., Tedrow, U.B., Koplan, B.A., Soejima, K. & Stevenson, W.G. 2007, "Catheter ablation of ventricular tachycardia after repair of congenital heart disease electroanatomic identification of the critical right ventricular isthmus", *Circulation,* vol. 116, no. 20, pp. 2241-2252.

Zhang, S., Skinner, J.L., Sims, A.L., Rollins, D.L., Walcott, G.P., Smith, W.M. & Ideker, R.E. 2000, "Three-dimensional mapping of spontaneous ventricular arrhythmias in a

canine thrombotic coronary occlusion model", *Journal of Cardiovascular Electrophysiology,* vol. 11, no. 7, pp. 762-772.

Zhang, X., Ramachandra, I., Liu, Z., Muneer, B., Pogwizd, S.M. & He, B. 2005, "Noninvasive three-dimensional electrocardiographic imaging of ventricular activation sequence", *American Journal of Physiology-Heart and Circulatory Physiology,* vol. 289, no. 6, pp. H2724-32.

Appendix A - Copyright Permissions

Ref. (Han et al., 2008)

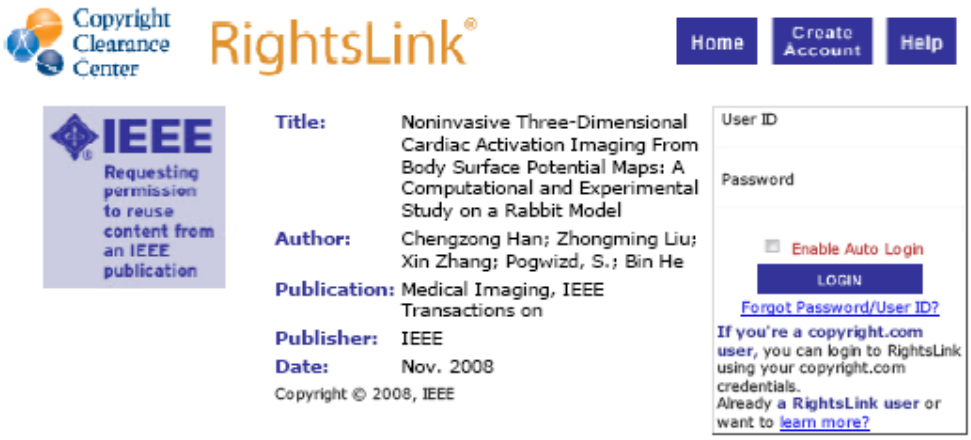

Thesis / Dissertation Reuse

The IEEE does not require individuals working on a thesis to obtain a formal reuse license, however, you may print out this statement to be used as a permission grant:

Requirements to be followed when using any portion (e.g., figure, graph, table, or textual material) of an IEEE copyrighted paper in a thesis:

1) In the case of textual material (e.g., using short quotes or referring to the work within these papers) users must give full credit to the original source (author, paper, publication) followed by the IEEE copyright line © 2011 IEEE.
2) In the case of illustrations or tabular material, we require that the copyright line © [Year of original publication] IEEE appear prominently with each reprinted figure and/or table.
3) If a substantial portion of the original paper is to be used, and if you are not the senior author, also obtain the senior author's approval.

Requirements to be followed when using an entire IEEE copyrighted paper in a thesis:

1) The following IEEE copyright/ credit notice should be placed prominently in the references: © [year of original publication] IEEE. Reprinted, with permission, from [author names, paper title, IEEE publication title, and month/year of publication]
2) Only the accepted version of an IEEE copyrighted paper can be used when posting the paper or your thesis on-line.
3) In placing the thesis on the author's university website, please display the following message in a prominent place on the website: In reference to IEEE copyrighted material which is used with permission in this thesis, the IEEE does not endorse any of [university/educational entity's name goes here]'s products or services. Internal or personal use of this material is permitted. If interested in reprinting/republishing IEEE copyrighted material for advertising or promotional purposes or for creating new collective works for resale or redistribution, please go to http://www.ieee.org/publications_standards/publications/rights/rights_link.html to learn how to obtain a License from RightsLink.

If applicable, University Microfilms and/or ProQuest Library, or the Archives of Canada may supply single copies of the dissertation.

Ref. (Han et al., 2011)

Copyright Clearance Center RightsLink®

Home | Account Info | Help

Title: Noninvasive imaging of three-dimensional cardiac activation sequence during pacing and ventricular tachycardia

Author: Chengzong Han,Steven M. Pogwizd,Cheryl R. Killingsworth,Bin He

Publication: Heart Rhythm

Publisher: Elsevier

Date: August 2011

Copyright © 2011, Elsevier

Logged in as: Chengzong Han

LOGOUT

Order Completed

Thank you very much for your order.

This is a License Agreement between Chengzong Han ("You") and Elsevier ("Elsevier"). The license consists of your order details, the terms and conditions provided by Elsevier, and the payment terms and conditions.

Get the printable license.

License Number	2963480799982
License date	Aug 07, 2012
Licensed content publisher	Elsevier
Licensed content publication	Heart Rhythm
Licensed content title	Noninvasive imaging of three-dimensional cardiac activation sequence during pacing and ventricular tachycardia
Licensed content author	Chengzong Han,Steven M. Pogwizd,Cheryl R. Killingsworth,Bin He
Licensed content date	August 2011
Licensed content volume number	8
Licensed content issue number	8
Number of pages	7
Type of Use	reuse in a thesis/dissertation
Portion	figures/tables/illustrations
Number of figures/tables /illustrations	8
Format	both print and electronic
Are you the author of this Elsevier article?	Yes
Will you be translating?	No
Order reference number	
Title of your thesis/dissertation	Noninvasive Imaging of Three-dimensional Ventricular Electrical Activity
Expected completion date	Aug 2012
Estimated size (number of pages)	120
Elsevier VAT number	GB 494 6272 12
Permissions price	0.00 USD
VAT/Local Sales Tax	0.0 USD / 0.0 GBP
Total	0.00 USD

Ref. (Han et al., 2012)

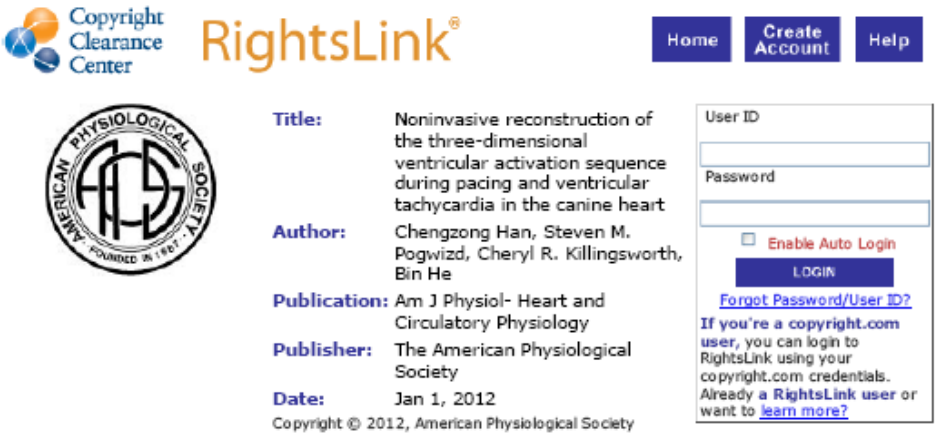

Appendix B – VITA

NAME Chengzong Han

CONTACT

7-105 Hasselmo Hall, 312 Church St SE, Minneapolis, MN 55455

hanxx158@umn.edu, hanchengzong@gmail.com

612-625-9741 (lab), 612-532-2265 (cell)

EDUCATION

Ph.D. in Biomedical Engineering
Department of Biomedical Engineering, University of Minnesota, Twin Cities, USA, 2006 – Present.
Expected graduation in Aug. 2012

M.S. in Electrical Engineering
College of Electrical Engineering, Zhejiang University, China, 2006.

B.S. in Electrical Engineering
College of Electrical Engineering, Zhejiang University, China, 2004.

EXPERIENCE

Research Assistant
Department of Biomedical Engineering, University of Minnesota, Twin Cities, USA, 2006 – Present.

- Conducted computer modeling, simulation, and programming.
- Conducted animal experiment and data analysis.
- Coordinated research projects and trained graduate students.

Research Assistant
College of Electrical Engineering, Zhejiang University, China, 2004 – 2006.

Teaching Assistant
Department of Biomedical Engineering, University of Minnesota, Twin Cities, USA.

- BMEn 8502 Physiological Control Systems, 2011.
- BMEn 5101 Advanced Bioelectricity and Instrumentation, 2010.
- BMEn 5401 Advanced Biomedical Functional Imaging, 2007.

HONORS AND AWARDS

- Open Finalist for Student Paper Competition in 33rd Annual International Conference of IEEE Engineering in Medicine and Biology Society, 2011.
- Predoctoral Fellowship from the American Heart Association, Midwest Affiliation, 2008-2009.
- Lillehei Heart Institute Poster Award in 6th Annual Conference of Life Sciences Alley, 2007.

- Graduate with Honor (top 1%), Zhejiang Province, China, 2004, 2006.
- Graduate with Honor, Zhejiang University, China, 2004, 2006.
- Second Prize in National Undergraduate Electronic Design Contest, China, 2003.

PROFESSIONAL MEMBERSHIP

- IEEE student membership
- IEEE Engineering in Medicine and Biology Society student membership

PUBLICATIONS

Journal Papers

- **Han C,** Pogwizd SM, Killingsworth CR, He B. Noninvasive reconstruction of the three-dimensional ventricular activation sequence during pacing and ventricular tachycardia in the canine heart. American Journal of Physiology-Heart and Circulatory Physiology, 302(1): H244-H252, 2012.
- **Han C,** Pogwizd SM, Killingsworth CR, He B. Noninvasive imaging of three-dimensional cardiac activation sequence during pacing and ventricular tachycardia. Heart Rhythm, 8(8): 1266-1272, 2011.
- **Han C,** Liu Z, Zhang X, Pogwizd SM, He B. Noninvasive three-dimensional cardiac activation imaging from body surface potential maps: a computational and experimental study on a rabbit model. IEEE Transactions on Medical Imaging, 27(11):1622-30, 2008.

Conference Abstracts/Proceedings

- **Han C,** Pogwizd SM, Killingsworth CR, He B. Imaging cardiac activation sequence during ventricular tachycardia in a canine model of nonischemic heart failure. 33nd Annual Scientific Sessions of the Heart Rhythm Society, 2012 (moderated poster).
- **Han C,** Pogwizd SM, Killingsworth CR, He B. Noninvasive reconstruction of the three-dimensional ventricular activation sequence during pacing and ventricular tachycardia in the rabbit heart. 33rd Annual International Conference of IEEE Engineering in Medicine and Biology Society, 2011 (oral).
- **Han C,** Pogwizd SM, Killingsworth CR, He B. Noninvasive reconstruction of the three-dimensional ventricular activation sequence from body surface potential maps in the canine heart. 32nd Annual Scientific Sessions of the Heart Rhythm Society, 2011 (poster).
- Zhou Z, Liu C, **Han C,** He B. Estimation of activation sequence from time course of equivalent current density in pathological

hearts - A simulation study. 8th International Symposium on Noninvasive Functional Source Imaging of the Brain and Heart & 8th International Conference on Bioelectromagnetism, 2011 (oral).

- **Han C,** Pogwizd SM, Killingsworth CR, Yan J, He B. Noninvasive three-dimensional cardiac activation imaging of ventricular tachycardia (VT) in the rabbit heart. Annual Scientific Sessions of the American Heart Association, 2010 (oral).
- **Han C,** Pogwizd SM, Killingsworth CR, Yan J, He B. Noninvasive three-dimensional cardiac activation imaging of ventricular arrhythmias in the rabbit heart. Computing in Cardiology, 2010 (oral).
- **Han C,** Pogwizd SM, Killingsworth CR, Liu C, Lai D, He B. Noninvasive imaging of the three-dimensional cardiac activation sequence of paced rhythm and ventricular tachycardia (VT) in the rabbit heart. 31st Annual Scientific Sessions of the Heart Rhythm Society, 2010 (oral).
- **Han C,** Liu C, Pogwizd SM, He B. Noninvasive three-dimensional cardiac activation imaging on a rabbit model. 31st Annual International Conference of IEEE Engineering in Medicine and Biology Society, 2009 (invited oral).
- **Han C,** Liu Z, Liu C, Pogwizd SM, He B. Noninvasive imaging of three-dimensional ventricular activation sequence in a rabbit model. 7th International Symposium on Noninvasive Functional Source Imaging of the Brain and Heart & 7th International Conference on Bioelectromagnetism, 2009 (poster).
- **Han C,** Liu Z, Liu C, Pogwizd SM, He B. Imaging three-dimensional ventricular activation sequence under dual-site pacing in a rabbit model. Joint Meeting of 6th International Symposium on Noninvasive Functional Source Imaging within the Human Brain and Heart and the International Conference on Functional Biomedical Imaging, 2007 (poster).
- **Han C,** Liu Z, Liu C, Pogwizd SM, He B. Three-dimensional activation sequence imaging in a rabbit model. 29th Annual International Conference of IEEE Engineering in Medicine and Biology Society, 2007 (poster).